



Measurement of differential t -channel single top (anti)quark production cross-sections at 13 TeV with the ATLAS detector

The ATLAS Collaboration

The production of single top quarks and top antiquarks via the t -channel exchange of a virtual W boson is measured in proton–proton collisions at a centre-of-mass energy of 13 TeV at the Large Hadron Collider. The full Run 2 data sample recorded with the ATLAS detector in the years 2015–2018 is used, corresponding to an integrated luminosity of 140 fb^{-1} . The absolute and normalised production cross-sections are measured differentially as a function of the transverse momentum and absolute rapidity of the top quark and top antiquark. In addition, the ratio of top quark to top antiquark production cross-sections is measured. The measured distributions are compared with next-to-leading-order quantum chromodynamics predictions obtained with different combinations of matrix-element generators, parton-shower programs and proton parton distribution functions, as well as to next-to-next-to-leading-order calculations. Overall, good agreement is observed between the measurements and the theoretical predictions. For most measured distributions, the sensitivity to differences between the predictions is limited by the systematic uncertainties in the measurement. The measured differential distributions are also interpreted in an effective field theory approach to constrain the Wilson-Coefficient $C_{Qq}^{3,1}$ associated with a four-quark operator. The interpretation accounts for the effect of the selection efficiency, which is altered significantly by non-zero contributions from $C_{Qq}^{3,1}$.

Contents

1	Introduction	3
2	ATLAS detector and data sample	4
3	Samples of simulated events	5
4	Object reconstruction and event selection	7
4.1	Object definitions	7
4.2	Event selection	8
5	Background estimation	9
6	Unfolding technique	12
7	Binning and convergence of unfolding	13
8	Systematic and statistical uncertainties	13
8.1	Sources of uncertainties	13
8.2	Evaluation of uncertainties	14
9	Results	18
9.1	Effective field theory interpretation	27
10	Conclusion	30
	Appendix	33

1 Introduction

The production of single top quarks was first observed in 2009 in proton–antiproton collisions at the Tevatron [1, 2] and was since then used to obtain valuable insights on the properties of the top quark [3]. At the Large Hadron Collider, the main production channel of single top quarks is the t -channel exchange of a virtual W boson. The total production cross-section of single top quarks and top antiquarks via the t -channel process (tq and $\bar{t}q$ production) was measured by both the ATLAS and CMS collaborations at centre-of-mass energies of 5.02 TeV [4], 7 TeV [5, 6], 8 TeV [7, 8] and 13 TeV [9, 10]. At 13 TeV, differential cross-sections were measured by CMS [11] using a partial Run 2 data sample with an integrated luminosity of 35.9 fb^{-1} .

Example Feynman diagrams for t -channel production of single top quarks and top antiquarks at leading-order (LO) in perturbation theory are depicted in Figure 1. A light quark from one of the colliding protons interacts with a b -quark from the other proton by exchanging a virtual W boson. Since the integral of the valence u -quark density of the proton is twice the integral of the valence d -quark density, the tq production cross-section is expected to be higher than the $\bar{t}q$ production cross-section. Subleading diagrams containing only sea quarks in the initial-state contribute to the production cross-section in a charge-symmetric way.

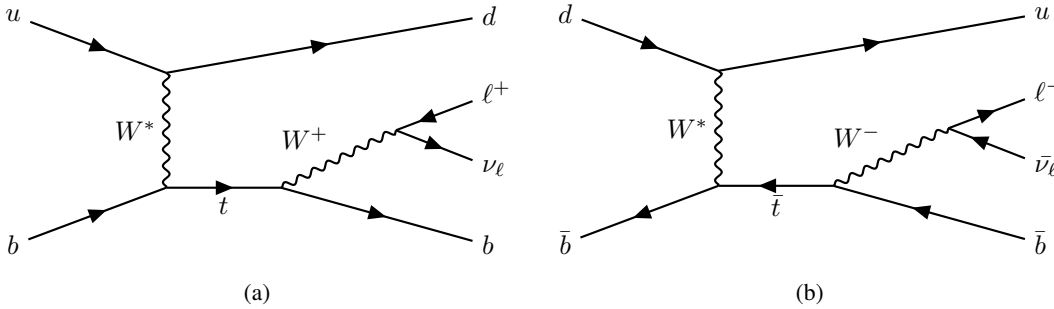


Figure 1: Example Feynman diagrams of (a) single top quark and (b) single top antiquark production via the t -channel exchange of a virtual W boson at LO in perturbation theory with the leptonic decay channel of the top (anti)quark.

In this paper, the ATLAS measurements of differential tq and $\bar{t}q$ production cross-sections are presented using the full Run 2 data sample, recorded with the ATLAS detector between 2015 and 2018 at $\sqrt{s} = 13 \text{ TeV}$, corresponding to an integrated luminosity of 140 fb^{-1} . Absolute and normalised differential cross-sections are measured as functions of the transverse momentum $p_{\text{T}}(t)$ or $p_{\text{T}}(\bar{t})$ and the absolute value of the rapidity $|y(t)|$ or $|y(\bar{t})|$ of the top quark and top antiquark. The cross-sections for tq and $\bar{t}q$ production are measured separately, along with their ratio.

The measurement targets events with leptonically decaying W bosons. Signal events are required to contain exactly one isolated electron or muon and large missing transverse momentum $E_{\text{T}}^{\text{miss}}$. Based on the LO event signature of tq and $\bar{t}q$ production, exactly two jets are required and exactly one of these jets must be identified as originating from a b -quark. The purity of the event selection in signal events is enhanced by dedicated kinematic requirements and the use of a neural network (NN), trained to separate signal and background events. The NN was trained for the ATLAS measurement of the total tq and $\bar{t}q$ production cross-sections at $\sqrt{s} = 13 \text{ TeV}$ [9], which serves as the basis for the differential analysis reported in this paper. Consequently, the event selection, simulated event samples, and systematic uncertainties used here are almost identical and are therefore described only briefly. Further details can be found in the paper [9].

Two signal regions are defined based on the sign of the lepton charge to measure the tq and $\bar{t}q$ production cross-sections separately. The measured cross-sections are corrected for geometric acceptance, detector resolution, and trigger and reconstruction efficiencies. The corrections are made by unfolding the measured distributions to parton level, using iterative Bayesian unfolding (IBU) [12]. The measured differential cross-sections are compared with predictions obtained at next-to-leading-order (NLO) in quantum chromodynamics (QCD) with different combinations of matrix-element event generators and parton-shower programs and with different parton distribution function (PDF) sets, and to next-to-next-to-leading-order (NNLO) predictions calculated with MCFM [13]. Measurements of the differential cross-sections and in particular the ratio of the differential $tq/\bar{t}q$ cross-sections as a function of $|y(t \text{ or } \bar{t})|$ can help to constrain the PDFs of the proton [14]. The tq and $\bar{t}q$ process offers the possibility to constrain the u/d -quark ratio and, as future prospect, the b -quark density.

The differential cross-sections as a function of $p_T(t)$ or $p_T(\bar{t})$ are also of interest for effective field theory (EFT) interpretations [15]. In the standard-model effective field theory (SMEFT) [16], at leading-order in QCD only three dimension-6 operators contribute to tq and $\bar{t}q$ production through interference with the SM: $O_{Qq}^{3,1}$, $O_{\phi Q}^3$, and O_{tW} . A non-zero contribution from the four-quark EFT operator $O_{Qq}^{3,1}$ affects both the tq and $\bar{t}q$ production cross-sections and the kinematic properties of the events, thereby altering the acceptance. In contrast, the $O_{\phi Q}^3$ operator only alters the inclusive production cross-section and O_{tW} modifies the kinematics of the top-quark decay [17]. The EFT interpretation aims to constrain the contribution of $O_{Qq}^{3,1}$ and is based on the measured $p_T(t)$ and $p_T(\bar{t})$ differential distributions at parton level. The dependence of the acceptance on the $O_{Qq}^{3,1}$ contribution is studied and a significant impact on the obtained constraints is found. Therefore, the interpretation takes this acceptance effect into account. The obtained constraints on an $O_{Qq}^{3,1}$ contribution improve the limits set by the EFT interpretation of the total tq and $\bar{t}q$ cross-section measurement [9].

A brief introduction of the ATLAS detector and the data samples is given in Section 2 and the samples of simulated events are described in Section 3. The object definitions and event selection are given in Section 4. Section 5 provides a description of the estimate of the background rate. The unfolding procedure and needed inputs are defined in Section 6 and Section 7. The uncertainties are described in Section 8. The unfolded results and an interpretation of the results in the context of EFT are presented in Section 9.

2 ATLAS detector and data sample

The ATLAS experiment [18] at the LHC is a multipurpose particle detector with a forward–backward symmetric cylindrical geometry and a near 4π coverage in solid angle.¹ It consists of an inner tracking detector surrounded by a thin superconducting solenoid providing a 2 T axial magnetic field, electromagnetic and hadronic calorimeters, and a muon spectrometer. The inner tracking detector covers the pseudorapidity range $|\eta| < 2.5$. It consists of silicon pixel, silicon microstrip, and transition radiation tracking detectors. Lead/liquid-argon (LAr) sampling calorimeters provide electromagnetic (EM) energy measurements with high granularity within the region $|\eta| < 3.2$. A steel/scintillator-tile hadronic calorimeter covers the central pseudorapidity range ($|\eta| < 1.7$). The endcap and forward regions are instrumented with LAr

¹ ATLAS uses a right-handed coordinate system with its origin at the nominal interaction point (IP) in the centre of the detector and the z -axis along the beam pipe. The x -axis points from the IP to the centre of the LHC ring, and the y -axis points upwards. Polar coordinates (r, ϕ) are used in the transverse plane, ϕ being the azimuthal angle around the z -axis. The pseudorapidity is defined in terms of the polar angle θ as $\eta = -\ln \tan(\theta/2)$ and is equal to the rapidity $y = \frac{1}{2} \ln \left(\frac{E+p_z}{E-p_z} \right)$ in the relativistic limit. Angular distance is measured in units of $\Delta R \equiv \sqrt{(\Delta y)^2 + (\Delta\phi)^2}$.

calorimeters for EM and hadronic energy measurements up to $|\eta| = 4.9$. The muon spectrometer surrounds the calorimeters and is based on three large superconducting air-core toroidal magnets with eight coils each. The field integral of the toroids ranges between 2.0 and 6.0 T m across most of the detector. The muon spectrometer includes a system of precision tracking chambers up to $|\eta| = 2.7$ and fast detectors for triggering up to $|\eta| = 2.4$. The luminosity is measured mainly by the LUCID-2 [19] detector which is located close to the beampipe. A two-level trigger system was used to select events [20]. The first-level trigger is implemented in hardware and used a subset of the detector information to accept events at a rate close to 100 kHz. This is followed by a software-based trigger that reduced the accepted rate of complete events to 1.25 kHz on average depending on the data-taking conditions. A software suite [21] is used in data simulation, in the reconstruction and analysis of real and simulated data, in detector operations, and in the trigger and data acquisition systems of the experiment.

The analysis uses proton–proton (pp) collision data recorded in the years 2015 to 2018 [22] at a centre-of-mass energy of 13 TeV and corresponds to an integrated luminosity of 140 fb^{-1} with a relative uncertainty of 0.83% [23]. Events were selected online during data taking by single-electron or single-muon triggers [24, 25]. Multiple triggers with different thresholds in transverse momentum (p_T) were combined in a logical OR to increase the selection efficiency. The lowest-threshold triggers utilised isolation requirements for reducing the trigger rate.

3 Samples of simulated events

Sets of simulated events from signal and background processes were produced with MC-based event generator programs to model the physics processes. After event generation, the response of the ATLAS detector was simulated using the GEANT4 toolkit [26] with a full detector model [27] or a fast simulation [28, 29] which employed a parameterisation of the calorimeter response.

Samples of simulated events involving top quarks were generated using the POWHEG BOX v2 [30–36] matrix element (ME) generator with the top-quark mass set to $m_t = 172.5 \text{ GeV}$. All processes were calculated in QCD NLO and used the NNPDF3.0_{NLO} PDF set [37] with the five-flavour scheme (5FS) except single top-quark production in the t -channel that was simulated with the NNPDF3.0_{NLO_NF4} PDF set, which implements the four-flavour scheme (4FS). Parton showers, hadronisation, and the underlying event were modelled using PYTHIA 8.230 [38] with the A14 [39] set of tuned parameters and the NNPDF2.3_{LO} PDF set [40]. When generating tW events, the diagram-removal scheme [41] was employed to treat the interference with $t\bar{t}$ production [42]. The decays of bottom and charm hadrons were simulated using the EVTGEN 1.6.0 program [43].

The production of W and Z bosons in association with jets, including heavy-flavour jets, was simulated with the SHERPA 2.2.11 generator [44] using NLO matrix elements for up to two partons and LO matrix elements for up to five partons. The default SHERPA parton shower [45] and the cluster hadronisation model [46] were used. The generation employed the dedicated set of tuned parameters developed by the SHERPA authors and the NNPDF3.0_{NLO} PDF set. The W +jets and Z +jets samples were normalised to NNLO QCD and NLO electroweak predictions [47] of the total cross-sections, obtained with the FEWZ package [48, 49].

Samples of on-shell diboson production (WW , WZ , and ZZ , abbreviated as VV in the following) were simulated with the same SHERPA configuration as described above for W +jets and Z +jets production. The matrix elements considered contain all diagrams with four electroweak vertices and were calculated at

NLO in QCD for up to one additional parton and at LO for up to three additional parton emissions. The diboson event samples were normalised to the total cross-sections provided by SHERPA.

Multijet events with fake or non-prompt leptons are modelled using different strategies depending on the lepton type. Non-prompt muons are estimated from collision data while fake electrons or non-prompt electrons from hadron decays are described with simulated dijet samples. The dijet event sample was simulated using PYTHIA 8.186 with LO matrix elements for dijet production. The generation used the NNPDF2.3_{LO} PDF set and the A14 set of tuned parameters.

For interpreting the measurement in the framework of EFT, samples of t -channel and s -channel production were generated with MADGRAPH5_AMC@NLO 2.7.3 using the SMEFTatNLO-NLO UFO model [16] with the 5FS and the NNPDF3.0_{NLO} PDF set. The operator $O_{Qq}^{3,1}$ was activated, which introduces a four-quark contact interaction. Separate samples of simulated events were generated for each $C_{Qq}^{3,1}/\Lambda^2 \in \{-0.6, -0.2, 0.0, 0.4, 1.0\}$ TeV^{-2} for single top-quark and top-antiquark production. The generated events were showered with PYTHIA 8.244 using the A14 set of tuned parameters and the NNPDF2.3_{LO} PDF set. In these samples, the top-quark (top-antiquark) is assumed to decay into W^+b ($W^-\bar{b}$) with a branching ratio of 100%.

The simulation of single-top-quark events depends on several parameters, which can be constrained by comparing to the measured differential distributions. These include PDFs, α_s , and the calculation scheme (i.e. 4FS vs. 5FS). Among these, the variations of the PDFs have the largest impact. Fixed-order (FO) calculations are typically performed in the 5FS, where the initial b -quark is taken directly from the proton PDF. In contrast, for MC event generation the 4FS is usually preferred [36]. In this scheme, the initial gluon splitting into the $b\bar{b}$ pair is included in the ME calculation and can be carried out with massive b -quarks. As a result, the modelling of the kinematics of the “spectator” b -quark is more reliable.

Fixed order differential calculations of the top-quark and top-antiquark kinematics are available up to NNLO in perturbation theory within the MCFM framework [50, 51] and made in the 5FS. The dynamic double deep inelastic scattering scale is used as suggested in [51]. In this scale choice, the momentum transfer along the W boson Q^2 is used as the scale for the light-quark-line corrections $\mu^2 = Q^2$ and for the heavy-quark-line corrections, $\mu^2 = Q^2 + m_t^2$ with the top quark mass m_t set to 172.5 GeV. The uncertainty in the calculations comprises the uncertainty in the renormalisation and factorisation scale choice and the uncertainty in the value of α_s . The signal samples for tq and $\bar{t}q$ production are normalised to the reference cross-sections calculated with MCFM at NNLO [52].

Within the parton level ME generators interfaced to parton shower programs, calculations are available up to NLO with implementations in the POWHEG Box v2 (ST_tch_4f) and MG_AMC@NLO [53] frameworks, in both the 4FS and 5FS, and interfaced to either the PYTHIA 8 or the HERWIG 7 [54, 55] parton shower generator programs. The POWHEG Box implementation is the same as used for the event generation of the nominal signal sample. An overview of the considered fixed order calculations and ME event generators is given in Table 1.

PDFs are provided by several groups worldwide, e.g. ABM [56], CTEQ [57], MSHT [58], NNPDF [37, 59, 60], and HERAPDF [61]. The ATLAS Collaboration also provides its own PDF sets [62, 63]. The PDFs from each group can differ in, for example, the data used, the value of α_s , the treatments of the heavy-quark masses and the implementation of higher-order QCD corrections. Predictions for the tq and $\bar{t}q$ production with different PDF sets are obtained using the POWHEG Box v2 implementation. An overview of the PDFs used for the comparison is given in Table 2, where available the 4FS variant is used. All PDF

Table 1: Summary of fixed order calculations and ME event generators used for the production of top-quark and top-antiquark kinematic-distributions of the tq and $\bar{t}q$ production.

Program	Precision	FS	Note
MCFM	LO / NLO / NNLO	5FS	FO calculation
MG_AMC@NLO	NLO	4FS / 5FS	Event generation
POWHEG ST_tch_4f	NLO	4FS	Event generation

sets are employed at NLO precision to match that of the ME calculation, except for ATLASPDF21, which is available only at NNLO precision.

Table 2: Summary of PDF sets employed for the production of top-quark and top-antiquark kinematic-distributions of the tq and $\bar{t}q$ production using the PowHEG ST_tch_4f generator.

PDF	LHAPDF ID [64]	Precision	FS
NNPDF3.0	260400–260500	NLO	4FS
NNPDF4.0	334700	NLO	4FS
MSHT20	27700	NLO	4FS
CT18	14400	NLO	5FS
PDF4LHC21	93500–93541	NLO	4FS
ATLASPDF21	65700–65753	NNLO	5FS
ABMP16	42930–42961	NLO	4FS

4 Object reconstruction and event selection

The final state of the tq and $\bar{t}q$ signal processes comprises a charged lepton, a neutrino, a b -quark and a light quark (see Figure 1) and is reconstructed by identifying corresponding objects measured in the detector. The presence of a high- p_T neutrino is indicated by large missing transverse momentum. In the context of this analysis, “charged lepton” refers to electrons and muons only.

4.1 Object definitions

Electron candidates are reconstructed from Inner Detector (ID) tracks matched to EM calorimeter energy clusters [65], where for the pseudorapidity of the clusters η_{cluster} , $|\eta_{\text{cluster}}| < 2.47$ is required. The detector transition region $1.37 < |\eta_{\text{cluster}}| < 1.52$ is excluded. Electron candidates are required to have $p_T > 10$ GeV. A likelihood-based discriminant is constructed to reject non-prompt electrons [65]. Muon candidates are reconstructed by combining ID and muon spectrometer tracks [66]. All tracks must be in the range of $|\eta| < 2.5$. Leptons must be consistent with the primary vertex via impact-parameter requirements, and are further subject to isolation criteria optimised to reject non-prompt and fake candidates [65, 66].

Jets are reconstructed from particle-flow objects [67] with the anti- k_r algorithm [68, 69] using a radius parameter of 0.4. The jet energy is calibrated by applying several simulation-based corrections and techniques correcting for differences between simulation and data [70]. The jets must satisfy $p_T > 30$ GeV and $|\eta| < 4.5$. Pile-up suppression is performed via the jet-vertex tagger (JVT) [71] and forward JVT (fJVT) [72] discriminants. Jets containing b -hadrons are identified (b -tagged) with the DL1r algorithm, which uses a deep feed-forward neural network with several b -tagging algorithms as inputs [73]. As requirement on the DL1r discriminant, the 60% efficiency working point is used. Since the DL1r algorithm uses measurements from the ID, the identification of b -jets is limited to the region with $|\eta| < 2.5$.

An overlap-removal procedure is applied to prevent double-counting of objects satisfying multiple reconstruction criteria. Reconstructed objects are removed in the following order: electrons sharing an ID track with a muon, jets within $\Delta R = 0.2$ of an electron, electrons within $\Delta R = 0.4$ of a remaining jet, jets within $\Delta R = 0.2$ of a muon if they have less than three associated tracks with $p_T > 0.5$ GeV, and muons within $\Delta R = 0.4$ of a remaining jet.

The missing transverse momentum \vec{p}_T^{miss} is reconstructed as the negative vector sum of the p_T of the reconstructed leptons and jets, and ID tracks that point to the primary vertex but are not associated with a reconstructed object [74]. The magnitude of \vec{p}_T^{miss} is denoted by E_T^{miss} .

The neutrino momentum is required for the reconstruction of the top (anti)quark. The x - and y -components of the neutrino momentum are approximated by the components of \vec{p}_T^{miss} . The z -component, $p_z(\nu)$, is determined by constraining the mass of the reconstructed W boson to match the measured world average $m(W) = 80.4$ GeV [75]. If the resulting quadratic equation has two real solutions, the one with the smallest $|p_z(\nu)|$ is chosen. In the case of complex solutions, a kinematic fit is performed such that the imaginary part vanishes and the distance between the transverse components of the neutrino momentum and \vec{p}_T^{miss} is minimised [76]. The W boson is formed by adding the four-vectors of the reconstructed neutrino and the charged lepton and the top (anti)quark is reconstructed by adding the four-vector of the W boson and the b -jet.

4.2 Event selection

The event selection imposes requirements based on the expected event signature of tq and $\bar{t}q$ production. Candidate events must contain exactly one charged lepton with $p_T > 28$ GeV matched to the trigger object. Two separate signal regions are defined according to the sign of the lepton charge, referred to as ℓ^+ SR and ℓ^- SR in the following.

Exactly two jets with $p_T > 30$ GeV are required, of which exactly one must be b -tagged. The b -tagged jet is explicitly required to have $|\eta| < 2.5$. For events with forward jets with $2.3 < |\eta|$, the requirement $p_T(\text{jet}) > 35$ GeV is imposed leading to an improved modelling of the $|\eta|$ distribution of untagged jets in the given regime. To reduce the multijet background, requirements are imposed on the missing transverse energy and the transverse W mass defined as $m_T(W) = \sqrt{2p_T(\ell)E_T^{\text{miss}}(1 - \cos \Delta\phi(\vec{p}_T^{\text{miss}}, \ell))}$. Events are required to have $E_T^{\text{miss}} > 30$ GeV and $m_T(W) > 50$ GeV. To further suppress the multijet background and to remove poorly reconstructed leptons with low p_T , an additional requirement is applied based on the azimuthal angle ϕ between the charged lepton and the leading jet (j_1), i.e. the jet with the largest p_T . The imposed requirement is $p_T(\ell) > 40 \text{ GeV} \cdot |\Delta\phi(j_1, \ell)|/\pi$ since the charged lepton and the leading jet are typically emitted back-to-back in multijet events. An additional selection criterion is imposed on the

invariant mass of the charged lepton and the b -tagged jet, $m(\ell b) < 160$ GeV, to exclude the off-shell region for top-quark decays which is not modelled well.

To reduce the contribution from background processes further, an additional selection criterion is introduced using the NN trained for the inclusive analysis to separate background and signal events [9]. The NN is implemented using the NeuroBayes package [77, 78] and trained on kinematic variables formed from reconstructed objects and global event observables. Seventeen input variables are used which describe angular distances and differences between the transverse momentum of reconstructed objects, the invariant mass and absolute rapidity of reconstructed objects and the sum of the transverse momenta of the reconstructed jets, charged lepton and neutrino. The modelling of the input variables was studied in Ref. [9] and agrees with the data within uncertainty. The simulated nominal signal samples and all MC simulated background processes are used for the training.

The NN assigns an output-score $D_{nn} \in [0, 1]$ to each event. Signal events are assigned a high D_{nn} score and background events are assigned low scores. The requirement of a high D_{nn} score reduces the contribution from background processes significantly, but it also reduces the signal acceptance. A very low contribution from background events is required to keep the associated rate uncertainties under control, but a high number of data events is needed to keep the statistical uncertainties low. The D_{nn} requirement is therefore optimised to balance these effects and the requirement $D_{nn} > 0.93$ is chosen. Introducing the D_{nn} requirement enhances the signal-to-background ratio in the ℓ^+ SR from 0.25 to 6.1 and in the ℓ^- SR from 0.17 to 3.8. The impact of the D_{nn} requirement on the systematic uncertainties related to the modelling of the signal process was found to be negligible.

5 Background estimation

The background contribution from processes with one prompt lepton is estimated from MC simulations and includes $t\bar{t}$ production, single-top production via the s -channel and the tW process, diboson production and the production of single W and Z bosons in association with jets. The production processes of a W boson in association with jets are referred to as $W + b\bar{b}$ and $W + c(\bar{c})$ in the following. While $W + c$ production gives a significant contribution, the $W + b$ process is heavily suppressed.

The multijet background is estimated by using a combination of simulated dijet events and data-driven techniques. Events with misidentified jets are modelled from simulated dijet events by classifying jets that deposit most of their energy in the EM calorimeter as electrons. Events with non-prompt muons are modelled from dedicated collision events which are enriched in non-prompt muons by applying the nominal selection with inverted or modified muon isolation requirements. Both of these methods are detailed in Ref. [79].

The normalisation of each background process is extracted from a dedicated simultaneous binned profile maximum-likelihood fit using the same methodology as Ref. [9]. The likelihood function is defined as the product of Poisson probability terms across all bins. The fitted event yields in each bin depend on nuisance parameters that account for systematic uncertainties. All nuisance parameters, except those representing MC statistical uncertainties, are constrained by Gaussian terms in the likelihood function. Control regions for the multijet background and the complete D_{nn} distributions excluding $D_{nn} > 0.93$, i.e. the signal region for the differential measurement, are used in the fit. No additional control regions are included for backgrounds with a prompt lepton. The complete set of experimental and background-related uncertainties are included via nuisance parameters. The event yields of the multijet backgrounds are left floating while

the yields of all other backgrounds are constrained to their predictions within the associated uncertainties. For the background processes involving top quarks, the relative uncertainties in the cross-sections of $\pm 4\%$ for $t\bar{t}$ and $\pm 3.7\%$ for $tW + \bar{t}W, t\bar{b}/\bar{t}b$ are assigned. An uncertainty of $\pm 40\%$ is assigned to the expected rate of $W + b\bar{b}$, covering differences seen in previous measurements [80] between the SHERPA prediction and ATLAS collision data. For the $W + c(\bar{c})$ and $Z, VV+\text{jets}$ backgrounds, an uncertainty of $\pm 20\%$ is assigned. Separate nuisance parameters are used for the cross-section uncertainties of $W + b\bar{b}$ production and $W + c(\bar{c})$ production in the regions with positive and negative lepton charge. The post-fit agreement of the expected and observed distributions is shown in Figure 2. The difference between prediction and observation in Figure 2(a) can be attributed to the signal modelling uncertainties being not included. No significant pulls of nuisance parameters are observed and a consistent inclusive tq or $\bar{t}q$ cross-section is obtained.

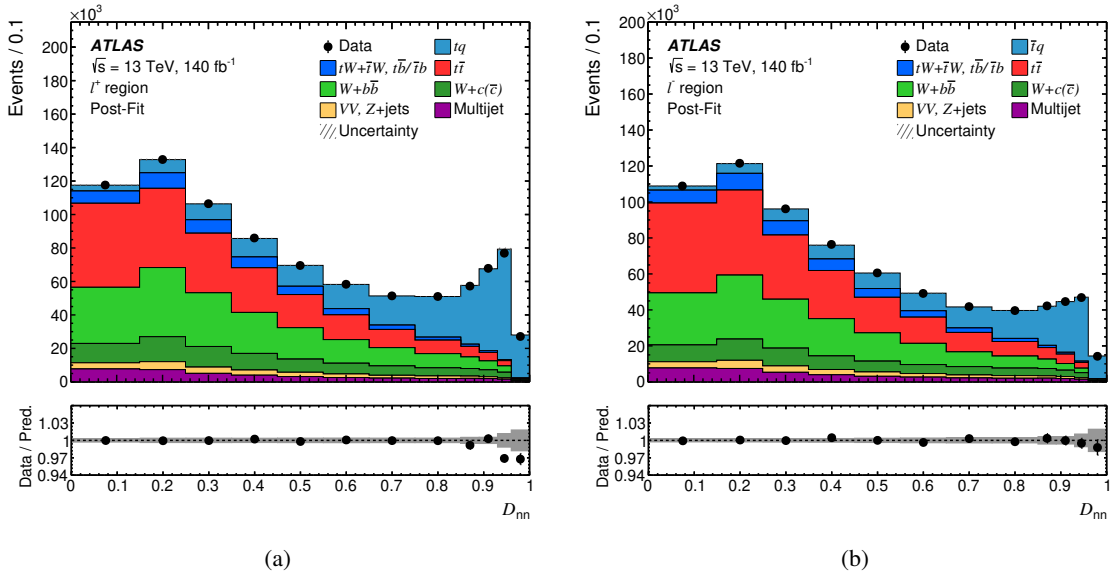


Figure 2: Post-fit agreement between data and the expected distributions in events containing (a) positively charged lepton and (b) negatively charged lepton. The experimental, background-related and MC statistical uncertainties are incorporated in the uncertainty bands. The region $D_{nn} > 0.93$ is excluded from the fit.

Per-process scale factors are obtained from the post-fit over pre-fit event yield ratio and the relative uncertainty in the post-fit yield is taken as the uncertainty in the expected rate of the respective process. The expected event yields in the SRs per process after the scale factors are applied to the background processes are presented in Table 3. Comparisons between the observed and expected distributions in both signal regions incorporating all uncertainties are shown in Figure 3. Here, $\ell^\pm \nu b$ is used to refer to the reconstructed top (anti)quark.

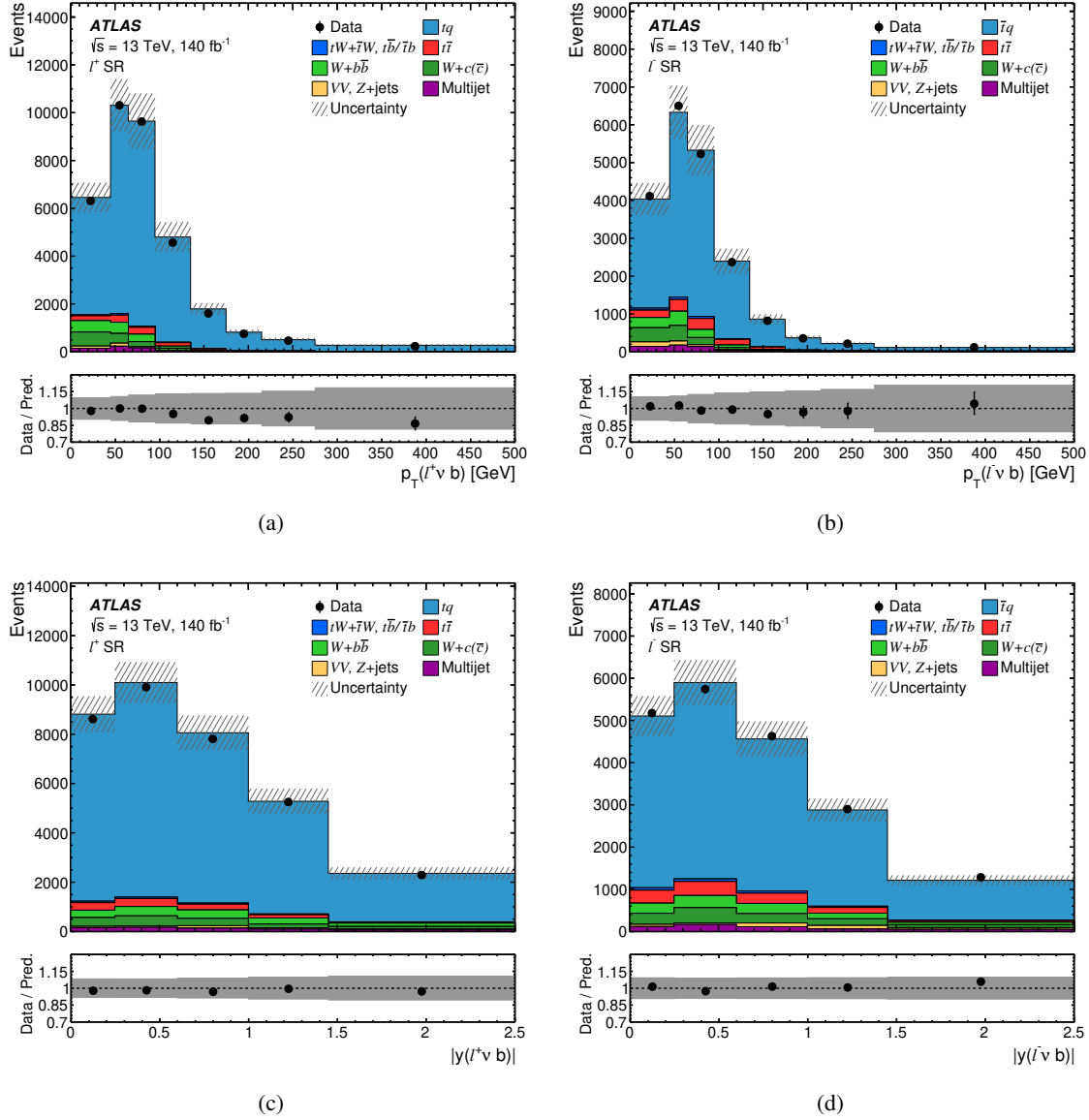


Figure 3: Comparison of the measured data to the expected distributions estimated from MC simulation in the (a),(c) ℓ^+ SR and (b),(d) ℓ^- SR (i.e. the requirement $D_{nn} > 0.93$ is imposed). The distributions are shown for variables (a) $p_T(\ell^+\nu b)$, (b) $p_T(\ell^-\nu b)$, (c) $|y(\ell^+\nu b)|$ and (d) $|y(\ell^-\nu b)|$, utilising the binning optimised for the unfolding as described in Section 7. The uncertainty bands incorporate the MC statistical uncertainty and all systematic uncertainties. The per-process scale factors are applied to the background processes.

Table 3: Expected event yields per process and observed event yields in the signal regions. The given uncertainties are the rate uncertainties defined as the relative uncertainty in the post-fit event yields.

Process	ℓ^+ SR		ℓ^- SR	
tq	29 740 \pm	590	15 \pm	15
$\bar{t}q$	7 \pm	7	15 550 \pm	300
$t\bar{t}$	1020 \pm	40	1050 \pm	40
$tW + \bar{t}W, t\bar{b}/\bar{t}b$	200 \pm	20	210 \pm	21
$Z, VV+\text{jets}$	290 \pm	60	300 \pm	60
$W + b\bar{b}$	1360 \pm	150	940 \pm	90
$W + c(\bar{c})$	1340 \pm	270	1080 \pm	170
Multijet	610 \pm	120	500 \pm	100
Total	34 580 \pm	680	19 630 \pm	380
Observed	33 883		19 730	

6 Unfolding technique

The unfolding aims to correct the measured distributions for resolution and efficiency effects caused by the detector. D’Agostini’s iterative approach [12], implemented in RooUnfold [81], is used to unfold the distributions. The distributions are unfolded to the parton level with stable top quarks, and extrapolated to the full kinematic phase space so that they can be easily compared with a variety of theory predictions.

The number of data events N_j^{data} measured in bin j of the distribution of the observable X after detector reconstruction can be parameterised in the following way

$$N_j^{\text{data}} = \sum_k M_{jk} \epsilon_k \mathcal{L}_{\text{int}} \Delta X_k \frac{d\hat{\sigma}_k}{dX_k} + \hat{B}_j.$$

Here \mathcal{L}_{int} denotes the integrated luminosity and ΔX_k is the width of bin k of the parton-level distribution of the observable X . The migration matrix element M_{jk} denotes the probability for a reconstructed event produced in bin k to be reconstructed in bin j . A strength of D’Agostini’s approach is that the migration matrix is not inverted. The nominal background \hat{B}_j is the expected sum of background events in bin j . The selection efficiency ϵ_k is defined as

$$\epsilon_k = \frac{N_k^{\text{sel}}}{N_k^{\text{prod}}},$$

where N_k^{prod} denotes the number of MC events produced in bin k and N_k^{sel} the number of events selected in bin k . Since no fiducial region is defined on the final-state, N_k^{sel} equals the number of events produced in bin k that satisfy the event selection at reconstruction level (cf. Section 4) in an arbitrary bin j .

7 Binning and convergence of unfolding

The migration matrices and efficiencies used for the unfolding are determined with the nominal signal samples. The binning of the distributions is optimised according to several criteria. The statistical uncertainty in the data yields is kept at a moderate level, i.e. below 10%, and the bin width is kept above the detector resolution. The migration of events to off-diagonal bins is kept sufficiently low, i.e. below 50%, to ensure the stability of the unfolding procedure. The bin edges are synchronised between both signal regions to allow for the measurement of the cross-section ratio.

The obtained migration matrices are shown in the Appendix in Figure 16. In both of the signal regions, a few data events are measured with $p_T(\ell^\pm \nu b) > 500$ GeV. The upper edge of the $p_T(\ell^\pm \nu b)$ distributions is not raised to incorporate all measured events because the differential cross-sections are normalised to the bin width. Instead, a shadow bin with an upper edge of 2000 GeV is added to account for migration effects. The cross-section is not measured in the shadow bin and it is therefore not shown in the following.

The unfolding procedure is regularised through the number of iterations. The parton-level prediction for a given distribution is used as a biased prior and in each iteration replaced by the result of the previous iteration. This procedure reduces the bias, i.e. the difference between the prediction and the true distribution, but leads to statistical fluctuations if too many iterations are performed. The number of iterations used for unfolding is optimised by minimising the statistical correlation between the bins of the unfolded distributions. For all distributions in all SRs, four iterations are chosen.

The unfolding procedure is validated to be robust against statistical fluctuations of the detector level distributions and changes in the shape of the signal process distributions. The latter is tested by altering the shape of the signal process at both the parton and detector levels according to the difference between the expected and the observed distributions. The altered detector level distributions are unfolded using the nominal migration matrix and efficiency and compared with the altered parton level distributions. The difference between the unfolded results and the parton level, i.e. the non-closure, is found to be below 2% for all distributions.

8 Systematic and statistical uncertainties

Several sources of systematic uncertainties affect the expected event yield from signal and background processes, as well as the distribution's shapes. The systematic uncertainties are divided into two major categories. Experimental uncertainties are associated with the reconstruction of the four-momenta of final-state objects: electrons, muons, untagged jets, b -tagged jets, and E_T^{miss} . The second category of uncertainties is related to the modelling of simulated processes.

8.1 Sources of uncertainties

The uncertainty in the integrated luminosity of the combined 2015–2018 data sample is 0.83% [23]. Scale factors are applied to simulated events to correct for reconstruction, identification, isolation and trigger performance differences between data and detector simulation for electrons and muons [65, 66, 82, 83]. The net effect of the probability of charge misidentification of reconstructed electrons is a migration of events at the level of 6×10^{-4} from the ℓ^+ SR to the ℓ^- SR (cf. [9]). The uncertainty in the jet energy scale (JES) [70] is decomposed into a set of 30 uncorrelated components. Sources of uncertainty contributing to

the JES uncertainty sources include the η intercalibration of forward jets within $0.8 < |\eta| < 4.5$ with those in the central barrel region ($|\eta| < 0.8$), pile-up modelling, jet flavour composition and response, differences between jets induced by b -quarks and those from gluons or light-quarks, single-particle response, detector modelling, non-closure, and effects of jets not fully contained within the calorimeter. The uncertainty of the jet energy resolution (JER) [70] comprises thirteen orthogonal components which account for jet p_T - and η -dependent differences between simulation and data. The uncertainty in the efficiency to satisfy the JVT requirement for pile-up suppression is also considered [71]. An uncertainty for E_T^{miss} is applied to account for a possible miscalibration of its soft-track component [74]. The b -tagging requirement made in the measurement requires consideration of uncertainties in the b -tagging efficiency of true b -jets and in the mistagging rates of light-quark jets and c -jets. The uncertainty in the b -tagging efficiency is decomposed into 45 orthogonal components [84]. The uncertainty in the rate of mistagging c -jets as b -jets is decomposed into 20 orthogonal components [85]. The uncertainty in the misidentification rate of light-quark jets is decomposed into 20 independent eigenvectors [86]. To account for differences in the pile-up distribution between simulation and data, the pile-up profile in the simulation is corrected to match the one in data. The uncertainty associated with the correction factor is applied in the measurement as a variation of the event weight. In the following, these uncertainties are summarised as *Experimental uncertainty*.

The rate uncertainties of the background processes are defined as described in Section 5 and summarised as *Background rate uncertainty*. Uncertainties in modelling parton showers and hadronisation are assigned to all top-quark production processes by comparing the nominal samples with alternative samples for which POWHEG BOX v2 was interfaced to HERWIG 7.2.1 [54, 55] (for $t\bar{t}$ production), HERWIG 7.1.6 (for $tW + \bar{t}W$ and $t\bar{b}$ production) or HERWIG 7.3.1 (for tq and $\bar{t}q$ production) instead of PYTHIA 8.230. Uncertainties related to the choice of the renormalisation scale μ_r and the factorisation scale μ_f for the matrix-element calculations are evaluated by varying the scales independently by factors of 2 and 0.5, separately for each of the top-quark production processes and for W +jets production. The uncertainty in matching the NLO matrix elements to the parton shower when generating $t\bar{t}$, $tW + \bar{t}W$ and tq and $\bar{t}q$ events is evaluated according to the prescription in Ref. [87]. The uncertainty in the choice of the h_{damp} parameter for the $t\bar{t}$ and $tW + \bar{t}W$ event generation is estimated by using additional samples produced with the h_{damp} parameter set to $3 \times m_t$. Uncertainties in the amount of initial-state and final-state radiation are assessed for the top-quark production processes by varying the parameter Var3c of the A14 parton-shower tune within the uncertainties of the tune and, for final-state radiation, by varying μ_r by factors of 0.5 and 2.0. The two variations are handled independently. The uncertainty due to the scheme for removing the interference of the $tW + \bar{t}W$ process with $t\bar{t}$ production is evaluated by comparing the nominal sample, using the diagram-removal scheme, with a sample produced with an alternative scheme (diagram subtraction) [41]. Uncertainties in the PDFs are evaluated for the top-quark production processes using the PDF4LHC15 prescription with 30 eigenvectors [88]. The uncertainty in the shape of the multijet background is evaluated by modifying the selection criteria for jet-electron and non-prompt-muon candidates, thereby generating templates for the systematically varied distributions. In the following plots, these uncertainties are summarised as *Signal modelling* and *Background modelling*.

8.2 Evaluation of uncertainties

To evaluate the impact of the experimental uncertainties, the rate uncertainties of the background processes and uncertainties related to the modelling of background processes, the expected event yield is estimated from the systematically varied distributions at reconstruction level. If an uncertainty is not defined for

a process, the nominal prediction is used for the estimate. The nominal background estimate is then subtracted and the resulting distributions are unfolded with the nominal migration matrix and efficiency. The difference between the unfolded result and the unfolded nominal signal distribution per bin is taken as the uncertainty. For uncertainties related to the modelling of the signal process, the systematically varied signal distribution is unfolded with the nominal migration matrix and efficiency and any difference with the systematically varied prediction at parton level is taken as the uncertainty.

The statistical uncertainty of the unfolded data is determined via pseudo-experiments. Each bin of the data distribution is fluctuated according to the expected statistical uncertainty to construct a pseudo-experiment. The pseudo-experiment is then unfolded with the nominal migration matrix and efficiency and the standard deviation of all unfolded pseudo-experiments is taken as the data's statistical uncertainty per bin.

To evaluate the statistical uncertainty due to the limited size of the MC signal sample, each bin of the migration matrix and efficiency is fluctuated according to a Gaussian distribution whose spread corresponds to the expected uncertainty due to the number of MC events in that bin. The nominal signal is unfolded with the fluctuated corrections and the standard deviation of all unfolded pseudo-experiments is taken as the MC statistical uncertainty.

One-sided uncertainties, such as the evaluation of the parton shower, are symmetrised by taking the full uncertainty with opposite sign as down variation. The total uncertainty in the unfolded cross-section is calculated per bin by adding the individual uncertainties in quadrature. The contributions from the individual uncertainties with positive signs are added to the total up variation and the contributions with negative signs are added to the total down variation. If both the up and the down variation of an uncertainty have a positive (negative) sign, the larger contribution is added to the total up (down) variation and the contribution to the total down (up) variation is set to zero.

The uncertainties in the ratio of the differential cross-sections are evaluated after the unfolding, taking correlations between the effect of the uncertainties in the measurements into account. The statistical uncertainties and the rate uncertainties in the $W + b\bar{b}$ and $W + c(\bar{c})$ background processes are decorrelated for tq and $\bar{t}q$ production and therefore added in quadrature.

The statistical uncertainty in the single components of the JES, JER and modelling related uncertainties are evaluated with the bootstrap method [89] as these uncertainties show fluctuations in all measured distributions. It was found that the fluctuations can be attributed to the statistical uncertainty of the systematic uncertainties, but the quoted uncertainties are consistent with the central values obtained with the bootstrap method. The statistical uncertainties of the JES and JER uncertainties are larger than those of the modelling related uncertainties and, expressed in terms of the fractional uncertainty in the measured cross-sections, reach magnitudes of about $\pm 0.5\%$ for the $|y(t)|$ or $|y(\bar{t})|$ distributions and about $\pm 1.0\%$ for the $p_T(t)$ or $p_T(\bar{t})$ distributions. The statistical uncertainties may be of interest for future combinations and are published in the HEPData entry for this analysis.

Summaries of the statistical and systematic uncertainties in all measured differential cross-sections are presented in Figures 4 and 5. The contributions of the different categories of uncertainties with a further breakdown of the experimental uncertainties are provided in the Appendix in Tables 6–15. The uncertainties in the absolute and normalised differential cross-sections are dominated by the signal-modelling-related and experimental uncertainties. The statistical uncertainties become significant in the high- p_T region of the absolute differential cross-section distributions, in the normalised differential cross-sections and in the cross-section ratios. For the latter, this can be attributed to the cancellation of systematic uncertainties. The uncertainties related to the rate and modelling of background processes are minor uncertainties for all

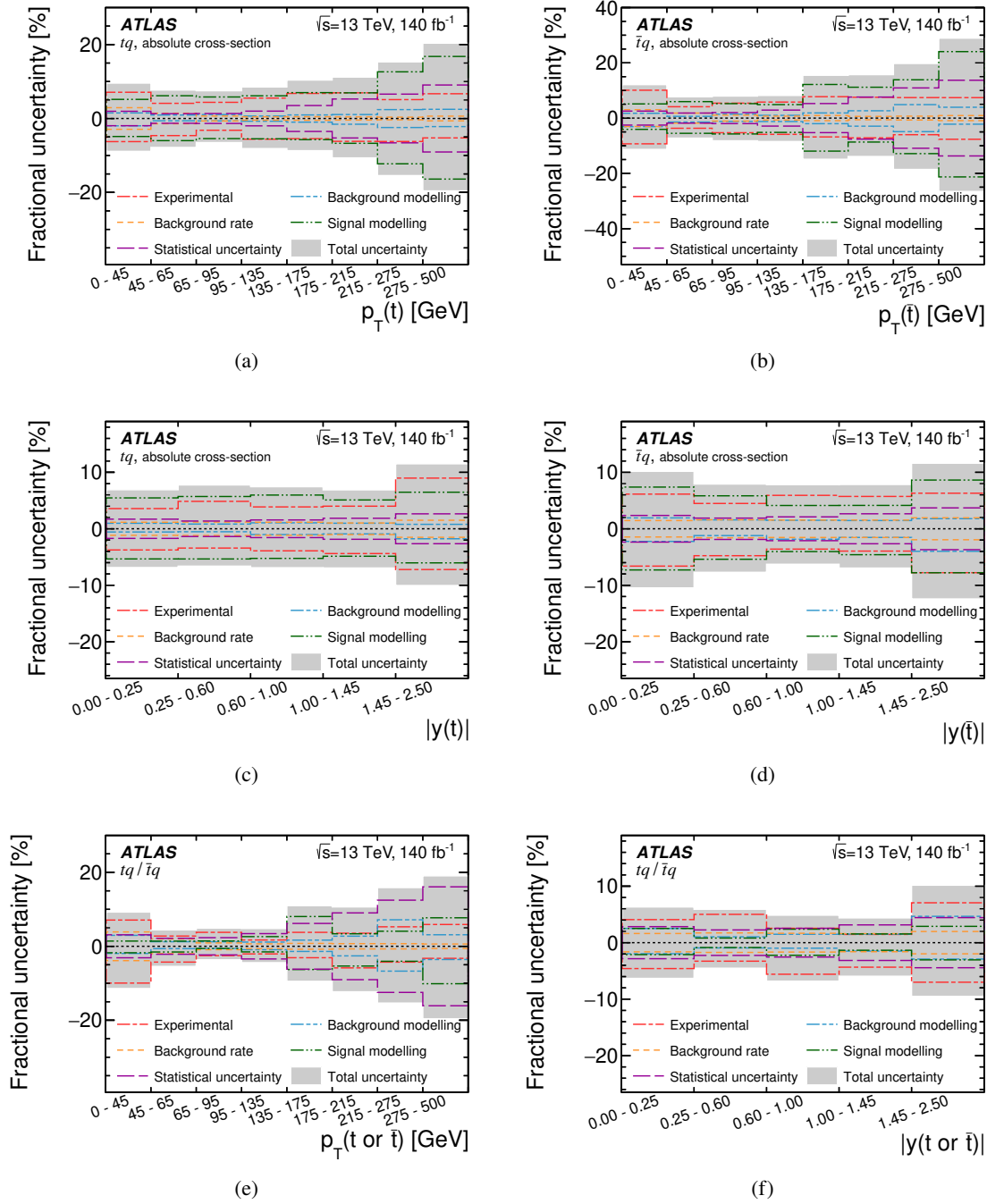


Figure 4: Summary of the uncertainties in the absolute differential tq or $\bar{t}q$ production cross-sections measured as a function of (a) $p_T(t)$, (b) $p_T(\bar{t})$, (c) $|y(t)|$ and (d) $|y(\bar{t})|$ and on the ratio of the differential tq and $\bar{t}q$ production cross-sections measured as a function of (e) $p_T(t \text{ or } \bar{t})$ and (f) $|y(t \text{ or } \bar{t})|$. Similar sources of uncertainties are grouped using their quadratic sum. The shaded band indicates the total uncertainty, defined as the quadratic sum of all sources of uncertainties.

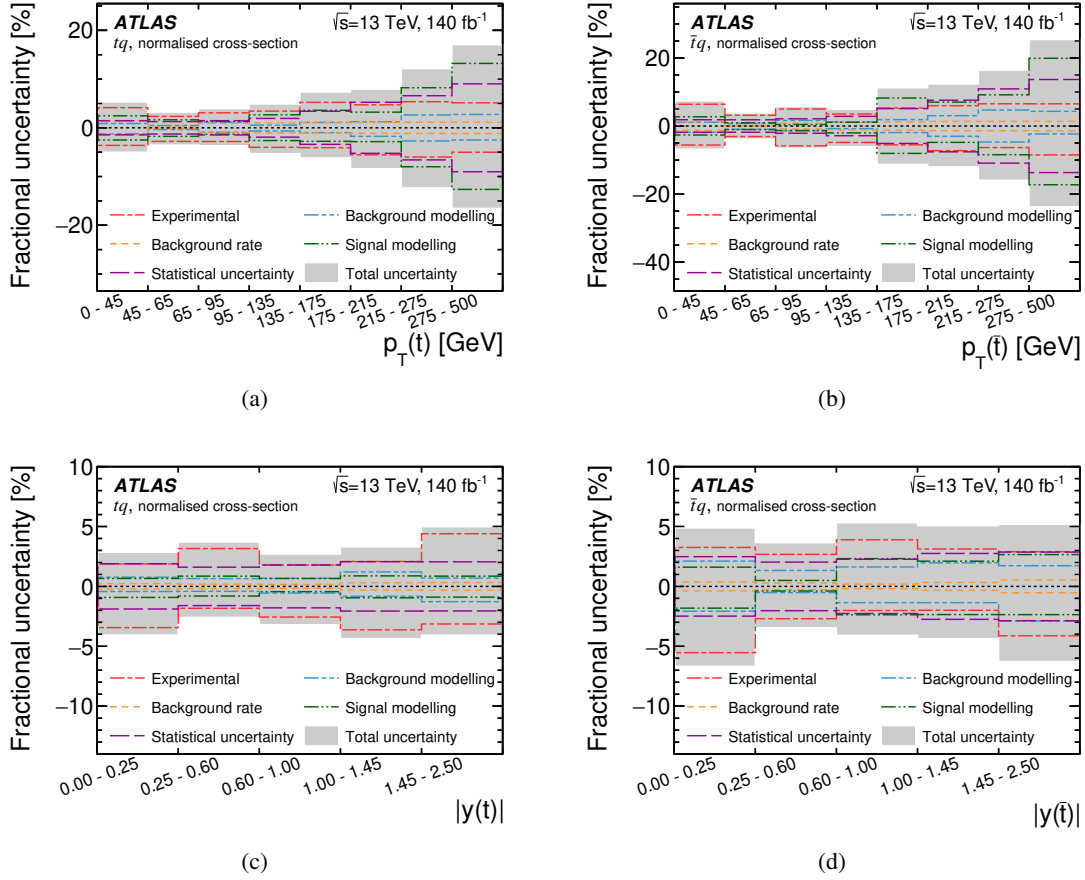


Figure 5: Summary of the uncertainties in the normalised differential tq or $\bar{t}q$ production cross-sections measured as a function of (a) $p_T(t)$, (b) $p_T(\bar{t})$, (c) $|y(t)|$ and (d) $|y(\bar{t})|$. Similar sources of uncertainties are grouped using their quadratic sum. The shaded band indicates the total uncertainty, defined as the quadratic sum of all sources of uncertainties.

measured cross-sections. Their contributions differ between the tq and $\bar{t}q$ production cross-sections as the fraction of background events differ between the signal regions.

9 Results

Differential tq and $\bar{t}q$ production cross-sections are measured as a function of $p_T(t)$ or $p_T(\bar{t})$ and $|y(t)|$ or $|y(\bar{t})|$. The absolute differential cross-sections are presented in Figures 6–8, the normalised differential cross-sections are shown in Figures 9–11 and the ratios of the cross-sections are shown in Figure 12. All measurement results are presented together with the theoretical predictions. The numerical values of the measured cross-sections are given in the Appendix in Tables 16–21 and the χ^2 probabilities for all theory predictions are listed in Tables 4 and 5. The χ^2 value of a given theory prediction is calculated as

$$\chi^2 = V_{N_b}^T \cdot \text{Cov}_{N_b}^{-1} \cdot V_{N_b},$$

where N_b denotes the number of bins, V_{N_b} denotes the vector of differences between the unfolded data and the prediction and Cov_{N_b} denotes the covariance matrix which incorporates all uncertainties in the measurement result described in Section 8.

The covariance matrix is obtained by performing pseudo-experiments. Each bin of the measured distribution at detector level is varied according to a Poisson distribution with the number of observed events in this bin as the mean value. Gaussian-distributed shifts are coherently added for the MC statistical uncertainty, each experimental uncertainty and each background related uncertainty by scaling each Poisson-fluctuated bin with the expected relative variation from the associated uncertainty effect. The resulting distribution is unfolded with the nominal migration matrix and efficiency. Signal modelling uncertainties are then coherently added with additional Gaussian-distributed shifts. For the normalised cross-sections, V_{N_b} and Cov_{N_b} are replaced by V_{N_b-1} and Cov_{N_b-1} by discarding the last element of V_{N_b} and the corresponding row and column of Cov_{N_b} .

The uncertainties in the theoretical predictions are added in quadrature on the diagonal elements of Cov_{N_b} . For the predictions obtained with different PDF sets, the MC statistical uncertainty and the PDF uncertainty are considered and the uncertainty in the predictions from different event generators additionally contains the uncertainty in the renormalisation and factorisation scale choice. The uncertainty in the FO calculations comprises the uncertainty in the renormalisation and factorisation scale choice and the uncertainty in the value of α_s .

Overall, a good agreement between the measured cross-sections and the theoretical predictions is observed. The FO calculations with MCFM at LO do not agree with the measured $p_T(t)$ and $p_T(\bar{t})$ spectra as expected for a 5FS calculation missing important diagrams. The predictions at NLO and NNLO show very good agreement with the unfolded data, with the NNLO predictions being generally closer to the data and showing a better compatibility. For the predictions obtained from different MC event generators, larger deviations between the predictions are only present in the high- p_T region of the absolute and differential cross-sections measured as a function of $p_T(t)$ or $p_T(\bar{t})$, but the deviations are mostly covered by the measurement uncertainties.

The predictions obtained with different PDF sets for the absolute differential cross-sections as a function of $|y(t)|$ or $|y(\bar{t})|$ differ from each other by up to 10%, but all agree with the measured result within the measurement uncertainties. The measured normalised differential production cross-sections as a function of $|y(t)|$ or $|y(\bar{t})|$ agree very well with the different predictions, although some deviations are visible for the differential $\bar{t}q$ cross-section. The χ^2 probabilities of the different predictions for both the normalised and absolute cross-sections are very similar to each other for a given distribution, except ABMP16, which has a noticeably lower probability than the other predictions for the $\bar{t}q$ production cross-sections binned in $|y(\bar{t})|$.

The predictions obtained with the ABMP16 PDF set overestimates the ratio of the differential cross-sections over the full measured $|y(t)|$ and $|y(\bar{t})|$ ranges. The other predictions are in excellent agreement with the measurement results.

At $\sqrt{s} = 8$ TeV [7], differential tq and $\bar{t}q$ production cross-sections were already measured separately as a function of $p_T(t)$ or $p_T(\bar{t})$ and $|y(t)|$ or $|y(\bar{t})|$. In contrast, the present measurement is performed at a different centre-of-mass energy and, in addition, achieves substantially higher precision for both the absolute and normalised differential cross-sections. Important factors for the improvement are the larger number of data events and a reduction of the contribution from background processes and their associated uncertainties. The greatest improvement is achieved for the normalised differential cross-sections as a function of $|y(t)|$ or $|y(\bar{t})|$, where this measurement reaches a precision of 3% to 6% compared with 7% to 15%. A previous analysis by CMS using a partial Run 2 data sample [11] measured combined tq and $\bar{t}q$ production cross-sections. This analysis provides the first separate measurement of differential tq and $\bar{t}q$ production at $\sqrt{s} = 13$ TeV and reaches a higher precision, as it utilises the full Run 2 data sample.

In both measurements discussed above, the differential cross-sections as a function of $p_T(t)$ or $p_T(\bar{t})$ were measured in a range of up to 300 GeV. This analysis measures the differential cross-sections up to 500 GeV, providing a significant extension of the probed $p_T(t$ or $\bar{t})$ region.

Table 4: χ^2 probabilities of the predictions for the absolute and normalised differential tq or $\bar{t}q$ production cross-sections and the ratio of the cross-sections as a function of $p_T(t)$, $p_T(\bar{t})$ and $p_T(t$ or $\bar{t})$ respectively. The uncertainties in the measured cross-sections and in the predictions are considered. The number of degrees of freedom (NDF) is listed for each distribution.

Prediction	$\frac{d\sigma(tq)}{dp_T(t)}$	$\frac{1}{\sigma(tq)} \frac{d\sigma(tq)}{dp_T(t)}$	$\frac{d\sigma(\bar{t}q)}{dp_T(\bar{t})}$	$\frac{1}{\sigma(\bar{t}q)} \frac{d\sigma(\bar{t}q)}{dp_T(\bar{t})}$	$\left(\frac{d\sigma(tq)}{dp_T(t)}\right) / \left(\frac{d\sigma(\bar{t}q)}{dp_T(\bar{t})}\right)$
	NDF=8	NDF=7	NDF=8	NDF=7	NDF=8
MCFM, with PDF4LHC21					
LO	0.03	0.0	0.02	0.0	0.99
NLO	0.55	0.50	0.83	0.69	1.0
NNLO	0.70	0.65	0.97	0.89	1.0
Generators, with NNPDF3.0					
POWHEG PYTHIA 8 (4FS)	0.78	0.59	0.98	0.91	1.0
MG_AMC@NLO (4FS)	0.60	0.19	0.96	0.86	1.0
MG_AMC@NLO (5FS)	0.60	0.60	0.96	0.93	1.0
MG_AMC@NLO dyn. scale (5FS)	0.68	0.65	0.90	0.84	1.0
POWHEG +HERWIG 7 (4FS)	0.85	0.66	0.99	0.93	1.0
PDFs, with POWHEG PYTHIA 8 (4FS)					
CT18	0.58	0.57	0.97	0.93	1.0
MSHT20	0.62	0.60	0.97	0.93	1.0
PDF4LHC21	0.63	0.63	0.96	0.92	1.0
ABMP16	0.64	0.70	0.96	0.90	0.34
NNPDF4.0	0.59	0.59	0.99	0.96	1.0
ATLASpdf21	0.55	0.62	0.91	0.92	1.0

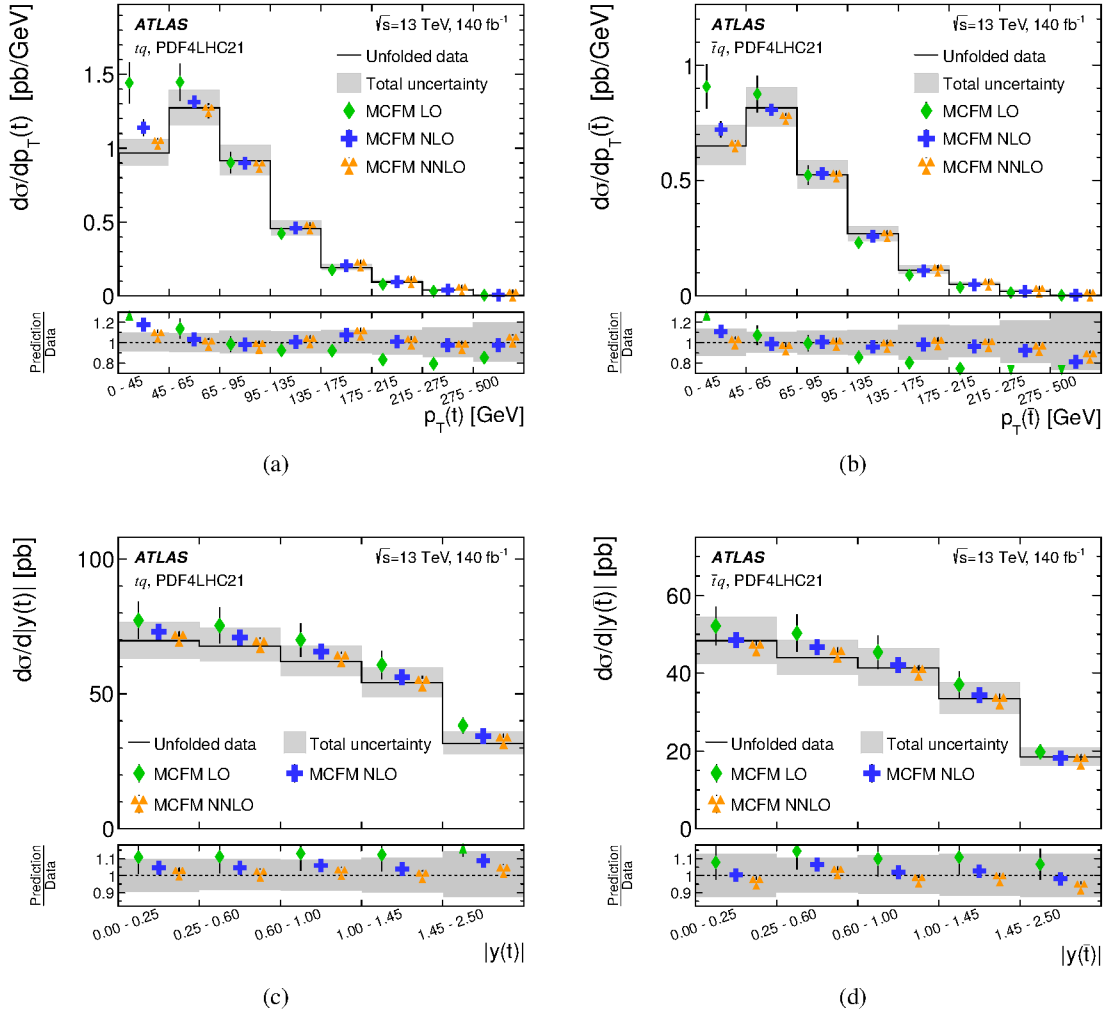


Figure 6: Absolute unfolded differential (a) (c) tq cross-sections and (b) (d) $\bar{t}q$ cross-sections as a function of (a) (b) $p_T(t)$ or $p_T(\bar{t})$ and (c) (d) $|y(t)|$ or $|y(\bar{t})|$. The shaded band indicates the total measurement uncertainty. The cross-sections are compared with the theoretical predictions from FO calculations done with MCFM at LO, NLO and NNLO. The uncertainty in the theoretical predictions comprises the uncertainty in the renormalisation and factorisation scale choice and the uncertainty in the value of α_s .

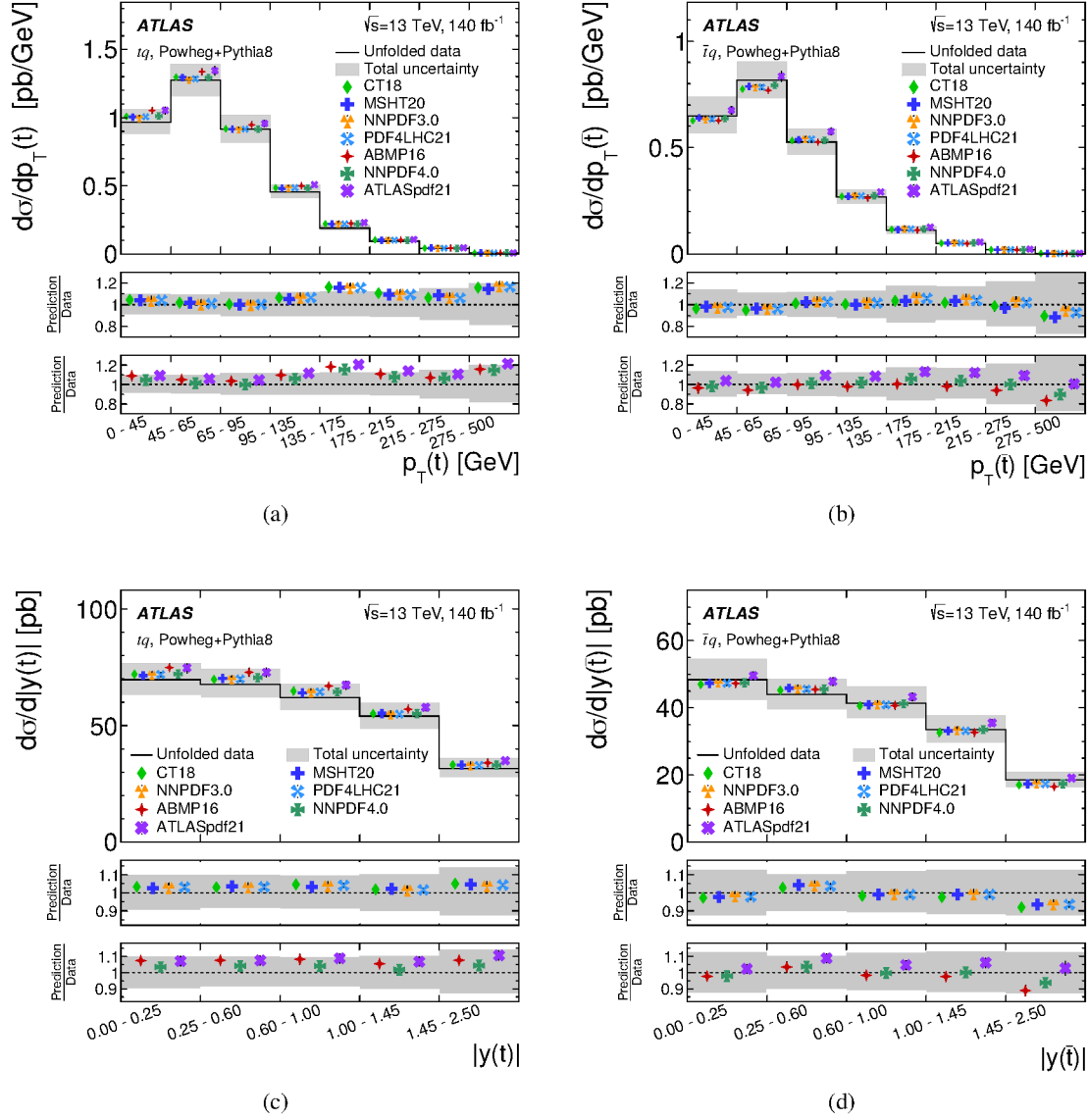


Figure 7: Absolute unfolded differential (a) (c) tq cross-sections and (b) (d) $\bar{t}q$ cross-sections as a function of (a) (b) $p_T(t)$ or $p_T(\bar{t})$ and (c) (d) $|y(t)|$ or $|y(\bar{t})|$. The shaded band indicates the total measurement uncertainty. The cross-sections are compared with the predictions from POWHEG + PYTHIA 8 with different PDF sets. The uncertainty in the theoretical predictions comprises the MC statistical uncertainty and the PDF uncertainty.

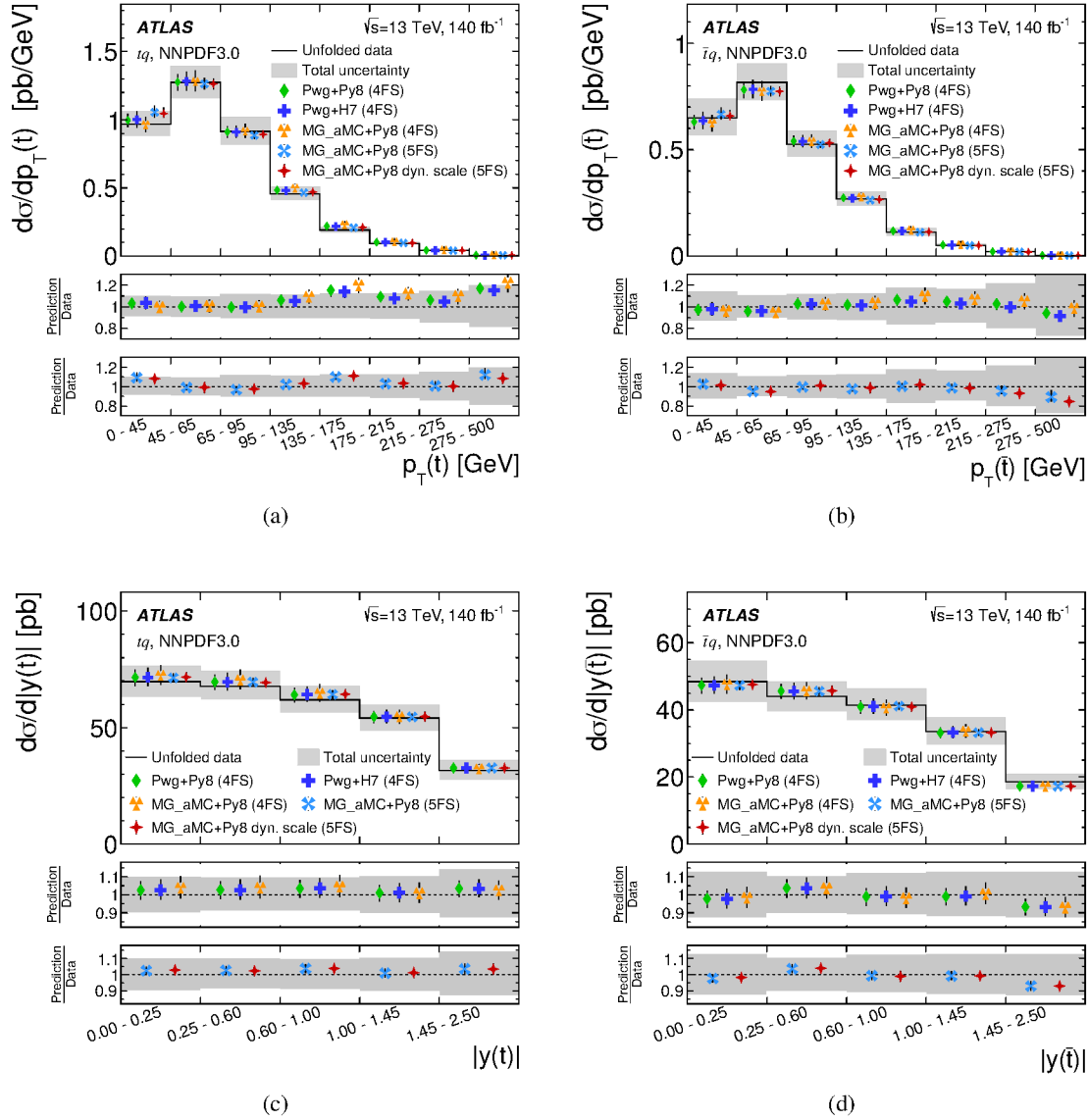


Figure 8: Absolute unfolded differential (a) (c) tq cross-sections and (b) (d) $t\bar{q}$ cross-sections as a function of (a) (b) $p_T(t)$ or $p_T(\bar{t})$ and (c) (d) $|y(t)|$ or $|y(\bar{t})|$. The shaded band indicates the total measurement uncertainty. The cross-sections are compared with the predictions from different MC event generators and parton shower programs. All predictions are generated with the NNPDF3.0 PDF set. The uncertainty in the theoretical predictions comprises the MC statistical uncertainty, the uncertainty in the renormalisation and factorisation scale choice and the PDF uncertainty.

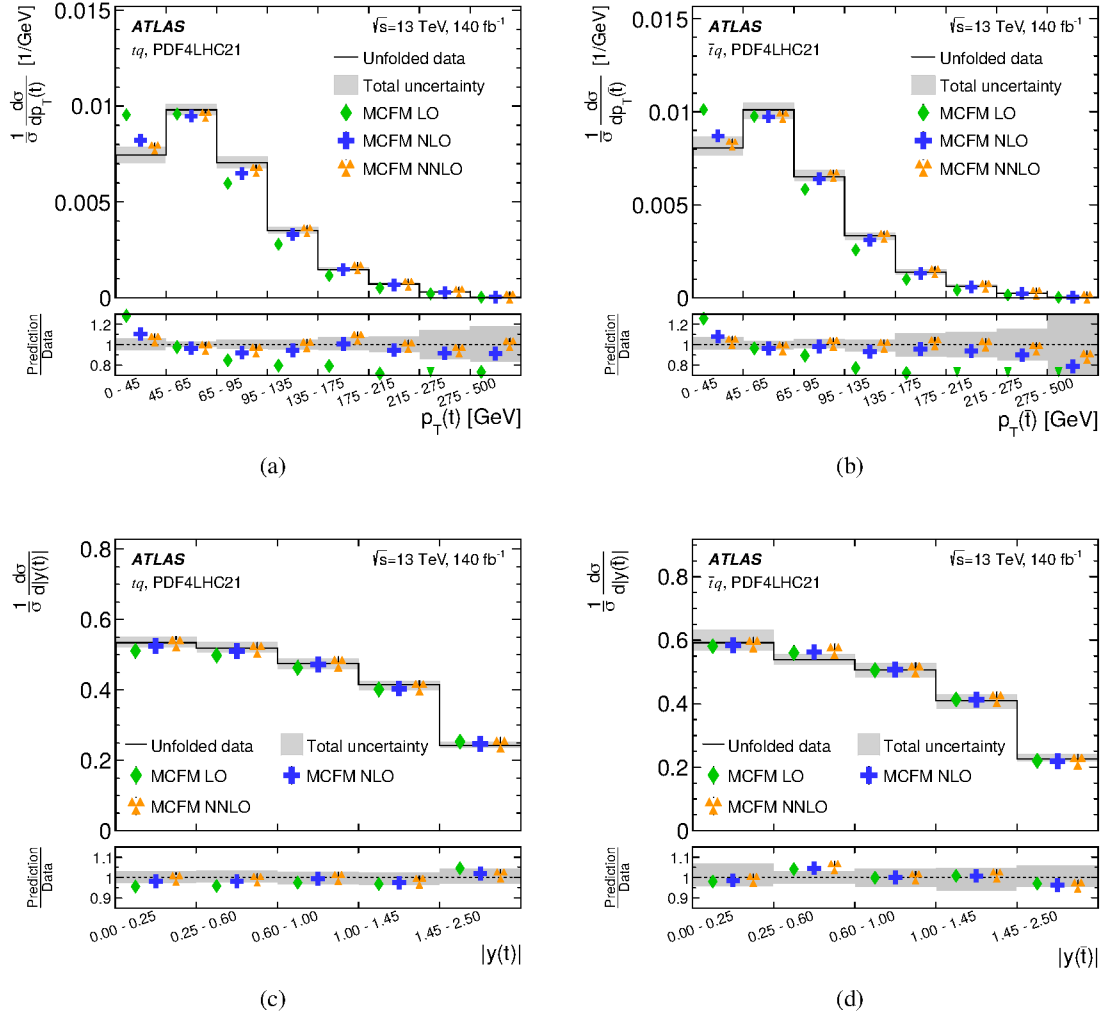


Figure 9: Normalised unfolded differential (a) (c) $t\bar{q}$ cross-sections and (b) (d) $\bar{t}q$ cross-sections as a function of (a) (b) $p_T(t)$ or $p_T(\bar{t})$ and (c) (d) $|y(t)|$ or $|y(\bar{t})|$. The shaded band indicates the total measurement uncertainty. The cross-sections are compared with the theoretical predictions from FO calculations done with MCFM at LO, NLO and NNLO. The uncertainty in the theoretical predictions from FO calculations comprises the uncertainty in the renormalisation and factorisation scale choice and the uncertainty in the value of α_s .

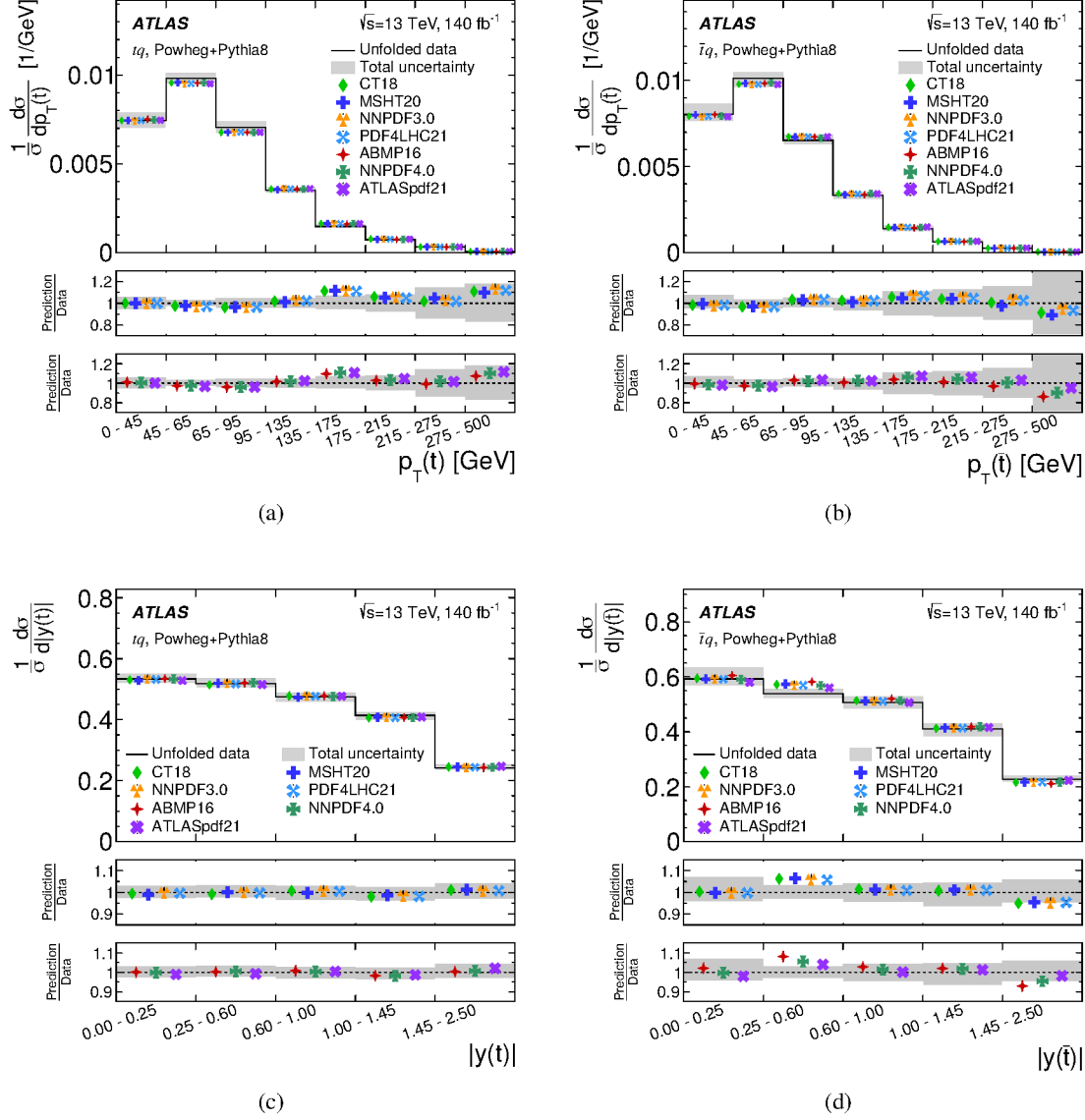


Figure 10: Normalised unfolded differential (a) (c) tq cross-sections and (b) (d) $\bar{t}q$ cross-sections as a function of (a) (b) $p_T(t)$ or $p_T(\bar{t})$ and (c) (d) $|y(t)|$ or $|y(\bar{t})|$. The shaded band indicates the total measurement uncertainty. The cross-sections are compared with the predictions from POWHEG + PYTHIA 8 with different PDF sets. The uncertainty in the theoretical predictions comprises the MC statistical uncertainty and the PDF uncertainty.

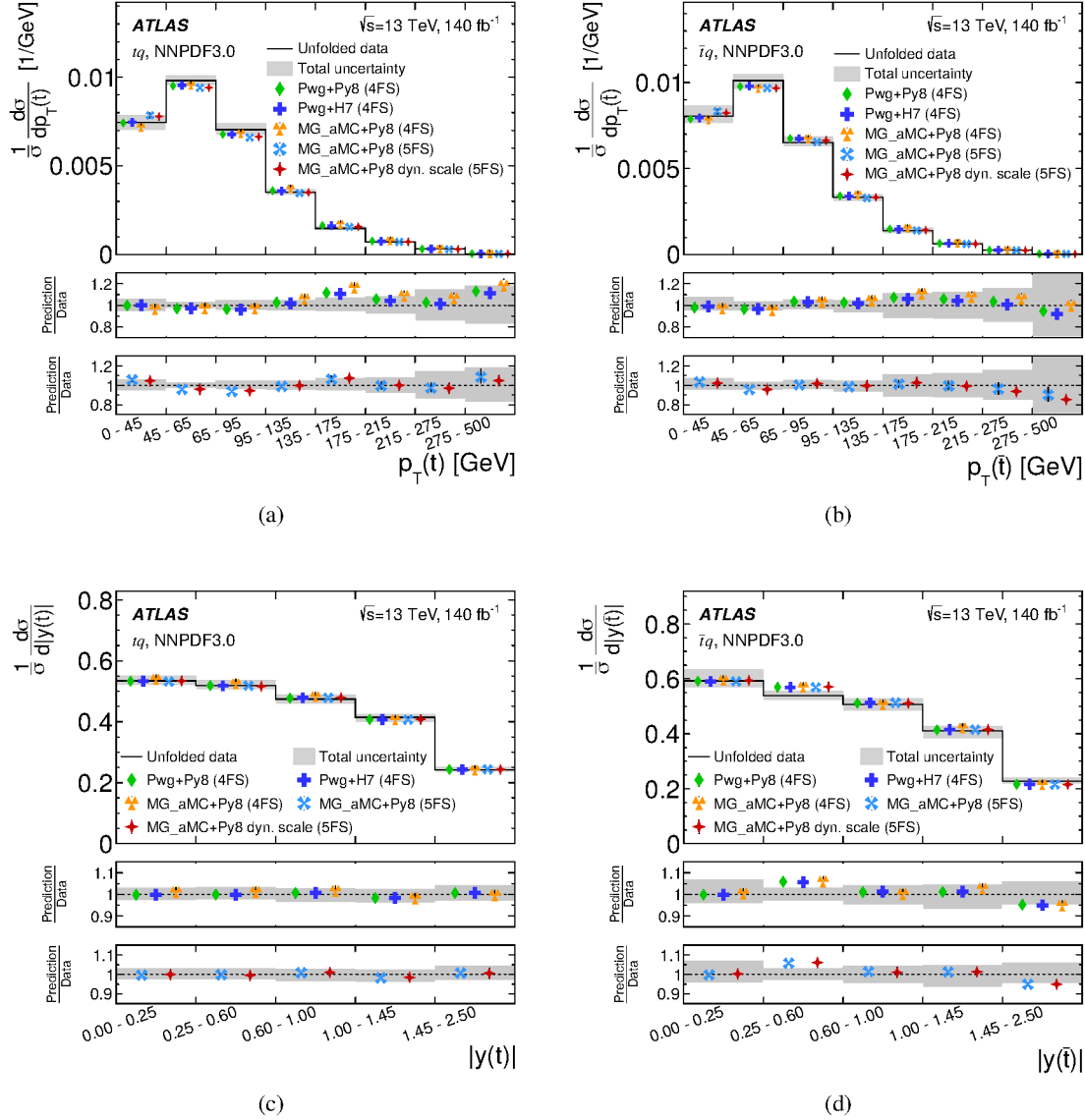


Figure 11: Normalised unfolded differential (a) (c) tq cross-sections and (b) (d) $\bar{t}q$ cross-sections as a function of (a) (b) $p_T(t)$ or $p_T(\bar{t})$ and (c) (d) $|y(t)|$ or $|y(\bar{t})|$. The shaded band indicates the total measurement uncertainty. The cross-sections are compared with the predictions from different MC event generators and parton shower programs. All predictions are generated with the NNPDF3.0 PDF set. The uncertainty in the theoretical predictions comprises the MC statistical uncertainty, the uncertainty in the renormalisation and factorisation scale choice and the PDF uncertainty.

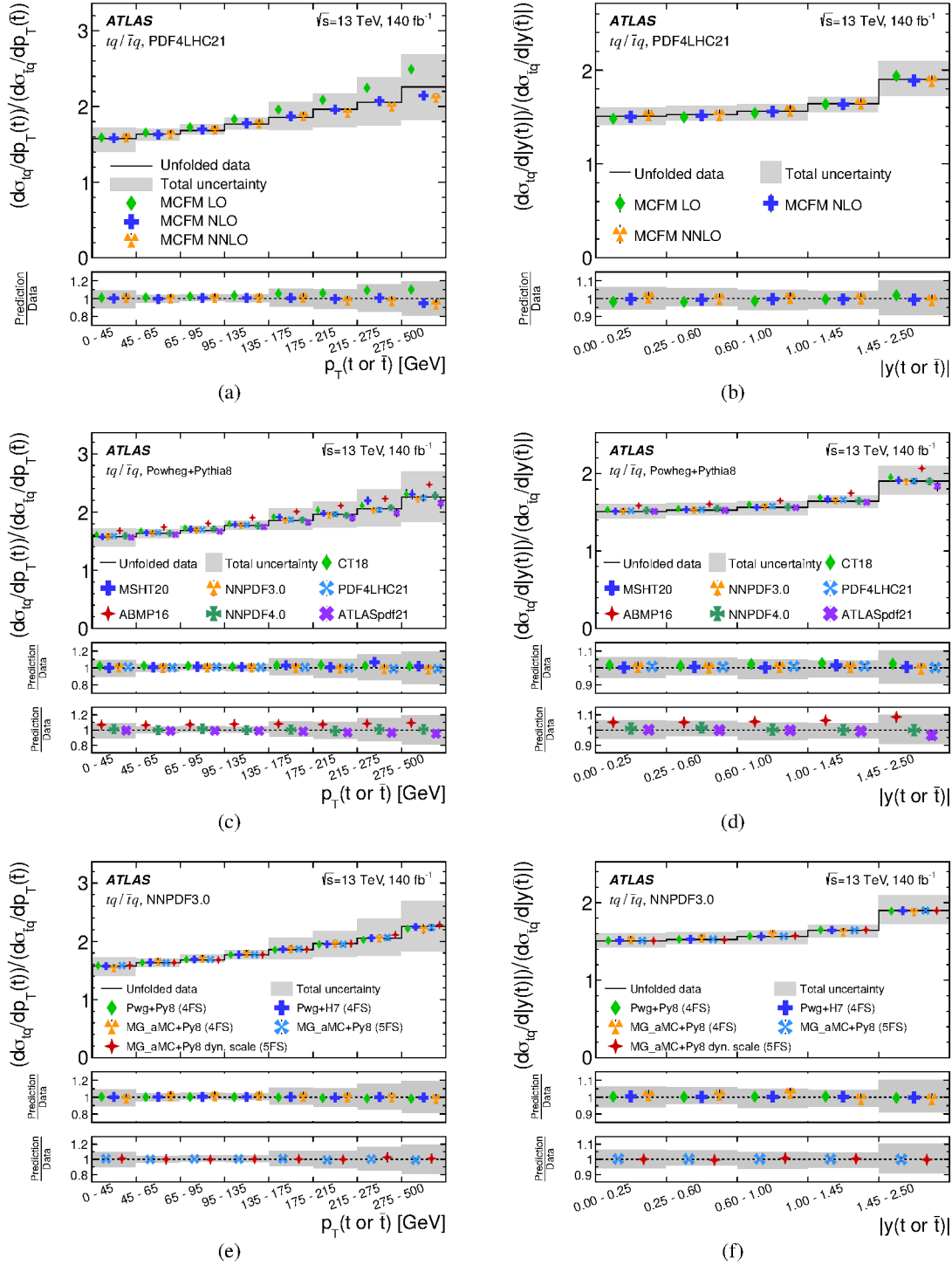


Figure 12: Ratio of the unfolded differential cross-sections as a function of (a) (c) (e) $p_T(t \text{ or } \bar{t})$ and (b) (d) (f) $|y(t \text{ or } \bar{t})|$. The shaded band indicates the total measurement uncertainty. The cross-sections are compared with theoretical predictions obtained from (a) (b) FO calculations done with MCFM at LO, NLO and NNLO, (c) (d) POWHEG +PYTHIA 8 with different PDF sets and (e) (f) different MC event generators and parton shower programs with the NNPDF3.0 PDF set. The uncertainty in the FO calculations comprises the uncertainty in the renormalisation and factorisation scale choice and the uncertainty in the value of α_s . The uncertainty in the predictions obtained with different PDF sets comprises the MC statistical uncertainty and the PDF uncertainty. The uncertainty in the predictions from different event generators comprises the MC statistical uncertainty, the uncertainty in the renormalisation and factorisation scale choice and the PDF uncertainty.

Table 5: χ^2 probabilities of the predictions for the absolute and normalised differential tq or $\bar{t}q$ production cross-sections and the ratio of the cross-sections as a function of $|y(t)|$, $|y(\bar{t})|$ and $|y(t \text{ or } \bar{t})|$ respectively. The uncertainties in the measured cross-sections and in the predictions are considered. The number of degrees of freedom (NDF) is listed for each distribution.

Prediction	$\frac{d\sigma(tq)}{d y(t) }$	$\frac{1}{\sigma(tq)} \frac{d\sigma(tq)}{d y(t) }$	$\frac{d\sigma(\bar{t}q)}{d y(\bar{t}) }$	$\frac{1}{\sigma(\bar{t}q)} \frac{d\sigma(\bar{t}q)}{d y(\bar{t}) }$	$\left(\frac{d\sigma(tq)}{d y(t) }\right) / \left(\frac{d\sigma(\bar{t}q)}{d y(\bar{t}) }\right)$
	NDF=5	NDF=4	NDF=5	NDF=4	NDF=5
MCFM, with PDF4LHC21					
LO	0.65	0.54	0.82	0.86	0.99
NLO	0.97	0.93	0.68	0.81	1.0
NNLO	1.0	0.98	0.81	0.74	1.0
Generators, with NNPDF3.0					
POWHEG PYTHIA 8 (4FS)	1.0	0.98	0.81	0.61	1.0
MG_AMC@NLO (4FS)	0.99	0.93	0.81	0.53	0.99
MG_AMC@NLO (5FS)	0.99	0.97	0.69	0.61	1.0
MG_AMC@NLO dyn. scale (5FS)	0.99	0.97	0.65	0.57	1.0
POWHEG +HERWIG 7 (4FS)	1.0	0.98	0.84	0.62	1.0
PDFs, with POWHEG PYTHIA 8 (4FS)					
CT18	0.98	0.96	0.68	0.55	0.96
MSHT20	1.0	1.0	0.61	0.52	1.0
PDF4LHC21	0.99	0.98	0.70	0.65	1.0
ABMP16	0.91	0.98	0.38	0.18	0.21
NNPDF4.0	0.99	0.99	0.70	0.61	1.0
ATLASpdf21	0.92	0.99	0.64	0.84	1.0

9.1 Effective field theory interpretation

The SMEFT provides a model-independent framework for indirect searches for new physics. Within this framework, the SM is regarded as a low-energy approximation of a more fundamental theory involving interactions at an energy scale Λ . The impact of new physics is parameterised by higher-dimensional operators maintaining SM symmetries. The effective dimension-6 Lagrangian is given by

$$\mathcal{L}_{\text{eff}} = \mathcal{L}_{\text{SM}} + \sum_i \frac{C_i}{\Lambda^2} O_i + \text{Hermitian conjugate},$$

where \mathcal{L}_{SM} is the SM Lagrangian. The O_i are effective dimension-6 operators and the C_i are the associated Wilson coefficients.

In this EFT interpretation, constraints on the contribution from the four-quark operator $O_{Qq}^{3,1}$ [90] are set. The relevant operators, expressed in the Warsaw basis [91], are

$$O_{qq}^{1(ijkl)} = (\bar{q}_i \gamma^\mu q_j)(\bar{q}_k \gamma_\mu q_l) \quad \text{and}$$

$$O_{qq}^{3(ijkl)} = (\bar{q}_i \gamma^\mu \tau^I q_j)(\bar{q}_k \gamma_\mu \tau^I q_l).$$

The q denote weak-isospin doublets and $ijkl \in 1, 2, 3$ are the quark generation indices. All contributing

four-quark processes depend solely on a linear combination of Wilson coefficients

$$C_{Qq}^{3,1} = \sum_{i=1,2} C_{qq}^{3(ii33)} + \frac{1}{6} C_{qq}^{1(i33i)} - \frac{1}{6} C_{qq}^{3(i33i)},$$

where Q represents the doublet of the third quark generation, therefore the four-quark interaction is fully characterised by $O_{Qq}^{3,1}$. There are two other dimension-6 operators which can alter single-top production and interfere with the SM diagrams at LO, namely $O_{\Phi Q}^3$ and O_{tW} [92]. They are not considered in this interpretation, i.e. their respective Wilson coefficients are set to zero. The operator $O_{Qq}^{3,1}$ leads to non-SM single top-quark production, as illustrated in Figure 13, for example via the process $\bar{b} + u \rightarrow t + d$. Top quarks produced in this way feature different angular distributions and transverse momentum spectra than those produced according to the SM.

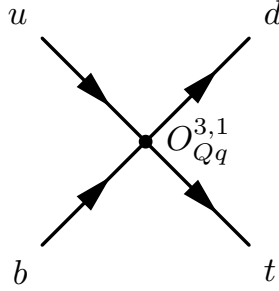


Figure 13: Representative LO Feynman diagram of a four-quark contact interaction leading to the production of a single top quark.

For large absolute values of $C_{Qq}^{3,1}/\Lambda^2$, the number of single top quarks and top antiquarks produced with a high transverse momentum is expected to increase. Therefore, the high- p_T region of the spectra provides a high sensitivity to $C_{Qq}^{3,1}/\Lambda^2$. Since the radiation of additional jets leads to increased jet- p_T , this analysis is not optimised for a high sensitivity to $C_{Qq}^{3,1}/\Lambda^2$, as the event selection requires candidate events to contain exactly two jets. Nevertheless, the differential cross-sections as a function of $p_T(t)$ or $p_T(\bar{t})$ are measured for high transverse momenta of up to 500 GeV, making an interpretation feasible.

The differential cross-sections as a function of $p_T(t)$ or $p_T(\bar{t})$ are parameterised by a polynomial of second degree in the EFT coefficient $C_{Qq}^{3,1}/\Lambda^2$

$$\begin{aligned} \frac{d\sigma_{(t \text{ or } \bar{t})}}{dp_T(t \text{ or } \bar{t})}(C_{Qq}^{3,1}/\Lambda^2) &= \left(\frac{d\sigma_{(t \text{ or } \bar{t})}}{dp_T(t \text{ or } \bar{t})} \right)_{\text{SM}} \cdot \Delta\tilde{\sigma}_{(t \text{ or } \bar{t})}(C_{Qq}^{3,1}/\Lambda^2), \quad \text{with} \\ \Delta\tilde{\sigma}_{(t \text{ or } \bar{t})}(C_{Qq}^{3,1}/\Lambda^2) &= \left(1 + a_1 \cdot C_{Qq}^{3,1}/\Lambda^2 + a_2 \cdot (C_{Qq}^{3,1}/\Lambda^2)^2 \right). \end{aligned} \quad (1)$$

The fixed-order predictions obtained with MCFM at NNLO are used in $(d\sigma_{(t \text{ or } \bar{t})}/dp_T(t \text{ or } \bar{t}))_{\text{SM}}$, which is the SM prediction. The expected relative change of the cross-sections as a function of $C_{Qq}^{3,1}/\Lambda^2$ is described by $\Delta\tilde{\sigma}_{(t \text{ or } \bar{t})}(C_{Qq}^{3,1}/\Lambda^2)$, where the term linear in $C_{Qq}^{3,1}/\Lambda^2$ covers the effect of the interference of SM and non-SM amplitudes and the term proportional to $(C_{Qq}^{3,1}/\Lambda^2)^2$ is entirely due to the four-quark operator. It is obtained by unfolding the EFT MC samples using the nominal migration matrix and selection efficiency;

and the resulting cross-section predictions are normalised to the prediction obtained from unfolding the EFT MC sample generated with $C_{Qq}^{3,1}/\Lambda^2$ set to zero.

The distributions from the EFT samples are unfolded to extract the parameterisations because a non-zero contribution from $C_{Qq}^{3,1}/\Lambda^2$ alters the kinematic properties of the event, which impacts the selection efficiency. It was validated that the impact is not primarily caused by the D_{nn} requirement. The selection efficiencies obtained for the EFT MC samples are shown in Figure 14. The decreased selection efficiencies for large positive values of $C_{Qq}^{3,1}/\Lambda^2$ negate the effect of the increased cross-section predictions. The magnitude of the effect is shown exemplarily for one bin of the differential tq cross-section in Figure 15, where the parameterisation of $\Delta\tilde{\sigma}_{(t \text{ or } \bar{t})}(C_{Qq}^{3,1}/\Lambda^2)$ obtained with the approach explained above is compared with the parameterisation obtained from parton-level predictions. The parameterisation obtained from parton-level predictions is not used for the interpretation.

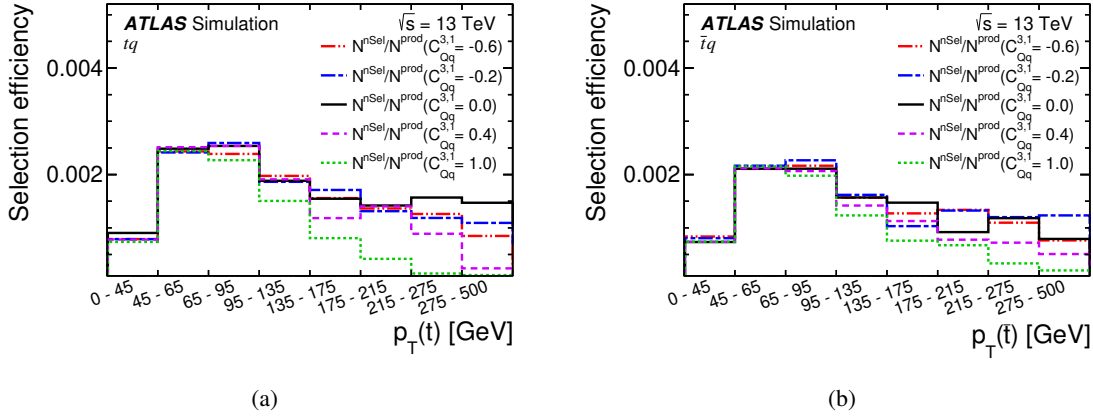
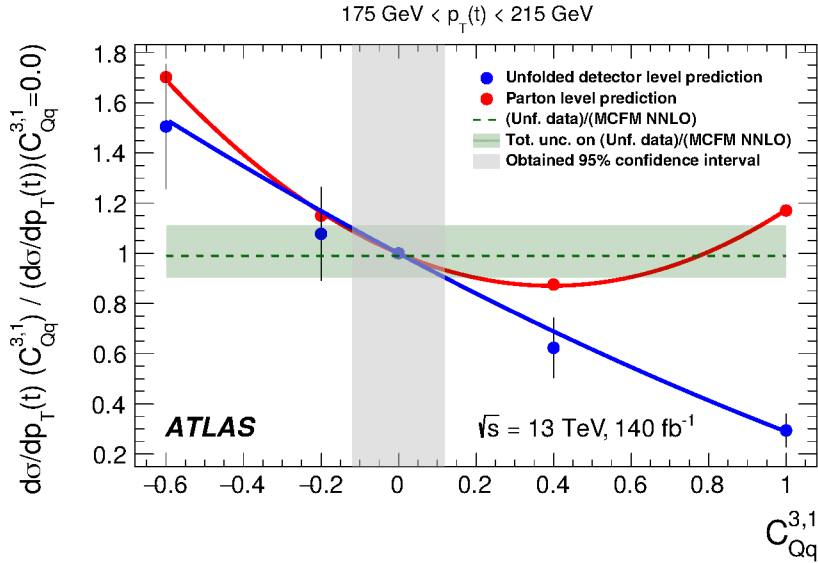


Figure 14: Selection efficiencies for the (a) $p_T(t)$ and (b) $p_T(\bar{t})$ spectra calculated for tq and $\bar{t}q$ production events generated with different values of $C_{Qq}^{3,1}/\Lambda^2$, with Λ set to 1 TeV.

The parameters a_1 and a_2 in Eq. (1) are determined via least-squares fits performed for each bin of the unfolded distributions. The uncertainties in the measured result, the SM prediction and the statistical uncertainty due to the limited size of the EFT MC samples are taken into account for the least-squares fit. The uncertainty due to the limited statistical power is evaluated by unfolding pseudo-experiments which are produced by fluctuating each bin of the detector level distributions according to a Gaussian distribution whose spread corresponds to the expected uncertainty due to the number of MC events in that bin. The standard deviation of all unfolded pseudo-experiments per bin is taken as statistical uncertainty. The statistical uncertainties of the different EFT MC samples are treated as uncorrelated. The correlation of the total uncertainty in the measurement result between bins is not considered for the least-squares fit. The parameterisations for $\Delta\tilde{\sigma}_{(t \text{ or } \bar{t})}(C_{Qq}^{3,1}/\Lambda^2)$ are given in Table 22.

The EFTfitter tool [93] is used to constrain $C_{Qq}^{3,1}/\Lambda^2$ in a Bayesian statistical framework. The total uncertainty in the measured results is taken into account and symmetrised by taking the larger of the two variations. Correlations between the single bins of the distributions are accounted for via the correlation matrices of the differential measurements. Uncertainties in the SM prediction are taken into account as well and comprise the uncertainty in the renormalisation and factorisation scale and the uncertainty in the value of α_s . The 95% confidence level (CL) interval for $C_{Qq}^{3,1}/\Lambda^2$ is determined to be

$$-0.12 \text{ TeV}^{-2} < C_{Qq}^{3,1}/\Lambda^2 < 0.12 \text{ TeV}^{-2}.$$



(a)

Figure 15: Comparison of the parameterisation for the expected relative change of the differential tq production cross-section as a function of $C_{Qq}^{3,1}/\Lambda^2$, with Λ set to 1 TeV, obtained from parton level predictions and by unfolding the detector level predictions with the nominal unfolding corrections. The uncertainties in the predictions are MC statistical uncertainties only. The dashed line indicates the measurement result over the theoretical prediction calculated with MCFM at NNLO (cf. Eq. (1)). The uncertainty band includes the total uncertainty in the measurement result and the uncertainty in the theory prediction, which considers the uncertainty in the renormalisation and factorisation scale choice and the value of α_s . The vertical shaded area shows the 95% confidence interval obtained in this interpretation.

The constraints improve upon the limits set by the ATLAS measurement of the total tq and $\bar{t}q$ cross-sections Ref. [9], where a confidence interval $C_{Qq}^{3,1}/\Lambda^2 \in [-0.37, 0.06] \text{ TeV}^{-2}$ at 95% CL was obtained.

10 Conclusion

The production of single top quarks and top antiquarks in tq and $\bar{t}q$ final states proceeds in the SM via the t -channel exchange of a virtual W boson. Differential tq and $\bar{t}q$ production cross-sections are measured in proton–proton collisions at a centre-of-mass energy of 13 TeV using the full Run 2 data sample recorded by the ATLAS detector at the LHC in the years 2015–2018, corresponding to an integrated luminosity of 140 fb^{-1} . Events are required to contain exactly one isolated electron or muon, high missing transverse momentum and exactly two jets, one of which must be identified as originating from a b -quark. A neural network is employed to separate signal from background events and a requirement of a high neural-network output score is imposed to achieve a high purity in signal events.

The absolute and normalised tq and $\bar{t}q$ production cross-sections are measured differentially at parton level as a function of the transverse momentum $p_T(t)$ or $p_T(\bar{t})$ and the absolute value of the rapidity $|y(t)|$ or $|y(\bar{t})|$ of the top quark and top antiquark. Differential tq and $\bar{t}q$ production cross-sections are measured separately and their ratio is measured as well. The measured cross-sections are compared with various predictions obtained from fixed order calculations up to NNLO in QCD and from MC event generators

interfaced to parton shower programs at NLO. Overall, a good agreement between the measurement results and the theory predictions is observed within the measurement uncertainties. The measurement is limited by systematic uncertainties, where the largest contributions are experimental uncertainties and uncertainties related to the modelling of the signal processes. Data statistical uncertainties are significant for the normalised differential cross-sections and the cross-section ratio.

This analysis provides the first separate measurement of differential tq and $\bar{t}q$ production at 13 TeV and the first measurement of the ratio of the differential $tq/\bar{t}q$ cross-sections. Compared with the measurements of the differential cross-sections at 8 TeV, a significant reduction of the uncertainties is achieved and measurement range for the differential cross-sections as a function of $p_T(t)$ or $p_T(\bar{t})$ is extended to 500 GeV .

The differential cross-sections as a function of $p_T(t)$ or $p_T(\bar{t})$ are interpreted in an EFT approach, setting limits at the 95% confidence level on contributions from the four-quark operator $O_{Qq}^{3,1}$. The impact of $O_{Qq}^{3,1}$ on the acceptance, caused by altered event kinematics, is taken into account. The 95% confidence interval $-0.12 \text{ TeV}^{-2} < C_{Qq}^{3,1}/\Lambda^2 < 0.12 \text{ TeV}^{-2}$ is obtained, improving the constraints set by an interpretation of the ATLAS measurement of the total tq and $\bar{t}q$ cross-sections.

Acknowledgements

We thank CERN for the very successful operation of the LHC and its injectors, as well as the support staff at CERN and at our institutions worldwide without whom ATLAS could not be operated efficiently.

The crucial computing support from all WLCG partners is acknowledged gratefully, in particular from CERN, the ATLAS Tier-1 facilities at TRIUMF/SFU (Canada), NDGF (Denmark, Norway, Sweden), CC-IN2P3 (France), KIT/GridKA (Germany), INFN-CNAF (Italy), NL-T1 (Netherlands), PIC (Spain), RAL (UK) and BNL (USA), the Tier-2 facilities worldwide and large non-WLCG resource providers. Major contributors of computing resources are listed in Ref. [94].

We gratefully acknowledge the support of ANPCyT, Argentina; YerPhI, Armenia; ARC, Australia; BMWFW and FWF, Austria; ANAS, Azerbaijan; CNPq and FAPESP, Brazil; NSERC, NRC and CFI, Canada; CERN; ANID, Chile; CAS, MOST and NSFC, China; Minciencias, Colombia; MEYS CR, Czech Republic; DNRf and DNSRC, Denmark; IN2P3-CNRS and CEA-DRF/IRFU, France; SRNSFG, Georgia; BMFTR, HGF and MPG, Germany; GSRI, Greece; RGC and Hong Kong SAR, China; ICHEP and Academy of Sciences and Humanities, Israel; INFN, Italy; MEXT and JSPS, Japan; CNRST, Morocco; NWO, Netherlands; RCN, Norway; MNiSW, Poland; FCT, Portugal; MNE/IFA, Romania; MSTDI, Serbia; MSSR, Slovakia; ARIS and MVZI, Slovenia; DSI/NRF, South Africa; MICIU/AEI, Spain; SRC and Wallenberg Foundation, Sweden; SERI, SNSF and Cantons of Bern and Geneva, Switzerland; NSTC, Taipei; TENMAK, Türkiye; STFC/UKRI, United Kingdom; DOE and NSF, United States of America.

Individual groups and members have received support from BCKDF, CANARIE, CRC and DRAC, Canada; CERN-CZ, FORTE and PRIMUS, Czech Republic; COST, ERC, ERDF, Horizon 2020, ICSC-NextGenerationEU and Marie Skłodowska-Curie Actions, European Union; Investissements d’Avenir Labex, Investissements d’Avenir Idex and ANR, France; DFG and AvH Foundation, Germany; Herakleitos, Thales and Aristeia programmes co-financed by EU-ESF and the Greek NSRF, Greece; BSF-NSF and MINERVA, Israel; NCN and NAWA, Poland; La Caixa Banking Foundation, CERCA Programme Generalitat de Catalunya and PROMETEO and GenT Programmes Generalitat Valenciana, Spain; Göran Gustafssons Stiftelse, Sweden; The Royal Society and Leverhulme Trust, United Kingdom.

In addition, individual members wish to acknowledge support from CERN: European Organization for Nuclear Research (CERN DOCT); Chile: Agencia Nacional de Investigación y Desarrollo (FONDECYT 1230812, FONDECYT 1240864, Fondecyt 3240661, Fondecyt Regular 1240721); China: Chinese Ministry of Science and Technology (MOST-2023YFA1605700, MOST-2023YFA1609300), National Natural Science Foundation of China (NSFC - 12175119, NSFC 12275265); Czech Republic: Czech Science Foundation (GACR - 24-11373S), Ministry of Education Youth and Sports (ERC-CZ-LL2327, FORTE CZ.02.01.01/00/22_008/0004632), PRIMUS Research Programme (PRIMUS/21/SCI/017); EU: H2020 European Research Council (ERC - 101002463); European Union: European Research Council (BARD No. 101116429, ERC - 948254, ERC 101089007), European Regional Development Fund (HE COFUND GA No.101081355, ERDF), European Union, Future Artificial Intelligence Research (FAIR-NextGenerationEU PE00000013), Italian Center for High Performance Computing, Big Data and Quantum Computing (ICSC, NextGenerationEU); France: Agence Nationale de la Recherche (ANR-21-CE31-0013, ANR-21-CE31-0022, ANR-22-EDIR-0002, ANR-24-CE31-0504-01); Germany: Deutsche Forschungsgemeinschaft (DFG - 469666682, DFG - CR 312/5-2); China: Research Grants Council (GRF); Italy: Istituto Nazionale di Fisica Nucleare (ICSC, NextGenerationEU), Ministero dell'Università e della Ricerca (NextGenEU 153D23001490006 M4C2.1.1, NextGenEU I53D23000820006 M4C2.1.1, NextGenEU I53D23001490006 M4C2.1.1, SOE2024_0000023); Japan: Japan Society for the Promotion of Science (JSPS KAKENHI JP22H01227, JSPS KAKENHI JP22H04944, JSPS KAKENHI JP22KK0227, JSPS KAKENHI JP24K23939, JSPS KAKENHI JP24KK0251, JSPS KAKENHI JP25H00650, JSPS KAKENHI JP25H01291, JSPS KAKENHI JP25K01023); Norway: Research Council of Norway (RCN-314472); Poland: Ministry of Science and Higher Education (IDUB AGH, POB8, D4 no 9722), Polish National Science Centre (NCN 2021/42/E/ST2/00350, NCN OPUS 2023/51/B/ST2/02507, NCN OPUS nr 2022/47/B/ST2/03059, NCN UMO-2019/34/E/ST2/00393, UMO-2022/47/O/ST2/00148, UMO-2023/49/B/ST2/04085, UMO-2023/51/B/ST2/00920, UMO-2024/53/N/ST2/00869); Portugal: Foundation for Science and Technology (FCT); Spain: Generalitat Valenciana (ASFAE/2022/008), Ministry of Science and Innovation (MCIN & NextGenEU PCI2022-135018-2, MICIN & FEDER PID2021-125273NB, RYC2019-028510-I, RYC2020-030254-I, RYC2021-031273-I, RYC2022-038164-I), Ministerio de Ciencia, Innovación y Universidades/Agencia Estatal de Investigación (PID2022-142604OB-C22); Sweden: Carl Trygger Foundation (Carl Trygger Foundation CTS 22:2312), Swedish Research Council (Swedish Research Council 2023-04654, VR 2021-03651, VR 2022-03845, VR 2022-04683, VR 2023-03403, VR 2024-05451), Knut and Alice Wallenberg Foundation (KAW 2018.0458, KAW 2022.0358, KAW 2023.0366); Switzerland: Swiss National Science Foundation (SNSF - PCEFP2_194658); United Kingdom: Royal Society (NIF-R1-231091); United States of America: U.S. Department of Energy (ECA DE-AC02-76SF00515), Neubauer Family Foundation.

Appendix

Migration matrices

The migration matrices are optimised according to the criteria explained in Section 7. The obtained migration matrices are presented in Figure 16.

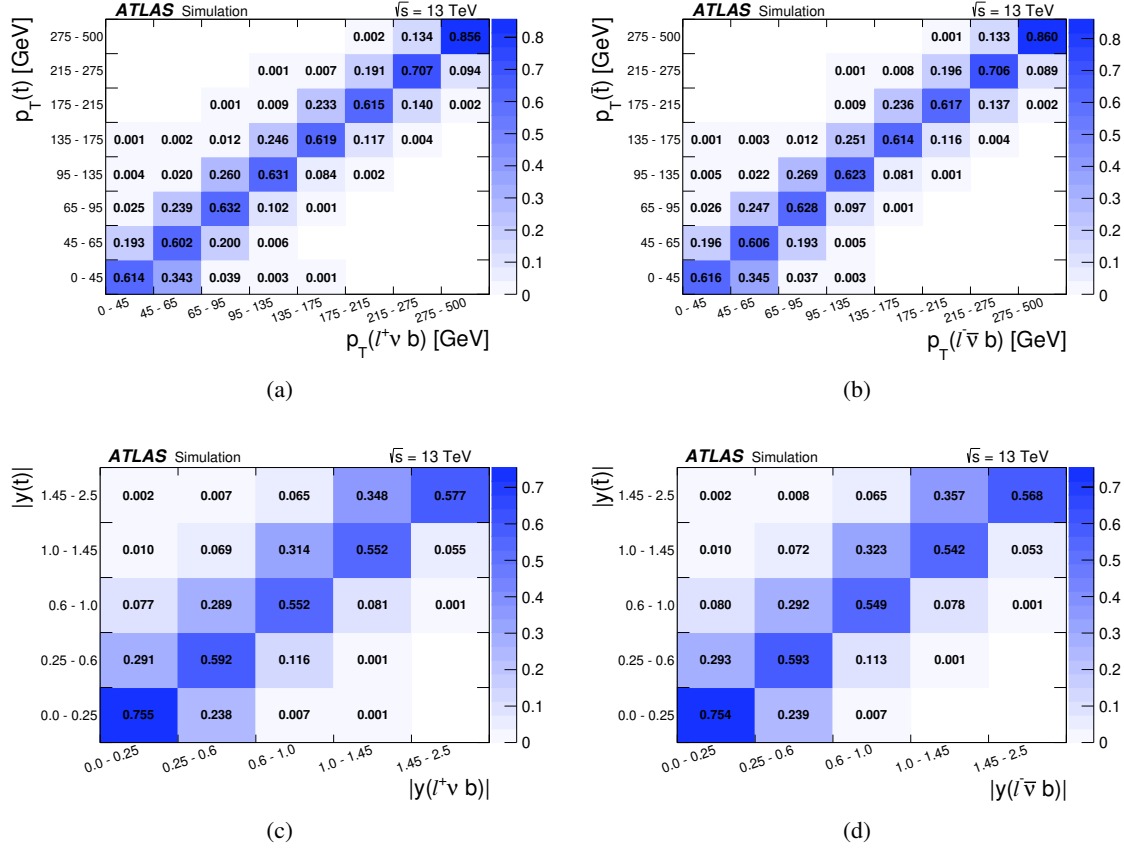


Figure 16: Migration matrices for the (a),(b) $p_T(\ell^+ \nu b)$ and (c),(d) $|y(\ell^+ \nu b)|$ distributions in the (a),(c) ℓ^+ SR and (b),(d) ℓ^- SR. The variables on parton-level are shown on the y-axis and the reconstructed variables are shown on the x-axis. The rows are normalised to unity.

Systematic and statistical uncertainties

The statistical and systematic uncertainties in the measured results are evaluated according to the description in Section 8. The impact of the different sources of uncertainties are given in Tables 6–15. Experimental uncertainties are further separated into components related to the JES, JER, (f)JVT, b -tagging, pile-up, E_T^{miss} and the charged lepton.

Table 6: Summary of the uncertainties in the absolute differential $t\bar{q}$ production cross-sections measured as a function of $p_T(t)$. Similar sources of uncertainties are grouped using their quadratic sum. The total uncertainty is defined as the quadratic sum of all sources of uncertainties.

Systematic	Systematic uncertainty in [%] on the absolute $t\bar{q}$ cross-section in the given $p_T(t)$ interval							
	[0, 45] GeV	[45, 65] GeV	[65, 95] GeV	[95, 135] GeV	[135, 175] GeV	[175, 215] GeV	[215, 275] GeV	[275, 500] GeV
JER	1.5/-4.2	2.4/-3.5	2.7/-1.0	0.95/-1.9	2.9/-0.63	0.81/-3.6	3.0/-0.42	1.7/-2.6
JES	5.7/-3.2	1.6/-1.0	2.3/-1.7	4.8/-4.8	5.6/-4.9	6.3/-4.5	3.4/-5.8	5.5/-3.9
(f)JVT	1.8/-1.8	1.3/-1.3	0.78/-0.78	0.25/-0.26	0.61/-0.63	0.49/-0.49	0.45/-0.46	0.52/-0.52
Lepton	1.4/-1.2	1.1/-1.1	1.0/-1.0	1.0/-0.99	1.0/-0.99	1.0/-1.0	1.1/-0.98	0.99/-1.0
E_T^{miss}	2.1/-0.0	0.72/-0.34	0.84/-0.28	0.99/-0.16	0.98/-0.13	1.8/-0.0	0.74/-0.81	2.5/-0.0
b -tagging	2.2/-2.2	1.7/-1.7	1.5/-1.5	1.4/-1.4	1.3/-1.3	1.3/-1.3	1.2/-1.2	1.3/-1.3
Pile-up	1.4/-1.4	1.3/-1.2	1.5/-1.3	1.4/-1.3	1.3/-1.2	1.1/-1.1	1.2/-1.1	1.3/-1.3
Luminosity	0.83/-0.83	0.83/-0.83	0.83/-0.83	0.83/-0.83	0.83/-0.83	0.83/-0.83	0.83/-0.83	0.83/-0.83
Signal modelling	5.2/-4.9	6.2/-6.0	5.8/-5.4	6.1/-5.5	7.0/-5.7	6.9/-6.7	12/-12	16/-16
Background modelling	1.5/-2.0	0.93/-0.62	1.1/-0.66	0.66/-0.74	0.96/-0.99	1.1/-1.6	2.4/-2.4	2.5/-2.2
Background rate	2.9/-2.9	1.4/-1.4	0.67/-0.67	0.45/-0.45	0.48/-0.48	0.43/-0.43	0.36/-0.36	0.64/-0.64
Total systematic	9.5/-8.7	7.6/-7.7	7.4/-6.4	8.3/-7.9	9.8/-8.0	9.9/-9.3	13/-13	18/-17
Statistical	2.0/-2.0	1.3/-1.3	1.3/-1.3	2.0/-2.0	3.5/-3.5	5.3/-5.3	6.6/-6.6	9.1/-9.1
Total uncertainty	9.7/-8.9	7.7/-7.9	7.5/-6.5	8.5/-8.1	10/-8.7	11/-10	15/-15	20/-19

Table 7: Summary of the uncertainties in the absolute differential $\bar{t}q$ production cross-sections measured as a function of $p_T(\bar{t})$. Similar sources of uncertainties are grouped using their quadratic sum. The total uncertainty is defined as the quadratic sum of all sources of uncertainties.

Systematic	Systematic uncertainty in [%] on the absolute $\bar{t}q$ cross-section in the given $p_T(\bar{t})$ interval							
	[0, 45] GeV	[45, 65] GeV	[65, 95] GeV	[95, 135] GeV	[135, 175] GeV	[175, 215] GeV	[215, 275] GeV	[275, 500] GeV
JER	7.2/-3.0	1.6/-1.2	3.1/-3.7	0.96/-2.6	2.2/-2.3	3.9/-3.9	3.3/-2.4	1.8/-5.4
JES	6.0/-8.1	2.1/-1.9	3.3/-2.7	5.1/-4.7	6.4/-5.9	5.8/-5.5	6.3/-4.9	6.5/-4.3
(f)JVT	1.6/-1.6	1.3/-1.3	0.61/-0.62	0.21/-0.22	0.73/-0.75	0.64/-0.65	0.49/-0.51	0.72/-0.71
Lepton	1.3/-1.4	1.2/-1.2	1.1/-1.2	1.0/-1.1	1.1/-1.1	1.1/-1.1	1.1/-1.2	1.2/-1.6
E_T^{miss}	1.8/-0.0	1.5/-0.11	1.2/-0.68	0.9/-0.25	2.9/-0.61	1.4/-0.25	0.11/-1.2	1.6/-1.6
b -tagging	2.4/-2.4	1.9/-1.9	1.6/-1.6	1.5/-1.5	1.4/-1.4	1.4/-1.4	1.4/-1.4	1.5/-1.5
Pile-up	0.91/-1.2	1.3/-1.2	1.6/-1.5	1.5/-1.3	1.4/-1.2	1.6/-1.5	0.96/-0.74	1.5/-1.3
Luminosity	0.83/-0.83	0.83/-0.83	0.83/-0.83	0.83/-0.83	0.83/-0.83	0.83/-0.83	0.83/-0.83	0.83/-0.83
Signal modelling	5.1/-4.1	6.0/-5.5	5.2/-5.7	4.9/-5.2	12/-11	11/-8.7	13/-12	24/-21
Background modelling	1.7/-3.1	0.63/-1.4	1.4/-1.2	1.0/-1.2	1.9/-2.0	2.6/-2.9	4.9/-4.9	3.9/-2.2
Background rate	3.0/-3.0	1.8/-1.8	1.1/-1.1	0.7/-0.7	0.93/-0.93	0.61/-0.61	0.7/-0.7	0.92/-0.92
Total systematic	11/-11	7.6/-7.1	7.8/-8.0	7.7/-8.0	14/-13	13/-11	16/-15	25/-22
Statistical	2.5/-2.5	1.8/-1.8	2.0/-2.0	2.9/-2.9	5.3/-5.3	7.6/-7.6	10/-10	13/-13
Total uncertainty	12/-11	7.8/-7.3	8.0/-8.2	8.2/-8.5	15/-14	15/-13	19/-18	28/-26

Table 8: Summary of the uncertainties in the absolute differential tq production cross-sections measured as a function of $|y(t)|$. Similar sources of uncertainties are grouped using their quadratic sum. The total uncertainty is defined as the quadratic sum of all sources of uncertainties.

Systematic	Systematic uncertainty in [%] on the absolute tq cross-section in the given $ y(t) $ interval				
	[0.0, 0.25]	[0.25, 0.6]	[0.6, 1.0]	[1.0, 1.45]	[1.45, 2.5]
JER	0.8/ -2.5	3.5/ -1.5	2.1/ -2.5	0.51/ -2.3	4.5/ -5.7
JES	2.3/ -1.1	2.1/ -1.7	1.9/ -1.6	2.9/ -2.8	6.4/ -3.4
(f)JVT	0.87/ -0.88	0.91/ -0.91	0.85/ -0.85	0.82/ -0.82	0.82/ -0.82
Lepton	1.1/ -1.1	1.1/ -1.1	1.0/ -1.0	1.0/ -1.0	1.3/ -1.1
E_T^{miss}	0.0/ -0.47	1.0/ -0.07	0.93/ -0.09	1.3/ -0.0	3.4/ -0.47
b -tagging	1.6/ -1.6	1.6/ -1.6	1.6/ -1.6	1.5/ -1.5	1.6/ -1.6
Pile-up	1.3/ -1.2	1.3/ -1.2	1.4/ -1.3	1.3/ -1.3	2.0/ -1.7
Luminosity	0.83/ -0.83	0.83/ -0.83	0.83/ -0.83	0.83/ -0.83	0.83/ -0.83
Signal modelling	5.5/ -5.3	5.7/ -5.3	6.0/ -5.2	5.1/ -4.9	6.5/ -6.0
Background modelling	0.97/ -0.57	0.83/ -0.53	1.1/ -1.0	0.98/ -0.9	0.79/ -1.8
Background rate	1.2/ -1.2	1.2/ -1.2	1.2/ -1.2	1.0/ -1.0	1.5/ -1.5
Total systematic	6.7/ -6.7	7.7/ -6.5	7.3/ -6.7	6.7/ -6.7	11/ -9.7
Statistical	1.7/ -1.7	1.4/ -1.4	1.6/ -1.6	1.9/ -1.9	2.6/ -2.6
Total uncertainty	6.9/ -6.9	7.8/ -6.6	7.5/ -6.9	6.9/ -7.0	11/ -10

Table 9: Summary of the uncertainties in the absolute differential $\bar{t}q$ production cross-sections measured as a function of $|y(\bar{t})|$. Similar sources of uncertainties are grouped using their quadratic sum. The total uncertainty is defined as the quadratic sum of all sources of uncertainties.

Systematic	Systematic uncertainty in [%] on the absolute $\bar{t}q$ cross-section in the given $ y(\bar{t}) $ interval				
	[0.0, 0.25]	[0.25, 0.6]	[0.6, 1.0]	[1.0, 1.45]	[1.45, 2.5]
JER	3.5/ -5.4	2.4/ -1.4	3.7/ -1.1	2.4/ -1.4	3.6/ -3.0
JES	3.9/ -2.6	2.5/ -3.6	3.5/ -2.2	4.0/ -2.5	4.0/ -6.5
(f)JVT	0.77/ -0.78	0.93/ -0.94	0.82/ -0.81	0.84/ -0.83	0.68/ -0.67
Lepton	1.3/ -1.2	1.2/ -1.3	1.3/ -1.2	1.1/ -1.4	1.2/ -1.2
E_T^{miss}	1.7/ -0.0	0.46/ -0.48	1.6/ -0.25	2.1/ -0.0	1.8/ -0.95
b -tagging	1.8/ -1.8	1.8/ -1.8	1.7/ -1.7	1.8/ -1.8	1.8/ -1.8
Pile-up	1.4/ -1.4	1.4/ -1.3	1.2/ -1.2	1.2/ -1.2	1.5/ -1.5
Luminosity	0.83/ -0.83	0.83/ -0.83	0.83/ -0.83	0.83/ -0.83	0.83/ -0.83
Signal modelling	7.4/ -7.3	5.8/ -5.4	4.1/ -4.0	4.1/ -4.6	8.6/ -7.8
Background modelling	1.9/ -2.2	1.6/ -1.2	1.5/ -1.9	1.5/ -1.5	1.8/ -4.0
Background rate	1.5/ -1.5	1.6/ -1.6	1.5/ -1.5	1.5/ -1.5	1.9/ -1.9
Total systematic	9.9/ -10	7.7/ -7.5	7.6/ -6.0	7.4/ -6.5	11/ -11
Statistical	2.4/ -2.4	1.9/ -1.9	2.1/ -2.1	2.7/ -2.7	3.7/ -3.7
Total uncertainty	10/ -10	7.9/ -7.7	7.9/ -6.3	7.9/ -7.0	11/ -12

Table 10: Summary of the uncertainties in the normalised differential tq production cross-sections measured as a function of $p_T(t)$. Similar sources of uncertainties are grouped using their quadratic sum. The total uncertainty is defined as the quadratic sum of all sources of uncertainties.

Systematic	Systematic uncertainty in [%] on the normalised tq cross-section in the given $p_T(t)$ interval							
	[0, 45] GeV	[45, 65] GeV	[65, 95] GeV	[95, 135] GeV	[135, 175] GeV	[175, 215] GeV	[215, 275] GeV	[275, 500] GeV
JER	0.5/-2.5	1.5/-1.4	2.4/-0.3	1.2/-1.4	3.5/-0.24	1.5/-3.7	4.3/-0.81	2.2/-2.0
JES	3.8/-2.4	1.7/-2.2	1.8/-2.6	3.1/-3.6	3.5/-3.6	4.1/-3.8	2.7/-5.6	4.0/-4.2
(f)JVT	0.81/-0.79	0.36/-0.35	0.18/-0.18	0.7/-0.71	1.6/-1.6	1.4/-1.5	1.4/-1.4	1.5/-1.5
Lepton	0.56/-0.19	0.04/-0.26	0.12/-0.41	0.18/-0.25	0.19/-0.32	0.16/-0.27	0.37/-0.26	0.26/-0.38
E_T^{miss}	1.1/-0.0	0.0/-0.97	0.0/-0.61	0.0/-0.27	0.11/-0.6	0.64/-0.01	0.23/-1.1	1.4/-0.0
b -tagging	0.79/-0.79	0.16/-0.16	0.51/-0.52	0.55/-0.56	0.64/-0.65	0.72/-0.73	0.86/-0.87	1.1/-1.1
Pile-up	0.06/-0.09	0.06/-0.06	0.07/-0.0	0.02/-0.0	0.11/-0.14	0.21/-0.34	0.17/-0.17	0.0/-0.09
Signal modelling	2.5/-2.5	1.6/-1.8	1.3/-1.3	2.7/-2.6	3.6/-2.8	3.2/-2.8	8.2/-8.0	13/-12
Background modelling	0.88/-1.3	0.46/-0.36	1.1/-0.91	0.55/-0.65	1.1/-0.99	1.2/-1.7	2.6/-2.7	2.7/-2.5
Background rate	1.5/-1.5	0.18/-0.18	0.94/-0.96	1.0/-1.0	1.0/-1.1	1.1/-1.1	1.1/-1.2	1.2/-1.2
Total systematic	5.1/-4.8	2.9/-3.3	3.7/-3.4	4.5/-4.9	6.5/-5.1	5.9/-6.6	10/-10	14/-13
Statistical	1.4/-1.4	1.3/-1.3	1.5/-1.5	1.9/-1.9	3.4/-3.4	5.2/-5.2	6.6/-6.6	9.0/-9.0
Total uncertainty	5.3/-5.0	3.2/-3.5	3.9/-3.7	4.9/-5.3	7.3/-6.2	7.9/-8.4	12/-12	17/-16

Table 11: Summary of the uncertainties in the normalised differential $\bar{t}q$ production cross-sections measured as a function of $p_T(\bar{t})$. Similar sources of uncertainties are grouped using their quadratic sum. The total uncertainty is defined as the quadratic sum of all sources of uncertainties.

Systematic	Systematic uncertainty in [%] on the normalised $\bar{t}q$ cross-section in the given $p_T(\bar{t})$ interval							
	[0, 45] GeV	[45, 65] GeV	[65, 95] GeV	[95, 135] GeV	[135, 175] GeV	[175, 215] GeV	[215, 275] GeV	[275, 500] GeV
JER	5.3/-2.5	1.4/-2.3	3.0/-4.7	0.87/-3.5	2.3/-3.7	3.6/-5.4	3.1/-3.4	1.7/-6.7
JES	3.3/-4.9	2.8/-2.0	3.9/-3.2	3.3/-3.1	4.1/-3.7	4.4/-4.5	5.5/-4.5	5.9/-4.3
(f)JVT	0.7/-0.68	0.41/-0.4	0.27/-0.29	0.67/-0.69	1.6/-1.7	1.5/-1.5	1.4/-1.4	1.6/-1.6
Lepton	0.32/-0.39	0.33/-0.03	0.38/-0.45	0.12/-0.32	0.43/-0.41	0.38/-0.41	0.2/-0.62	0.42/-1.2
E_T^{miss}	0.77/-0.14	0.2/-0.07	0.11/-0.89	0.19/-0.75	1.6/-0.56	0.24/-0.51	0.0/-2.3	0.57/-1.7
b -tagging	0.81/-0.8	0.18/-0.18	0.55/-0.55	0.68/-0.69	0.77/-0.77	0.83/-0.84	0.93/-0.94	1.3/-1.3
Pile-up	0.11/-0.36	0.03/-0.0	0.37/-0.22	0.24/-0.06	0.14/-0.0	0.38/-0.23	0.52/-0.31	0.23/-0.07
Signal modelling	2.7/-2.6	0.96/-1.0	0.45/-1.3	1.1/-2.0	8.2/-8.0	7.0/-4.8	9.2/-8.4	19/-17
Background modelling	1.1/-1.8	0.74/-0.97	1.7/-1.4	1.2/-0.77	1.9/-1.9	3.0/-3.0	4.7/-4.7	4.3/-2.3
Background rate	1.3/-1.3	0.14/-0.14	0.83/-0.85	1.2/-1.2	1.2/-1.2	1.4/-1.4	1.4/-1.4	1.4/-1.4
Total systematic	7.2/-6.6	3.4/-3.4	5.3/-6.2	4.1/-5.4	10/-10	9.8/-9.3	12/-11	21/-19
Statistical	1.9/-1.9	1.8/-1.8	2.1/-2.1	2.8/-2.8	5.1/-5.1	7.6/-7.6	10/-10	13/-13
Total uncertainty	7.4/-6.8	3.9/-3.9	5.7/-6.6	5.0/-6.1	11/-11	12/-12	16/-15	25/-23

Table 12: Summary of the uncertainties in the normalised differential tq production cross-sections measured as a function of $|y(t)|$. Similar sources of uncertainties are grouped using their quadratic sum. The total uncertainty is defined as the quadratic sum of all sources of uncertainties.

Systematic	Systematic uncertainty in [%] on the normalised tq cross-section in the given $ y(t) $ interval				
	[0.0, 0.25]	[0.25, 0.6]	[0.6, 1.0]	[1.0, 1.45]	[1.45, 2.5]
JER	1.3/ -2.2	3.1/ -0.32	1.4/ -1.5	2.0/ -3.2	2.5/ -2.8
JES	1.3/ -1.6	0.69/ -1.7	1.0/ -1.9	0.46/ -1.6	3.0/ -1.2
(f)JVT	0.02/ -0.03	0.06/ -0.06	0.02/ -0.02	0.03/ -0.03	0.04/ -0.04
Lepton	0.17/ -0.37	0.22/ -0.18	0.18/ -0.28	0.3/ -0.31	0.5/ -0.2
E_T^{miss}	0.07/ -2.1	0.13/ -0.63	0.11/ -0.73	0.25/ -0.43	1.8/ -0.27
b -tagging	0.08/ -0.08	0.07/ -0.07	0.06/ -0.06	0.16/ -0.16	0.13/ -0.13
Pile-up	0.24/ -0.21	0.2/ -0.27	0.12/ -0.16	0.12/ -0.23	0.43/ -0.33
Signal modelling	0.66/ -0.92	0.85/ -0.8	0.66/ -0.44	0.88/ -0.95	0.86/ -0.9
Background modelling	0.77/ -0.43	0.65/ -0.41	0.68/ -0.56	1.2/ -0.83	0.69/ -1.3
Background rate	0.23/ -0.23	0.19/ -0.19	0.17/ -0.17	0.3/ -0.31	0.32/ -0.33
Total systematic	2.1/ -3.6	3.3/ -2.0	2.0/ -2.7	2.6/ -3.9	4.5/ -3.5
Statistical	1.9/ -1.9	1.6/ -1.6	1.8/ -1.8	2.1/ -2.1	2.1/ -2.1
Total uncertainty	2.9/ -4.1	3.7/ -2.6	2.7/ -3.2	3.3/ -4.4	5.0/ -4.1

Table 13: Summary of the uncertainties in the normalised differential $\bar{t}q$ production cross-sections measured as a function of $|y(\bar{t})|$. Similar sources of uncertainties are grouped using their quadratic sum. The total uncertainty is defined as the quadratic sum of all sources of uncertainties.

Systematic	Systematic uncertainty in [%] on the normalised $\bar{t}q$ cross-section in the given $ y(\bar{t}) $ interval				
	[0.0, 0.25]	[0.25, 0.6]	[0.6, 1.0]	[1.0, 1.45]	[1.45, 2.5]
JER	2.6/ -5.5	2.5/ -1.8	3.3/ -1.5	2.2/ -1.7	2.5/ -2.5
JES	1.7/ -0.57	0.87/ -1.6	1.9/ -1.3	2.0/ -0.66	1.4/ -3.2
(f)JVT	0.02/ -0.03	0.14/ -0.14	0.06/ -0.04	0.05/ -0.05	0.13/ -0.12
Lepton	0.54/ -0.32	0.19/ -0.54	0.57/ -0.26	0.36/ -0.74	0.31/ -0.32
E_T^{miss}	0.67/ -0.12	0.0/ -1.1	0.37/ -0.07	1.0/ -0.26	0.5/ -0.65
b -tagging	0.12/ -0.12	0.06/ -0.06	0.1/ -0.1	0.1/ -0.1	0.18/ -0.18
Pile-up	0.04/ -0.09	0.07/ -0.0	0.09/ -0.15	0.15/ -0.17	0.15/ -0.15
Signal modelling	1.6/ -1.8	0.5/ -0.38	2.3/ -2.4	2.1/ -2.4	2.7/ -2.4
Background modelling	2.1/ -2.1	1.3/ -0.51	1.6/ -1.4	2.0/ -1.4	1.7/ -2.9
Background rate	0.36/ -0.37	0.28/ -0.28	0.19/ -0.19	0.33/ -0.33	0.54/ -0.53
Total systematic	4.2/ -6.2	3.0/ -2.8	4.8/ -3.4	4.3/ -3.4	4.3/ -5.6
Statistical	2.5/ -2.5	2.0/ -2.0	2.3/ -2.3	2.8/ -2.8	2.9/ -2.9
Total uncertainty	4.9/ -6.7	3.7/ -3.5	5.3/ -4.1	5.1/ -4.4	5.2/ -6.3

Table 14: Summary of the uncertainties in the ratio of the differential production cross-sections measured as a function of $p_T(t \text{ or } \bar{t})$. Similar sources of uncertainties are grouped using their quadratic sum. The total uncertainty is defined as the quadratic sum of all sources of uncertainties.

Systematic	Systematic uncertainty in [%] on the cross-section ratio in the given $p_T(t \text{ or } \bar{t})$ interval							
	[0, 45] GeV	[45, 65] GeV	[65, 95] GeV	[95, 135] GeV	[135, 175] GeV	[175, 215] GeV	[215, 275] GeV	[275, 500] GeV
JER	2.0/ -9.6	2.2/ -3.8	3.2/ -1.9	1.4/ -0.96	3.4/ -1.3	1.8/ -5.5	4.1/ -2.4	4.9/ -2.1
JES	6.7/ -2.5	1.6/ -1.3	1.9/ -1.5	0.8/ -1.8	1.5/ -1.5	2.9/ -1.9	2.6/ -3.5	2.0/ -2.5
(f)JVT	0.18/ -0.21	0.03/ -0.04	0.17/ -0.17	0.04/ -0.04	0.13/ -0.12	0.16/ -0.15	0.06/ -0.07	0.19/ -0.19
Lepton	1.2/ -0.33	0.1/ -0.43	0.48/ -0.48	0.35/ -0.06	0.32/ -0.42	0.28/ -0.3	0.9/ -0.1	1.1/ -0.23
E_T^{miss}	0.45/ -0.0	0.0/ -1.2	0.4/ -0.33	0.34/ -0.26	0.47/ -2.3	0.68/ -0.09	1.8/ -0.63	2.4/ -0.0
b -tagging	0.33/ -0.32	0.29/ -0.29	0.23/ -0.23	0.21/ -0.2	0.18/ -0.18	0.2/ -0.2	0.32/ -0.32	0.34/ -0.34
Pile-up	0.54/ -0.23	0.04/ -0.0	0.21/ -0.16	0.06/ -0.09	0.0/ -0.14	0.43/ -0.57	0.26/ -0.38	0.04/ -0.18
Signal modelling	1.4/ -1.7	1.4/ -1.5	1.4/ -0.6	2.6/ -1.5	8.1/ -6.3	3.4/ -5.3	4.1/ -4.1	7.7/ -10
Background modelling	3.0/ -1.9	1.2/ -0.64	1.2/ -0.58	1.1/ -0.92	1.7/ -1.4	2.7/ -2.6	7.2/ -6.7	3.1/ -3.6
Background rate	3.9/ -3.9	2.0/ -2.0	0.92/ -0.92	0.66/ -0.66	0.79/ -0.78	0.71/ -0.71	0.71/ -0.71	0.62/ -0.61
Total systematic	8.7/ -10	3.9/ -5.0	4.3/ -2.8	3.4/ -2.8	9.1/ -7.2	5.7/ -8.4	9.8/ -9.0	10/ -11
Statistical	3.1/ -3.1	2.2/ -2.2	2.3/ -2.3	3.4/ -3.4	6.2/ -6.2	9.0/ -9.0	12/ -12	16/ -16
Total uncertainty	9.3/ -11	4.4/ -5.4	4.9/ -3.7	4.8/ -4.4	10/ -9.5	10/ -12	15/ -15	19/ -19

Table 15: Summary of the uncertainties in the ratio of the differential production cross-sections measured as a function of $|y(t \text{ or } \bar{t})|$. Similar sources of uncertainties are grouped using their quadratic sum. The total uncertainty is defined as the quadratic sum of all sources of uncertainties.

Systematic	Systematic uncertainty in [%] on the cross-section ratio in the given $ y(t \text{ or } \bar{t}) $ interval				
	[0.0, 0.25]	[0.25, 0.6]	[0.6, 1.0]	[1.0, 1.45]	[1.45, 2.5]
JER	3.7/ -3.5	4.3/ -3.1	2.1/ -5.1	0.69/ -3.7	4.5/ -6.6
JES	1.7/ -1.9	2.4/ -0.88	1.4/ -2.0	0.73/ -2.0	5.0/ -2.3
(f)JVT	0.1/ -0.1	0.04/ -0.06	0.09/ -0.13	0.01/ -0.02	0.15/ -0.15
Lepton	0.09/ -0.6	0.66/ -0.21	0.23/ -0.56	0.82/ -0.21	1.2/ -0.56
E_T^{miss}	0.0/ -2.1	0.71/ -0.0	0.16/ -0.71	0.52/ -1.0	1.8/ -0.0
b -tagging	0.24/ -0.24	0.27/ -0.27	0.25/ -0.25	0.42/ -0.41	0.3/ -0.29
Pile-up	0.27/ -0.08	0.09/ -0.16	0.15/ -0.03	0.1/ -0.09	0.43/ -0.24
Signal modelling	2.5/ -2.1	0.82/ -0.86	2.4/ -2.2	1.5/ -1.3	2.9/ -3.0
Background modelling	2.5/ -2.0	1.0/ -0.93	1.5/ -0.98	1.5/ -1.5	4.7/ -2.9
Background rate	1.6/ -1.6	1.7/ -1.7	1.7/ -1.7	1.6/ -1.6	2.0/ -2.0
Total systematic	5.7/ -5.6	5.5/ -3.9	4.1/ -6.3	3.1/ -5.0	9.2/ -8.4
Statistical	2.8/ -2.8	2.3/ -2.3	2.5/ -2.5	3.1/ -3.1	4.4/ -4.4
Total uncertainty	6.3/ -6.3	5.9/ -4.5	4.9/ -6.8	4.4/ -5.9	10/ -9.5

Measurement results

The measured results for the parton-level tq and $\bar{t}q$ production cross-sections are shown graphically in Section 9. The numerical values are given in Tables 16–21.

Table 16: Absolute and normalised differential tq production cross-sections as a function of $p_T(t)$.

$p_T(t)$ [GeV]	$\frac{d\sigma_{tq}}{dp_T(t)}$ [fb GeV ⁻¹]			$\frac{1}{\sigma} \frac{d\sigma_{tq}}{dp_T(t)}$ [10^{-3} GeV ⁻¹]		
	stat.	syst.		stat.	syst.	
0–45	966	± 18	90/–83	7.44	± 0.15	0.37/–0.34
45–65	1274	± 16	95/–98	9.81	± 0.13	0.28/–0.32
65–95	914	± 12	67/–58	7.04	± 0.09	0.26/–0.24
95–135	456	± 9	37/–35	3.51	± 0.07	0.16/–0.17
135–175	191	± 7	18/–15	1.470	± 0.052	0.095/–0.075
175–215	93.6	± 4.9	9.3/–8.7	0.721	± 0.038	0.043/–0.047
215–275	40.4	± 2.7	5.6/–5.6	0.311	± 0.021	0.032/–0.032
275–500	6.1	± 0.6	1.1/–1.1	0.0470	± 0.0043	0.0068/–0.0065

Table 17: Absolute and normalised differential $\bar{t}q$ production cross-sections as a function of $p_T(\bar{t})$.

$p_T(\bar{t})$ [GeV]	$\frac{d\sigma_{\bar{t}q}}{dp_T(\bar{t})}$ [fb GeV ⁻¹]			$\frac{1}{\sigma} \frac{d\sigma_{\bar{t}q}}{dp_T(\bar{t})}$ [10^{-3} GeV ⁻¹]		
	stat.	syst.		stat.	syst.	
0–45	649	± 16	76/–71	8.05	± 0.20	0.56/–0.51
45–65	815	± 14	60/–57	10.11	± 0.18	0.34/–0.34
65–95	526	± 10	40/–41	6.52	± 0.13	0.35/–0.41
95–135	269	± 8	20/–21	3.33	± 0.10	0.13/–0.18
135–175	112	± 6	16/–15	1.38	± 0.07	0.14/–0.14
175–215	50.1	± 3.8	6.9/–5.8	0.621	± 0.047	0.061/–0.058
215–275	20.6	± 2.3	3.4/–3.1	0.256	± 0.028	0.031/–0.030
275–500	3.42	± 0.47	0.87/–0.78	0.0425	± 0.0058	0.0091/–0.0082

Table 18: Absolute and normalised differential tq production cross-sections as a function of $|y(t)|$.

$ y(t) $	$\frac{d\sigma_{tq}}{d y(t) }$ [pb]			$\frac{1}{\sigma} \frac{d\sigma_{tq}}{d y(t) }$		
	stat.	syst.		stat.	syst.	
0.0–0.25	69.7	± 1.2	4.6/–4.6	0.534	± 0.009	0.012/–0.020
0.25–0.6	67.7	± 0.9	5.2/–4.4	0.519	± 0.007	0.018/–0.011
0.6–1.0	62.0	± 1.0	4.5/–4.2	0.475	± 0.007	0.010/–0.013
1.0–1.45	54.1	± 1.0	3.6/–3.6	0.414	± 0.008	0.011/–0.016
1.45–2.5	31.6	± 0.8	3.5/–3.1	0.2420	± 0.0064	0.0100/–0.0075

Table 19: Absolute and normalised differential $\bar{t}q$ production cross-sections as a function of $|y(\bar{t})|$.

$ y(\bar{t}) $	$\frac{d\sigma_{\bar{t}q}}{d y(\bar{t}) }$ [pb]			$\frac{1}{\sigma} \frac{d\sigma_{\bar{t}q}}{d y(\bar{t}) }$		
	stat.	syst.		stat.	syst.	
0.0–0.25	48.4	± 1.1	4.8/–4.9	0.592	± 0.014	0.025/–0.037
0.25–0.6	43.9	± 0.8	3.4/–3.3	0.538	± 0.010	0.017/–0.016
0.6–1.0	41.3	± 0.9	3.1/–2.4	0.506	± 0.011	0.025/–0.018
1.0–1.45	33.5	± 0.9	2.5/–2.2	0.410	± 0.011	0.018/–0.014
1.45–2.5	18.5	± 0.7	2.0/–2.2	0.2268	± 0.0084	0.0082/–0.0120

Table 20: Ratio of the absolute differential tq and $\bar{t}q$ production cross-sections as a function of $p_T(t$ or $\bar{t})$.

$p_T(t$ or $\bar{t})$ [GeV]	$\left(\frac{d\sigma(tq)}{dp_T(t)}\right)/\left(\frac{d\sigma(\bar{t}q)}{dp_T(\bar{t})}\right)$		
	stat.	syst.	
0–45	1.573	± 0.048	0.137/–0.172
45–65	1.634	± 0.035	0.063/–0.081
65–95	1.683	± 0.039	0.072/–0.047
95–135	1.766	± 0.060	0.059/–0.049
135–175	1.86	± 0.11	0.17/–0.13
175–215	1.96	± 0.18	0.11/–0.16
215–275	2.06	± 0.26	0.20/–0.18
275–500	2.26	± 0.36	0.23/–0.25

Table 21: Ratio of the absolute differential tq and $\bar{t}q$ production cross-sections as a function of $|y(t \text{ or } \bar{t})|$.

$ y(t \text{ or } \bar{t}) $	$(\frac{d\sigma(tq)}{d y(t) })/(\frac{d\sigma(\bar{t}q)}{d y(\bar{t}) })$		
	stat.		syst.
0.0–0.25	1.507	± 0.043	0.085/–0.085
0.25–0.6	1.525	± 0.034	0.083/–0.060
0.6–1.0	1.562	± 0.040	0.065/–0.099
1.0–1.45	1.642	± 0.052	0.050/–0.083
1.45–2.5	1.90	± 0.08	0.17/–0.16

EFT interpretation

Table 22: Best fit results for the expected relative change in the differential tq and $\bar{t}q$ cross-sections as a function of $C_{Qq}^{3,1}/\Lambda^2$. The predictions for the expected relative change are obtained by unfolding the distributions of the EFT MC samples with the nominal migration matrix and efficiency. The parameterisations are determined from least-square fits to the predictions normalised to the prediction from the EFT MC sample generated with $C_{Qq}^{3,1}/\Lambda^2$ set to zero. According to Eq. (1), the parameterisations take the form $\Delta\tilde{\sigma}_{(t \text{ or } \bar{t})}(C_{Qq}^{3,1}/\Lambda^2) = (1 + a_1 \cdot C_{Qq}^{3,1}/\Lambda^2 + a_2 \cdot (C_{Qq}^{3,1}/\Lambda^2)^2)$

$p_T(t) \text{ or } p_T(\bar{t}) \text{ range}$	$\Delta\tilde{\sigma}_{tq}(C_{Qq}^{3,1}/\Lambda^2)$		$\Delta\tilde{\sigma}_{\bar{t}q}(C_{Qq}^{3,1}/\Lambda^2)$	
	a_1	a_2	a_1	a_2
$0 \text{ GeV} \leq p_T(t) \text{ or } p_T(\bar{t}) \leq 45 \text{ GeV}$	–0.175	0.0	–0.260	+0.142
$45 \text{ GeV} \leq p_T(t) \text{ or } p_T(\bar{t}) \leq 65 \text{ GeV}$	–0.145	0.0	–0.205	+0.187
$65 \text{ GeV} \leq p_T(t) \text{ or } p_T(\bar{t}) \leq 95 \text{ GeV}$	–0.263	+0.050	–0.216	+0.014
$95 \text{ GeV} \leq p_T(t) \text{ or } p_T(\bar{t}) \leq 135 \text{ GeV}$	–0.389	0.0	–0.429	+0.063
$135 \text{ GeV} \leq p_T(t) \text{ or } p_T(\bar{t}) \leq 175 \text{ GeV}$	–0.735	+0.143	–0.593	+0.231
$175 \text{ GeV} \leq p_T(t) \text{ or } p_T(\bar{t}) \leq 215 \text{ GeV}$	–0.813	+0.099	–1.107	+0.695
$215 \text{ GeV} \leq p_T(t) \text{ or } p_T(\bar{t}) \leq 275 \text{ GeV}$	–0.897	+0.043	–1.184	+0.640
$275 \text{ GeV} \leq p_T(t) \text{ or } p_T(\bar{t}) \leq 500 \text{ GeV}$	–2.452	+1.694	–2.576	+3.426

References

- [1] D0 Collaboration, *Observation of Single Top-Quark Production*, *Phys. Rev. Lett.* **103** (2009) 092001, arXiv: [0903.0850](#).
- [2] CDF Collaboration, *Observation of Electroweak Single Top-Quark Production*, *Phys. Rev. Lett.* **103** (2009) 092002, arXiv: [0903.0885](#).
- [3] A. Giammanco and R. Schwienhorst, *Single top-quark production at the Tevatron and the LHC*, *Rev. Mod. Phys.* **90** (2018) 035001, arXiv: [1710.10699](#).
- [4] ATLAS Collaboration, *Measurement of t -channel single-top-quark production in pp collisions at $\sqrt{s} = 5.02$ TeV with the ATLAS detector*, *Phys. Lett. B* **854** (2024) 138726, arXiv: [2310.01518 \[hep-ex\]](#).
- [5] ATLAS Collaboration, *Comprehensive measurements of t -channel single top-quark production cross sections at $\sqrt{s} = 7$ TeV with the ATLAS detector*, *Phys. Rev. D* **90** (2014) 112006, arXiv: [1406.7844 \[hep-ex\]](#).
- [6] CMS Collaboration, *Measurement of the single-top-quark t -channel cross section in pp collisions at $\sqrt{s} = 7$ TeV*, *JHEP* **12** (2012) 035, arXiv: [1209.4533 \[hep-ex\]](#).
- [7] ATLAS Collaboration, *Fiducial, total and differential cross-section measurements of t -channel single top-quark production in pp collisions at 8 TeV using data collected by the ATLAS detector*, *Eur. Phys. J. C* **77** (2017) 531, arXiv: [1702.02859 \[hep-ex\]](#).
- [8] CMS Collaboration, *Measurement of the t -channel single-top-quark production cross section and of the $|V_{tb}|$ CKM matrix element in pp collisions at $\sqrt{s} = 8$ TeV*, *JHEP* **06** (2014) 090, arXiv: [1403.7366 \[hep-ex\]](#).
- [9] ATLAS Collaboration, *Measurement of t -channel production of single top quarks and antiquarks in pp collisions at 13 TeV using the full ATLAS Run 2 data sample*, *JHEP* **05** (2024) 305, arXiv: [2403.02126 \[hep-ex\]](#), Erratum: *JHEP* **06** (2025) 024.
- [10] CMS Collaboration, *Measurement of the single top quark and antiquark production cross sections in the t channel and their ratio in proton–proton collisions at $\sqrt{s} = 13$ TeV*, *Phys. Lett. B* **800** (2020) 135042, arXiv: [1812.10514 \[hep-ex\]](#).
- [11] CMS Collaboration, *Measurement of differential cross sections and charge ratios for t -channel single top quark production in proton–proton collisions at $\sqrt{s} = 13$ TeV*, *Eur. Phys. J. C* **80** (2020) 370, arXiv: [1907.08330 \[hep-ex\]](#).
- [12] G. D’Agostini, *A multidimensional unfolding method based on Bayes’ theorem*, *Nucl. Instrum. Meth. A* **362** (1995) 487.
- [13] J. Campbell and T. Neumann, *Precision Phenomenology with MCFM*, *JHEP* **12** (2019) 034, arXiv: [1909.09117 \[hep-ph\]](#).
- [14] E. R. Nocera, M. Ubiali and C. Voisey, *Single top production in PDF fits*, *JHEP* **2020** (2020) 67, arXiv: [1912.09543](#).
- [15] N. P. Hartland et al., *A Monte Carlo global analysis of the Standard Model Effective Field Theory: the top quark sector*, *JHEP* **2019** (2019) 100, arXiv: [1901.05965](#).
- [16] C. Degrande et al., *Automated one-loop computations in the standard model effective field theory*, *Phys. Rev. D* **103** (2021) 096024, arXiv: [2008.11743 \[hep-ph\]](#).

- [17] M. de Beurs, E. Laenen, M. Vreeswijk and E. Vryonidou, *Effective operators in t -channel single top production and decay*, *Eur. Phys. J. C* **78** (2018) 919, arXiv: [1807.03576 \[hep-ph\]](#).
- [18] ATLAS Collaboration, *The ATLAS Experiment at the CERN Large Hadron Collider*, *JINST* **3** (2008) S08003.
- [19] G. Avoni et al., *The new LUCID-2 detector for luminosity measurement and monitoring in ATLAS*, *JINST* **13** (2018) P07017.
- [20] ATLAS Collaboration, *Performance of the ATLAS trigger system in 2015*, *Eur. Phys. J. C* **77** (2017) 317, arXiv: [1611.09661 \[hep-ex\]](#).
- [21] ATLAS Collaboration, *Software and computing for Run 3 of the ATLAS experiment at the LHC*, *Eur. Phys. J. C* **85** (2025) 234, arXiv: [2404.06335 \[hep-ex\]](#),
Erratum: *Eur. Phys. J. C* **85** (2025) 907.
- [22] ATLAS Collaboration, *ATLAS data quality operations and performance for 2015–2018 data-taking*, *JINST* **15** (2020) P04003, arXiv: [1911.04632 \[physics.ins-det\]](#).
- [23] ATLAS Collaboration, *Luminosity determination in pp collisions at $\sqrt{s} = 13$ TeV using the ATLAS detector at the LHC*, *Eur. Phys. J. C* **83** (2023) 982, arXiv: [2212.09379 \[hep-ex\]](#).
- [24] ATLAS Collaboration, *Performance of electron and photon triggers in ATLAS during LHC Run 2*, *Eur. Phys. J. C* **80** (2020) 47, arXiv: [1909.00761 \[hep-ex\]](#).
- [25] ATLAS Collaboration, *Performance of the ATLAS muon triggers in Run 2*, *JINST* **15** (2020) P09015, arXiv: [2004.13447 \[physics.ins-det\]](#).
- [26] S. Agostinelli et al., *GEANT4 – a simulation toolkit*, *Nucl. Instrum. Meth. A* **506** (2003) 250.
- [27] ATLAS Collaboration, *The ATLAS Simulation Infrastructure*, *Eur. Phys. J. C* **70** (2010) 823, arXiv: [1005.4568 \[physics.ins-det\]](#).
- [28] ATLAS Collaboration, *The simulation principle and performance of the ATLAS fast calorimeter simulation FastCaloSim*, ATL-PHYS-PUB-2010-013, 2010, URL: <https://cds.cern.ch/record/1300517>.
- [29] W. Lukas, *Fast Simulation for ATLAS: Atlfast-II and ISF*, *J. Phys.: Conf. Ser.* **396** (2012) 022031.
- [30] P. Nason, *A new method for combining NLO QCD with shower Monte Carlo algorithms*, *JHEP* **11** (2004) 040, arXiv: [hep-ph/0409146](#).
- [31] S. Frixione, G. Ridolfi and P. Nason, *A positive-weight next-to-leading-order Monte Carlo for heavy flavour hadroproduction*, *JHEP* **09** (2007) 126, arXiv: [0707.3088 \[hep-ph\]](#).
- [32] S. Frixione, P. Nason and C. Oleari, *Matching NLO QCD computations with parton shower simulations: the POWHEG method*, *JHEP* **11** (2007) 070, arXiv: [0709.2092 \[hep-ph\]](#).
- [33] S. Alioli, P. Nason, C. Oleari and E. Re, *NLO single-top production matched with shower in POWHEG: s - and t -channel contributions*, *JHEP* **09** (2009) 111, arXiv: [0907.4076 \[hep-ph\]](#), Erratum: *JHEP* **02** (2010) 011.
- [34] S. Alioli, P. Nason, C. Oleari and E. Re, *A general framework for implementing NLO calculations in shower Monte Carlo programs: the POWHEG BOX*, *JHEP* **06** (2010) 043, arXiv: [1002.2581 \[hep-ph\]](#).

- [35] E. Re, *Single-top Wt -channel production matched with parton showers using the POWHEG method*, *Eur. Phys. J. C* **71** (2011) 1547, arXiv: [1009.2450 \[hep-ph\]](#).
- [36] R. Frederix, E. Re and P. Torrielli, *Single-top t -channel hadroproduction in the four-flavour scheme with POWHEG and aMC@NLO*, *JHEP* **09** (2012) 130, arXiv: [1207.5391 \[hep-ph\]](#).
- [37] NNPDF Collaboration, R. D. Ball et al., *Parton distributions for the LHC run II*, *JHEP* **04** (2015) 040, arXiv: [1410.8849 \[hep-ph\]](#).
- [38] T. Sjöstrand, S. Mrenna and P. Skands, *A brief introduction to PYTHIA 8.1*, *Comput. Phys. Commun.* **178** (2008) 852, arXiv: [0710.3820 \[hep-ph\]](#).
- [39] ATLAS Collaboration, *ATLAS Pythia 8 tunes to 7 TeV data*, ATL-PHYS-PUB-2014-021, 2014, URL: <https://cds.cern.ch/record/1966419>.
- [40] NNPDF Collaboration, R. D. Ball et al., *Parton distributions with LHC data*, *Nucl. Phys. B* **867** (2013) 244, arXiv: [1207.1303 \[hep-ph\]](#).
- [41] S. Frixione, E. Laenen, P. Motylinski, C. White and B. R. Webber, *Single-top hadroproduction in association with a W boson*, *JHEP* **07** (2008) 029, arXiv: [0805.3067 \[hep-ph\]](#).
- [42] ATLAS Collaboration, *Studies on top-quark Monte Carlo modelling for Top2016*, ATL-PHYS-PUB-2016-020, 2016, URL: <https://cds.cern.ch/record/2216168>.
- [43] D. J. Lange, *The EvtGen particle decay simulation package*, *Nucl. Instrum. Meth. A* **462** (2001) 152.
- [44] E. Bothmann et al., *Event generation with Sherpa 2.2*, *SciPost Phys.* **7** (2019) 034, arXiv: [1905.09127 \[hep-ph\]](#).
- [45] S. Schumann and F. Krauss, *A parton shower algorithm based on Catani–Seymour dipole factorisation*, *JHEP* **03** (2008) 038, arXiv: [0709.1027 \[hep-ph\]](#).
- [46] J.-C. Winter, F. Krauss and G. Soff, *A modified cluster-hadronisation model*, *Eur. Phys. J. C* **36** (2004) 381, arXiv: [hep-ph/0311085](#).
- [47] C. Anastasiou, L. Dixon, K. Melnikov and F. Petriello, *High-precision QCD at hadron colliders: Electroweak gauge boson rapidity distributions at next-to-next-to leading order*, *Phys. Rev. D* **69** (2004) 094008, arXiv: [hep-ph/0312266](#).
- [48] R. Gavin, Y. Li, F. Petriello and S. Quackenbush, *FEWZ 2.0: A code for hadronic Z production at next-to-next-to-leading order*, *Comput. Phys. Commun.* **182** (2011) 2388, arXiv: [1011.3540 \[hep-ph\]](#).
- [49] S. Quackenbush, R. Gavin, Y. Li and F. Petriello, *W physics at the LHC with FEWZ 2.1*, *Comput. Phys. Commun.* **184** (2013) 209, arXiv: [1201.5896](#).
- [50] J. Campbell, T. Neumann and Z. Sullivan, *Single-top-quark production in the t -channel at NNLO*, *JHEP* **02** (2021) 040, arXiv: [2012.01574 \[hep-ph\]](#).
- [51] J. Campbell, T. Neumann and Z. Sullivan, *Testing parton distribution functions with t -channel single-top-quark production*, *Phys. Rev. D* **104** (2021) 094042, arXiv: [2109.10448 \[hep-ph\]](#).

- [52] ATLAS and CMS Collaborations, *Reference Single Top-Quark Cross-Sections for ATLAS and CMS Analyses*, ATL-PHYS-PUB-2025-035, 2025, URL: <https://cds.cern.ch/record/2942746>.
- [53] J. Alwall et al., *The automated computation of tree-level and next-to-leading order differential cross sections, and their matching to parton shower simulations*, *JHEP* **07** (2014) 079, arXiv: [1405.0301](https://arxiv.org/abs/1405.0301) [hep-ph].
- [54] M. Bähr et al., *Herwig++ physics and manual*, *Eur. Phys. J. C* **58** (2008) 639, arXiv: [0803.0883](https://arxiv.org/abs/0803.0883) [hep-ph].
- [55] J. Bellm et al., *Herwig 7.0/Herwig++ 3.0 release note*, *Eur. Phys. J. C* **76** (2016) 196, arXiv: [1512.01178](https://arxiv.org/abs/1512.01178) [hep-ph].
- [56] S. Alekhin, J. Blümlein, S. Moch and R. Plačákytė, *Parton distribution functions, α_s , and heavy-quark masses for LHC Run II*, *Phys. Rev. D* **96** (2017) 014011, arXiv: [1701.05838](https://arxiv.org/abs/1701.05838) [hep-ph].
- [57] T.-J. Hou et al., *Progress in the CTEQ-TEA NNLO global QCD analysis*, (2019), arXiv: [1908.11394](https://arxiv.org/abs/1908.11394) [hep-ph].
- [58] S. Bailey, T. Cridge, L. A. Harland-Lang, A. D. Martin and R. S. Thorne, *Parton distributions from LHC, HERA, Tevatron and fixed target data: MSHT20 PDFs*, *Eur. Phys. J. C* **81** (2021) 341, arXiv: [2012.04684](https://arxiv.org/abs/2012.04684) [hep-ph].
- [59] R. D. Ball et al., *Parton distributions from high-precision collider data*, *Eur. Phys. J. C* **77** (2017) 663, arXiv: [1706.00428](https://arxiv.org/abs/1706.00428) [hep-ph].
- [60] NNPDF Collaboration, R. D. Ball et al., *The path to proton structure at 1% accuracy*, *Eur. Phys. J. C* **82** (2022) 428, arXiv: [2109.02653](https://arxiv.org/abs/2109.02653) [hep-ph].
- [61] H1 and ZEUS Collaborations, *Combination of measurements of inclusive deep inelastic $e^\pm p$ scattering cross sections and QCD analysis of HERA data*, *Eur. Phys. J. C* **75** (2015) 580, arXiv: [1506.06042](https://arxiv.org/abs/1506.06042) [hep-ex].
- [62] ATLAS Collaboration, *Precision measurement and interpretation of inclusive W^+ , W^- and Z/γ^* production cross sections with the ATLAS detector*, *Eur. Phys. J. C* **77** (2017) 367, arXiv: [1612.03016](https://arxiv.org/abs/1612.03016) [hep-ex].
- [63] ATLAS Collaboration, *Determination of the parton distribution functions of the proton using diverse ATLAS data from pp collisions at $\sqrt{s} = 7, 8$ and 13 TeV*, *Eur. Phys. J. C* **82** (2022) 438, arXiv: [2112.11266](https://arxiv.org/abs/2112.11266) [hep-ex].
- [64] A. Buckley et al., *LHAPDF6: parton density access in the LHC precision era*, *Eur. Phys. J. C* **75** (2015) 132, arXiv: [1412.7420](https://arxiv.org/abs/1412.7420).
- [65] ATLAS Collaboration, *Electron and photon performance measurements with the ATLAS detector using the 2015–2017 LHC proton–proton collision data*, *JINST* **14** (2019) P12006, arXiv: [1908.00005](https://arxiv.org/abs/1908.00005) [hep-ex].
- [66] ATLAS Collaboration, *Muon reconstruction and identification efficiency in ATLAS using the full Run 2 pp collision data set at $\sqrt{s} = 13$ TeV*, *Eur. Phys. J. C* **81** (2021) 578, arXiv: [2012.00578](https://arxiv.org/abs/2012.00578) [hep-ex].
- [67] ATLAS Collaboration, *Jet reconstruction and performance using particle flow with the ATLAS Detector*, *Eur. Phys. J. C* **77** (2017) 466, arXiv: [1703.10485](https://arxiv.org/abs/1703.10485) [hep-ex].

- [68] M. Cacciari, G. P. Salam and G. Soyez, *The anti- k_t jet clustering algorithm*, *JHEP* **04** (2008) 063, arXiv: [0802.1189 \[hep-ph\]](#).
- [69] M. Cacciari, G. P. Salam and G. Soyez, *FastJet user manual*, *Eur. Phys. J. C* **72** (2012) 1896, arXiv: [1111.6097 \[hep-ph\]](#).
- [70] ATLAS Collaboration, *Jet energy scale and resolution measured in proton–proton collisions at $\sqrt{s} = 13$ TeV with the ATLAS detector*, *Eur. Phys. J. C* **81** (2021) 689, arXiv: [2007.02645 \[hep-ex\]](#).
- [71] ATLAS Collaboration, *Performance of pile-up mitigation techniques for jets in pp collisions at $\sqrt{s} = 8$ TeV using the ATLAS detector*, *Eur. Phys. J. C* **76** (2016) 581, arXiv: [1510.03823 \[hep-ex\]](#).
- [72] ATLAS Collaboration, *Identification and rejection of pile-up jets at high pseudorapidity with the ATLAS detector*, *Eur. Phys. J. C* **77** (2017) 580, arXiv: [1705.02211 \[hep-ex\]](#), Erratum: *Eur. Phys. J. C* **77** (2017) 712.
- [73] ATLAS Collaboration, *ATLAS flavour-tagging algorithms for the LHC Run 2 pp collision dataset*, *Eur. Phys. J. C* **83** (2023) 681, arXiv: [2211.16345 \[physics.data-an\]](#).
- [74] ATLAS Collaboration, *Performance of missing transverse momentum reconstruction with the ATLAS detector using proton–proton collisions at $\sqrt{s} = 13$ TeV*, *Eur. Phys. J. C* **78** (2018) 903, arXiv: [1802.08168 \[hep-ex\]](#).
- [75] Particle Data Group, *Review of Particle Physics*, *PTEP* **2022** (2022) 083C01.
- [76] T. Chwalek, *Measurement of W-Boson Helicity-Fractions in Top-Quark Decays with the CDF II Experiment and Prospects for an Early $t\bar{t}$ Cross-Section Measurement with the CMS Experiment*, Ph.D. Thesis, Karlsruhe U., IEKP-KA-2010-05, FERMILAB-THESIS-2010-74, CERN-THESIS-2010-255, 2010, URL: <https://cds.cern.ch/record/1416031>.
- [77] M. Feindt, *A Neural Bayesian Estimator for Conditional Probability Densities*, IEKP-KA/04-05, 2004, arXiv: [physics/0402093 \[physics.data-an\]](#).
- [78] M. Feindt and U. Kerzel, *The NeuroBayes neural network package*, *Nucl. Instrum. Meth. A* **559** (2006) 190.
- [79] ATLAS Collaboration, *Estimation of non-prompt and fake lepton backgrounds in final states with top quarks produced in proton–proton collisions at $\sqrt{s} = 8$ TeV with the ATLAS Detector*, ATLAS-CONF-2014-058, 2014, URL: <https://cds.cern.ch/record/1951336>.
- [80] ATLAS Collaboration, *Search for flavour-changing neutral-current interactions of a top quark and a gluon in pp collisions at $\sqrt{s} = 13$ TeV with the ATLAS detector*, *Eur. Phys. J. C* **82** (2022) 334, arXiv: [2112.01302 \[hep-ex\]](#).
- [81] T. Auye, ‘Unfolding algorithms and tests using RooUnfold’, *Proceedings, 2011 Workshop on Statistical Issues Related to Discovery Claims in Search Experiments and Unfolding (PHYSTAT 2011)* (CERN, Geneva, Switzerland, 17th–20th Jan. 2011) 313, arXiv: [1105.1160 \[physics.data-an\]](#).
- [82] ATLAS Collaboration, *Electron and photon energy calibration with the ATLAS detector using LHC Run 2 data*, *JINST* **19** (2024) P02009, arXiv: [2309.05471 \[hep-ex\]](#).

- [83] ATLAS Collaboration, *Studies of the muon momentum calibration and performance of the ATLAS detector with pp collisions at $\sqrt{s} = 13$ TeV*, *Eur. Phys. J. C* **83** (2023) 686, arXiv: [2212.07338 \[hep-ex\]](#).
- [84] ATLAS Collaboration, *ATLAS b -jet identification performance and efficiency measurement with $t\bar{t}$ events in pp collisions at $\sqrt{s} = 13$ TeV*, *Eur. Phys. J. C* **79** (2019) 970, arXiv: [1907.05120 \[hep-ex\]](#).
- [85] ATLAS Collaboration, *Measurement of the c -jet mistagging efficiency in $t\bar{t}$ events using pp collision data at $\sqrt{s} = 13$ TeV collected with the ATLAS detector*, *Eur. Phys. J. C* **82** (2022) 95, arXiv: [2109.10627 \[hep-ex\]](#).
- [86] ATLAS Collaboration, *Calibration of the light-flavour jet mistagging efficiency of the b -tagging algorithms with Z +jets events using 139 fb^{-1} of ATLAS proton–proton collision data at $\sqrt{s} = 13$ TeV*, *Eur. Phys. J. C* **83** (2023) 728, arXiv: [2301.06319 \[hep-ex\]](#).
- [87] S. Höche, S. Mrenna, S. Payne, C. T. Preuss and P. Skands, *A Study of QCD Radiation in VBF Higgs Production with Vincia and Pythia*, *SciPost Phys.* **12** (2022) 010, arXiv: [2106.10987 \[hep-ph\]](#).
- [88] J. Butterworth et al., *PDF4LHC recommendations for LHC Run II*, *J. Phys. G* **43** (2016) 023001, arXiv: [1510.03865 \[hep-ph\]](#).
- [89] ATLAS Collaboration, *Evaluating statistical uncertainties and correlations using the bootstrap method*, ATL-PHYS-PUB-2021-011, 2021, URL: <https://cds.cern.ch/record/2759945>.
- [90] TopFitter collaboration, *Constraining top quark effective theory in the LHC Run II era*, *JHEP* **4** (2016) 15, arXiv: [1512.03360 \[hep-ph\]](#).
- [91] B. Grzadkowski, M. Iskrzyński, M. Misiak and J. Rosiek, *Dimension-six terms in the Standard Model Lagrangian*, *JHEP* **2010** (2010) 85, arXiv: [1008.4884](#).
- [92] ATLAS Collaboration, *Constraints on effective field theories via quadruple-differential angular decay rates from t -channel single-top-quark production at $\sqrt{s} = 13$ TeV with the ATLAS detector*, (2025), arXiv: [2510.23372 \[hep-ex\]](#).
- [93] N. Castro, J. Erdmann, C. Grunwald, K. Kröninger and N.-A. Rosien, *EFTfitter: a tool for interpreting measurements in the context of effective field theories*, *Eur. Phys. J. C* **76** (2016) 432, arXiv: [1605.05585](#).
- [94] ATLAS Collaboration, *ATLAS Computing Acknowledgements*, ATL-SOFT-PUB-2025-001, 2025, URL: <https://cds.cern.ch/record/2922210>.

The ATLAS Collaboration

G. Aad ¹⁰³, E. Aakvaag ¹⁷, B. Abbott ¹²², S. Abdelhameed ^{118a}, K. Abeling ⁵⁵, N.J. Abicht ⁴⁹, S.H. Abidi ³⁰, M. Aboeela ⁴⁵, A. Aboulhorma ^{36e}, H. Abramowicz ¹⁵⁶, Y. Abulaiti ¹¹⁹, B.S. Acharya ^{69a,69b,m}, A. Ackermann ^{63a}, C. Adam Bourdarios ⁴, L. Adamczyk ^{86a}, S.V. Addepalli ¹⁴⁸, M.J. Addison ¹⁰², J. Adelman ¹¹⁷, A. Adiguzel ^{22c}, T. Adye ¹³⁶, A.A. Affolder ¹³⁸, Y. Afik ⁴⁰, M.N. Agaras ¹³, A. Aggarwal ¹⁰¹, C. Agheorghiesei ^{28c}, F. Ahmadov ^{39,ad}, S. Ahuja ⁹⁶, S. Ahuja ¹⁶⁸, X. Ai ^{142b}, G. Aielli ^{76a,76b}, A. Aikot ¹⁶⁸, M. Ait Tamliah ^{36e}, B. Aitbenkikh ^{36a}, T.P.A. Åkesson ⁹⁹, A.V. Akimov ¹⁵⁰, D. Akiyama ¹⁷³, N.N. Akolkar ²⁵, S. Aktas ¹⁷¹, G.L. Alberghi ^{24b}, J. Albert ¹⁷⁰, U. Alberti ²⁰, P. Albicocco ⁵³, G.L. Albouy ⁶⁰, S. Alderweireldt ⁵², Z.L. Alegria ¹²³, M. Aleksa ³⁷, I.N. Aleksandrov ³⁹, C. Alexa ^{28b}, T. Alexopoulos ¹⁰, F. Alfonsi ^{24b}, M. Algren ⁵⁶, M. Alhroob ¹⁷², B. Ali ¹³⁴, H.M.J. Ali ^{92,w}, S. Ali ³², S.W. Alibocus ⁹³, M. Aliev ^{34c}, G. Alimonti ^{71a}, W. Alkahi ⁵⁵, C. Allaire ⁶⁶, B.M.M. Allbrooke ¹⁵¹, D.R. Allen ¹²³, J.S. Allen ¹⁰², J.F. Allen ⁵², P.P. Allport ²¹, A. Aloisio ^{72a,72b}, F. Alonso ⁹¹, C. Alpigiani ¹⁴¹, Z.M.K. Alsolami ⁹², A. Alvarez Fernandez ¹⁰¹, M. Alves Cardoso ⁵⁶, M.G. Alviggi ^{72a,72b}, M. Aly ¹⁰², Y. Amaral Coutinho ^{82b}, A. Ambler ¹⁰⁵, C. Amelung ³⁷, M. Amerl ¹⁰², C.G. Ames ¹¹⁰, T. Amezza ¹²⁹, D. Amidei ¹⁰⁷, B. Amini ⁵⁴, K. Amirie ¹⁶⁰, A. Amirkhanov ³⁹, S.P. Amor Dos Santos ^{132a}, K.R. Amos ¹⁶⁸, D. Amperiadou ¹⁵⁷, S. An ⁸³, C. Anastopoulos ¹⁴⁴, T. Andeen ¹¹, J.K. Anders ⁹³, A.C. Anderson ⁵⁹, A. Andreatza ^{71a,71b}, S. Angelidakis ⁹, A. Angerami ⁴², A.V. Anisenkov ³⁹, A. Annovi ^{74a}, C. Antel ³⁷, E. Antipov ¹⁵⁰, M. Antonelli ⁵³, F. Anulli ^{75a}, M. Aoki ⁸³, T. Aoki ¹⁵⁸, M.A. Aparo ¹⁵¹, L. Aperio Bella ⁴⁸, M. Apicella ³¹, C. Appelt ¹⁵⁶, A. Apyan ²⁷, M. Arampatzis ¹⁰, S.J. Arbiol Val ⁸⁷, C. Arcangeletti ⁵³, A.T.H. Arce ⁵¹, J-F. Arguin ¹⁰⁹, S. Argyropoulos ¹⁵⁷, J.-H. Arling ⁴⁸, O. Arnaez ⁴, H. Arnold ¹⁵⁰, G. Artoni ^{75a,75b}, H. Asada ¹¹², K. Asai ¹²⁰, S. Asatryan ¹⁷⁸, N.A. Asbah ³⁷, R.A. Ashby Pickering ¹⁷², A.M. Aslam ⁹⁶, K. Assamagan ³⁰, R. Astalos ^{29a}, K.S.V. Astrand ⁹⁹, S. Atashi ¹⁶⁴, R.J. Atkin ^{34a}, H. Atmani ^{36f}, P.A. Atlasiddha ¹³⁰, K. Augsten ¹³⁴, A.D. Auriol ⁴¹, V.A. Austrup ¹⁰², A.S. Avad ⁹⁵, G. Avolio ³⁷, K. Axiotis ⁵⁶, A. Azzam ¹³, D. Babal ^{29b}, H. Bachacou ¹³⁷, K. Bachas ^{157,q}, A. Bachi ³⁵, E. Bachmann ⁵⁰, M.J. Backes ^{63a}, A. Badea ⁴⁰, T.M. Baer ¹⁰⁷, P. Bagnaia ^{75a,75b}, M. Bahmani ¹⁹, D. Bahner ⁵⁴, K. Bai ¹²⁵, J.T. Baines ¹³⁶, L. Baines ⁹⁵, O.K. Baker ¹⁷⁷, E. Bakos ¹⁶, D. Bakshi Gupta ⁸, L.E. Balabram Filho ^{82b}, V. Balakrishnan ¹²², R. Balasubramanian ⁴, E.M. Baldin ³⁸, P. Balek ^{86a}, E. Ballabene ^{24b,24a}, F. Balli ¹³⁷, L.M. Baltes ^{63a}, W.K. Balunas ³³, J. Balz ¹⁰¹, I. Bamwidhi ^{118b}, E. Banas ⁸⁷, M. Bandieramonte ¹³¹, A. Bandyopadhyay ²⁵, S. Bansal ²⁵, L. Barak ¹⁵⁶, M. Barakat ⁴⁸, E.L. Barberio ¹⁰⁶, D. Barberis ^{18b}, M. Barbero ¹⁰³, M.Z. Barel ¹¹⁶, T. Barillari ¹¹¹, M-S. Barisits ³⁷, T. Barklow ¹⁴⁸, P. Baron ¹³⁵, D.A. Baron Moreno ¹⁰², A. Baroncelli ⁶², A.J. Barr ¹²⁸, J.D. Barr ⁹⁷, F. Barreiro ¹⁰⁰, J. Barreiro Guimarães da Costa ¹⁴, M.G. Barros Teixeira ^{132a}, S. Barsov ³⁸, F. Bartels ^{63a}, R. Bartoldus ¹⁴⁸, A.E. Barton ⁹², P. Bartos ^{29a}, M. Baselga ⁴⁹, S. Bashiri ⁸⁷, A. Bassalat ^{66,b}, M.J. Basso ^{161a}, S. Bataju ⁴⁵, R. Bate ¹⁶⁹, R.L. Bates ⁵⁹, S. Batlamous ¹⁰⁰, M. Battaglia ¹³⁸, D. Battulga ¹⁹, M. Baue ^{75a,75b}, M. Bauer ⁷⁹, P. Bauer ²⁵, L.T. Bayer ⁴⁸, L.T. Bazzano Hurrell ³¹, J.B. Beacham ¹¹¹, T. Beau ¹²⁹, J.Y. Beauchamp ⁹¹, P.H. Beauchemin ¹⁶³, P. Bechtel ²⁵, H.P. Beck ^{20,p}, K. Becker ¹⁷², A.J. Beddall ⁸¹, V.A. Bednyakov ³⁹, C.P. Bee ¹⁵⁰, L.J. Beemster ¹⁶, M. Begalli ^{82d}, M. Begel ³⁰, J.K. Behr ⁴⁸, J.F. Beirer ³⁷, F. Beisiegel ²⁵, M. Belfkir ^{118b}, G. Bella ¹⁵⁶, L. Bellagamba ^{24b}, A. Bellerive ³⁵, C.D. Bellgraph ⁶⁸, P. Bellos ²¹, K. Beloborodov ³⁸, I. Benaoumeur ²¹, D. Benckroun ^{36a}, F. Bendebba ^{36a}, Y. Benhammou ¹⁵⁶, K.C. Benkendorfer ⁶¹, L. Beresford ⁴⁸,

M. Beretta [id⁵³](#), E. Bergeaas Kuutmann [id¹⁶⁶](#), N. Berger [id⁴](#), B. Bergmann [id¹³⁴](#), J. Beringer [id^{18a}](#),
G. Bernardi [id⁵](#), C. Bernius [id¹⁴⁸](#), F.U. Bernlochner [id²⁵](#), A. Berrocal Guardia [id¹³](#), T. Berry [id⁹⁶](#),
P. Berta [id¹³⁵](#), A. Berti [id^{132a}](#), R. Bertrand [id¹⁰³](#), S. Bethke [id¹¹¹](#), A. Betti [id^{75a,75b}](#), A.J. Bevan [id⁹⁵](#),
L. Bezio [id⁵⁶](#), N.K. Bhalla [id⁵⁴](#), S. Bharthuar [id¹¹¹](#), S. Bhatta [id¹⁵⁰](#), P. Bhattarai [id¹⁴⁸](#), Z.M. Bhatti [id¹¹⁹](#),
K.D. Bhide [id⁵⁴](#), V.S. Bhopatkar [id¹²³](#), R.M. Bianchi [id¹³¹](#), G. Bianco [id^{24b,24a}](#), O. Biebel [id¹¹⁰](#),
M. Biglietti [id^{77a}](#), C.S. Billingsley [id⁴⁵](#), Y. Bimgdi [id^{36f}](#), M. Bindi [id⁵⁵](#), A. Bingham [id¹⁷⁶](#), A. Bingul [id^{22b}](#),
C. Bini [id^{75a,75b}](#), G.A. Bird [id³³](#), M. Birman [id¹⁷⁴](#), M. Biros [id¹³⁵](#), S. Biryukov [id¹⁵¹](#), T. Bisanz [id⁴⁹](#),
E. Bisceglie [id^{24b,24a}](#), J.P. Biswal [id¹³⁶](#), D. Biswas [id¹⁴⁶](#), I. Bloch [id⁴⁸](#), A. Blue [id⁵⁹](#), U. Blumenschein [id⁹⁵](#),
V.S. Bobrovnikov [id³⁹](#), L. Boccardo [id^{57b,57a}](#), M. Boehler [id⁵⁴](#), B. Boehm [id¹⁷¹](#), D. Bogavac [id¹³](#),
A.G. Bogdanchikov [id³⁸](#), L.S. Boggia [id¹²⁹](#), V. Boisvert [id⁹⁶](#), P. Bokan [id³⁷](#), T. Bold [id^{86a}](#), M. Bomben [id⁵](#),
M. Bona [id⁹⁵](#), M. Boonekamp [id¹³⁷](#), A.G. Borbély [id⁵⁹](#), I.S. Bordulev [id³⁸](#), G. Borissov [id⁹²](#),
D. Bortoletto [id¹²⁸](#), D. Boscherini [id^{24b}](#), M. Bosman [id¹³](#), K. Bouaouda [id^{36a}](#), N. Bouchhar [id¹⁶⁸](#),
L. Boudet [id⁴](#), J. Boudreau [id¹³¹](#), E.V. Bouhova-Thacker [id⁹²](#), D. Boumediene [id⁴¹](#), R. Bouquet [id^{57b,57a}](#),
A. Boveia [id¹²¹](#), J. Boyd [id³⁷](#), D. Boye [id³⁰](#), I.R. Boyko [id³⁹](#), L. Bozianu [id⁵⁶](#), J. Bracinik [id²¹](#),
N. Brahimi [id⁴](#), G. Brandt [id¹⁷⁶](#), O. Brandt [id³³](#), B. Brau [id¹⁰⁴](#), J.E. Brau [id¹²⁵](#), R. Brenner [id¹⁷⁴](#),
L. Brenner [id¹¹⁶](#), R. Brenner [id¹⁶⁶](#), S. Bressler [id¹⁷⁴](#), G. Brianti [id^{78a,78b}](#), D. Britton [id⁵⁹](#), D. Britzger [id¹¹¹](#),
I. Brock [id²⁵](#), R. Brock [id¹⁰⁸](#), G. Brooijmans [id⁴²](#), A.J. Brooks [id⁶⁸](#), E.M. Brooks [id^{161b}](#), E. Brost [id³⁰](#),
L.M. Brown [id^{170,161a}](#), L.E. Bruce [id⁶¹](#), T.L. Bruckler [id¹²⁸](#), P.A. Bruckman de Renstrom [id⁸⁷](#),
B. Brüers [id⁴⁸](#), A. Bruni [id^{24b}](#), G. Bruni [id^{24b}](#), D. Brunner [id^{47a,47b}](#), M. Bruschi [id^{24b}](#), N. Bruscino [id^{75a,75b}](#),
T. Buanes [id¹⁷](#), Q. Buat [id¹⁴¹](#), D. Buchin [id¹¹¹](#), A.G. Buckley [id⁵⁹](#), O. Bulekov [id⁸¹](#), B.A. Bullard [id¹⁴⁸](#),
S. Burdin [id⁹³](#), C.D. Burgard [id⁴⁹](#), A.M. Burger [id⁹⁰](#), B. Burghgrave [id⁸](#), O. Burlayenko [id⁵⁴](#),
J. Burleson [id¹⁶⁷](#), J.C. Burzynski [id¹⁴⁷](#), E.L. Busch [id⁴²](#), V. Büscher [id¹⁰¹](#), P.J. Bussey [id⁵⁹](#), O. But [id²⁵](#),
J.M. Butler [id²⁶](#), C.M. Buttar [id⁵⁹](#), J.M. Butterworth [id⁹⁷](#), P. Butti [id³⁷](#), W. Buttinger [id¹³⁶](#),
C.J. Buxo Vazquez [id¹⁰⁸](#), A.R. Buzykaev [id³⁹](#), S. Cabrera Urbán [id¹⁶⁸](#), L. Cadamuro [id⁶⁶](#), H. Cai [id³⁷](#),
Y. Cai [id^{24b,113c,24a}](#), Y. Cai [id^{113a}](#), V.M.M. Cairo [id³⁷](#), O. Cakir [id^{3a}](#), N. Calace [id³⁷](#), P. Calafiura [id^{18a}](#),
G. Calderini [id¹²⁹](#), P. Calfayan [id³⁵](#), L. Calic [id⁹⁹](#), G. Callea [id⁵⁹](#), L.P. Caloba [id^{82b}](#), D. Calvet [id⁴¹](#),
S. Calvet [id⁴¹](#), R. Camacho Toro [id¹²⁹](#), S. Camarda [id³⁷](#), D. Camarero Munoz [id²⁷](#), P. Camarri [id^{76a,76b}](#),
C. Camincher [id¹⁷⁰](#), M. Campanelli [id⁹⁷](#), A. Camplani [id⁴³](#), V. Canale [id^{72a,72b}](#), A.C. Canbay [id^{3a}](#),
E. Canonero [id⁹⁶](#), J. Cantero [id¹⁶⁸](#), Y. Cao [id¹⁶⁷](#), F. Capocasa [id²⁷](#), M. Capua [id^{44b,44a}](#), A. Carbone [id^{71a,71b}](#),
R. Cardarelli [id^{76a}](#), J.C.J. Cardenas [id⁸](#), M.P. Cardiff [id²⁷](#), G. Carducci [id^{44b,44a}](#), T. Carli [id³⁷](#),
G. Carlino [id^{72a}](#), J.I. Carlotto [id¹³](#), B.T. Carlson [id^{131,r}](#), E.M. Carlson [id¹⁷⁰](#), J. Carmignani [id⁹³](#),
L. Carminati [id^{71a,71b}](#), A. Carnelli [id⁴](#), M. Carnesale [id³⁷](#), S. Caron [id¹¹⁵](#), E. Carquin [id^{139g}](#), I.B. Carr [id¹⁰⁶](#),
S. Carrá [id^{73a,73b}](#), G. Carratta [id^{24b,24a}](#), C. Carrion Martinez [id¹⁶⁸](#), A.M. Carroll [id¹²⁵](#), M.P. Casado [id^{13,h}](#),
P. Casolaro [id^{72a,72b}](#), M. Caspar [id⁴⁸](#), W.R. Castiglioni [id⁴⁰](#), F.L. Castillo [id⁴](#), L. Castillo Garcia [id¹³](#),
V. Castillo Gimenez [id¹⁶⁸](#), N.F. Castro [id^{132a,132e}](#), A. Catinaccio [id³⁷](#), J.R. Catmore [id¹²⁷](#), T. Cavaliere [id⁴](#),
V. Cavaliere [id³⁰](#), L.J. Caviedes Betancourt [id^{23b}](#), E. Celebi [id⁸¹](#), S. Cella [id³⁷](#), V. Cepaitis [id⁵⁶](#),
K. Cerny [id¹²⁴](#), A.S. Cerqueira [id^{82a}](#), A. Cerri [id^{74a,am}](#), L. Cerrito [id^{76a,76b}](#), F. Cerutti [id^{18a}](#),
B. Cervato [id^{71a,71b}](#), A. Cervelli [id^{24b}](#), G. Cesarini [id⁵³](#), S.A. Cetin [id⁸¹](#), P.M. Chabrilat [id¹²⁹](#),
R. Chakkappai [id⁶⁶](#), S. Chakraborty [id¹⁷²](#), A. Chambers [id⁶¹](#), J. Chan [id^{18a}](#), W.Y. Chan [id¹⁵⁸](#),
J.D. Chapman [id³³](#), E. Chapon [id¹³⁷](#), B. Chargeishvili [id^{154b}](#), D.G. Charlton [id²¹](#), C. Chauhan [id¹³⁵](#),
Y. Che [id^{113a}](#), S. Chekanov [id⁶](#), G.A. Chelkov [id^{39,a}](#), B. Chen [id¹⁵⁶](#), B. Chen [id¹⁷⁰](#), H. Chen [id³⁰](#),
J. Chen [id^{143a}](#), J. Chen [id¹⁴⁷](#), M. Chen [id¹²⁸](#), S. Chen [id⁸⁸](#), S.J. Chen [id^{113a}](#), X. Chen [id^{143a}](#), X. Chen [id^{15,ah}](#),
Z. Chen [id⁶²](#), C.L. Cheng [id¹⁷⁵](#), H.C. Cheng [id^{64a}](#), S. Cheong [id¹⁴⁸](#), A. Cheplakov [id³⁹](#),
E. Cherepanova [id¹¹⁶](#), R. Cherkaoui El Moursli [id^{36e}](#), E. Cheu [id⁷](#), K. Cheung [id⁶⁵](#), L. Chevalier [id¹³⁷](#),
V. Chiarella [id⁵³](#), G. Chiarelli [id^{74a}](#), G. Chiodini [id^{70a}](#), A.S. Chisholm [id²¹](#), A. Chitan [id^{28b}](#),
M. Chitishvili [id¹⁶⁸](#), M.V. Chizhov [id^{39,s}](#), K. Choi [id¹¹](#), Y. Chou [id¹⁴¹](#), E.Y.S. Chow [id¹¹⁵](#), K.L. Chu [id¹⁷⁴](#),
M.C. Chu [id^{64a}](#), X. Chu [id^{14,113c}](#), Z. Chubinidze [id⁵³](#), J. Chudoba [id¹³³](#), J.J. Chwastowski [id⁸⁷](#),

D. Cieri ^{id111}, K.M. Ciesla ^{id86a}, V. Cindro ^{id94}, A. Ciocio ^{id18a}, F. Cirotto ^{id72a,72b}, Z.H. Citron ^{id174},
 M. Citterio ^{id71a}, D.A. Ciubotaru ^{id28b}, A. Clark ^{id56}, P.J. Clark ^{id52}, N. Clarke Hall ^{id97}, C. Clarry ^{id160},
 S.E. Clawson ^{id48}, C. Clement ^{id47a,47b}, L. Clissa ^{id24b,24a}, Y. Coadou ^{id103}, M. Cobal ^{id69a,69c},
 A. Coccaro ^{id57b}, R.F. Coelho Barrue ^{id132a}, R. Coelho Lopes De Sa ^{id104}, S. Coelli ^{id71a},
 M.M. Cohen ^{id130}, L.S. Colangeli ^{id160}, B. Cole ^{id42}, P. Collado Soto ^{id100}, J. Collot ^{id60},
 R. Coluccia ^{id70a,70b}, P. Conde Muiño ^{id132a,132g}, M.P. Connell ^{id34c}, S.H. Connell ^{id34c}, E.I. Conroy ^{id128},
 M. Contreras Cossio ^{id11}, F. Conventi ^{id72a,aj}, A.M. Cooper-Sarkar ^{id128}, L. Corazzina ^{id75a,75b},
 F.A. Corchia ^{id24b,24a}, A. Cordeiro Oudot Choi ^{id141}, L.D. Corpe ^{id41}, M. Corradi ^{id75a,75b},
 F. Corriveau ^{id105,ab}, A. Cortes-Gonzalez ^{id158}, M.J. Costa ^{id168}, F. Costanza ^{id4}, D. Costanzo ^{id144},
 J. Couthures ^{id4}, G. Cowan ^{id96}, K. Cranmer ^{id175}, L. Cremer ^{id49}, D. Cremonini ^{id24b,24a},
 S. Crépe-Renaudin ^{id60}, F. Crescioli ^{id129}, T. Cresta ^{id73a,73b}, M. Cristinziani ^{id146},
 M. Cristoforetti ^{id78a,78b}, E. Critelli ^{id97}, V. Croft ^{id116}, G. Crosetti ^{id44b,44a}, A. Cueto ^{id100}, H. Cui ^{id97},
 Z. Cui ^{id7}, B.M. Cunnett ^{id151}, W.R. Cunningham ^{id59}, F. Curcio ^{id168}, J.R. Curran ^{id52},
 M.J. Da Cunha Sargedas De Sousa ^{id57b,57a}, J.V. Da Fonseca Pinto ^{id82b}, C. Da Via ^{id102},
 W. Dabrowski ^{id86a}, T. Dado ^{id37}, S. Dahbi ^{id153}, T. Dai ^{id107}, D. Dal Santo ^{id20}, C. Dallapiccola ^{id104},
 M. Dam ^{id43}, G. D'amen ^{id30}, V. D'Amico ^{id110}, J.R. Dandoy ^{id35}, M. D'Andrea ^{id57b,57a},
 D. Dannheim ^{id37}, G. D'anniballe ^{id74a,74b}, M. Danninger ^{id147}, V. Dao ^{id150}, G. Darbo ^{id57b},
 S.J. Das ^{id30}, F. Dattola ^{id48}, S. D'Auria ^{id71a,71b}, A. D'Avanzo ^{id72a,72b}, T. Davidek ^{id135},
 J. Davidson ^{id172}, I. Dawson ^{id95}, K. De ^{id8}, C. De Almeida Rossi ^{id160}, R. De Asmundis ^{id72a},
 N. De Biase ^{id48}, S. De Castro ^{id24b,24a}, N. De Groot ^{id115}, P. de Jong ^{id116}, H. De la Torre ^{id117},
 A. De Maria ^{id113a}, A. De Salvo ^{id75a}, U. De Sanctis ^{id76a,76b}, F. De Santis ^{id70a,70b}, A. De Santo ^{id151},
 J.B. De Vivie De Regie ^{id60}, J. Debevc ^{id94}, D.V. Dedovich ^{id39}, J. Degens ^{id93}, A.M. Deiana ^{id45},
 J. Del Peso ^{id100}, L. Delagrangue ^{id129}, F. Deliot ^{id137}, C.M. Delitzsch ^{id49}, M. Della Pietra ^{id72a,72b},
 D. Della Volpe ^{id56}, A. Dell'Acqua ^{id37}, L. Dell'Asta ^{id71a,71b}, M. Delmastro ^{id4}, C.C. Delogu ^{id57b,57a},
 P.A. Delsart ^{id60}, S. Demers ^{id177}, M. Demichev ^{id39}, S.P. Denisov ^{id38}, H. Denizli ^{id22a,1},
 M.G. Depala ^{id93}, L. D'Eramo ^{id41}, D. Derendarz ^{id87}, F. Derue ^{id129}, P. Dervan ^{id93,*}, A.M. Desai ^{id1},
 K. Desch ^{id25}, F.A. Di Bello ^{id74a,74b}, A. Di Ciaccio ^{id76a,76b}, L. Di Ciaccio ^{id4}, A. Di Domenico ^{id75a,75b},
 C. Di Donato ^{id72a,72b}, A. Di Girolamo ^{id37}, G. Di Gregorio ^{id66}, A. Di Luca ^{id78a,78b},
 B. Di Micco ^{id77a,77b}, R. Di Nardo ^{id77a,77b}, K.F. Di Petrillo ^{id40}, M. Diamantopoulou ^{id35}, F.A. Dias ^{id116},
 M.A. Diaz ^{id139a,139b}, A.R. Didenko ^{id39}, M. Didenko ^{id168}, S.D. Diefenbacher ^{id18a}, E.B. Diehl ^{id107},
 S. Díez Cornell ^{id48}, C. Díez Pardos ^{id146}, C. Dimitriadi ^{id149}, A. Dimitrievska ^{id21}, A. Dimri ^{id150},
 Y. Ding ^{id62}, J. Dingfelder ^{id25}, T. Dingley ^{id128}, I-M. Dinu ^{id28b}, S.J. Dittmeier ^{id63b}, F. Dittus ^{id37},
 M. Divisek ^{id135}, B. Dixit ^{id93}, F. Djama ^{id103}, T. Djobava ^{id154b}, C. Doglioni ^{id102,99}, A. Dohnalova ^{id29a},
 Z. Dolezal ^{id135}, K. Domijan ^{id86a}, K.M. Dona ^{id40}, M. Donadelli ^{id82d}, B. Dong ^{id108}, J. Donini ^{id41},
 A. D'Onofrio ^{id72a,72b}, M. D'Onofrio ^{id93}, J. Dopke ^{id136}, A. Doria ^{id72a}, N. Dos Santos Fernandes ^{id132a},
 I.A. Dos Santos Luz ^{id82e}, P. Dougan ^{id102}, M.T. Dova ^{id91}, A.T. Doyle ^{id59}, M.P. Drescher ^{id55},
 E. Dreyer ^{id174}, I. Drivas-koulouris ^{id10}, M. Drnevich ^{id119}, D. Du ^{id62}, T.A. du Pree ^{id116}, Z. Duan ^{id113a},
 M. Dubau ^{id4}, F. Dubinin ^{id39}, M. Dubovsky ^{id29a}, E. Duchovni ^{id174}, G. Duckeck ^{id110}, P.K. Duckett ^{id97},
 O.A. Ducu ^{id28b}, D. Duda ^{id52}, A. Dudarev ^{id37}, M.M. Dudek ^{id87}, E.R. Duden ^{id27}, M. D'uffizi ^{id102},
 L. Duflot ^{id66}, M. Dührssen ^{id37}, I. Duminica ^{id28g}, A.E. Dumitriu ^{id28b}, M. Dunford ^{id63a},
 K. Dunne ^{id47a,47b}, A. Duperrin ^{id103}, H. Duran Yildiz ^{id3a}, A. Durglishvili ^{id154b}, G.I. Dyckes ^{id18a},
 M. Dyndal ^{id86a}, B.S. Dziedzic ^{id37}, Z.O. Earnshaw ^{id151}, G.H. Eberwein ^{id128}, B. Eckerova ^{id29a},
 S. Eggebrecht ^{id55}, E. Egidio Purcino De Souza ^{id82e}, G. Eigen ^{id17}, K. Einsweiler ^{id18a}, T. Ekelof ^{id166},
 P.A. Ekman ^{id99}, S. El Farkh ^{id36b}, Y. El Ghazali ^{id62}, H. El Jarrari ^{id105}, A. El Moussaouy ^{id36a},
 D. Elitez ^{id37}, M. Ellert ^{id166}, F. Ellinghaus ^{id176}, T.A. Elliot ^{id96}, N. Ellis ^{id37}, J. Elmsheuser ^{id30},
 M. Elsayy ^{id118a}, M. Elsing ^{id37}, D. Emeliyanov ^{id136}, Y. Enari ^{id83}, S. Epari ^{id109},
 D. Ernani Martins Neto ^{id87}, F. Ernst ^{id37}, M. Escalier ^{id66}, C. Escobar ^{id168}, E. Etzion ^{id156},

G. Evans [ID132a,132b](#), H. Evans [ID68](#), L.S. Evans [ID48](#), A. Ezhilov [ID38](#), S. Ezzarqtouni [ID36a](#),
 F. Fabbri [ID24b,24a](#), L. Fabbri [ID24b,24a](#), G. Facini [ID97](#), V. Fadeyev [ID138](#), R.M. Fakhruddinov [ID38](#),
 D. Fakoudis [ID101](#), S. Falciano [ID75a](#), L.F. Falda Ulhoa Coelho [ID27](#), F. Fallavollita [ID111](#), G. Falsetti [ID44b,44a](#),
 J. Faltova [ID135](#), C. Fan [ID167](#), K.Y. Fan [ID64b](#), Y. Fan [ID14](#), Y. Fang [ID14,113c](#), M. Fanti [ID71a,71b](#),
 M. Faraj [ID69a,69b](#), Z. Farazpay [ID98](#), A. Farbin [ID8](#), A. Farilla [ID77a](#), K. Farman [ID153](#), T. Farooque [ID108](#),
 J.N. Farr [ID177](#), M.S. Farrington [ID61](#), S.M. Farrington [ID136,52](#), F. Fassi [ID36e](#), D. Fassouliotis [ID9](#),
 L. Fayard [ID66](#), P. Federic [ID135](#), P. Federicova [ID133](#), O.L. Fedin [ID38,a](#), M. Feickert [ID175](#), L. Feligioni [ID103](#),
 D.E. Fellers [ID18a](#), C. Feng [ID142a](#), Y. Feng [ID14](#), Z. Feng [ID116](#), M.J. Fenton [ID164](#), L. Ferencz [ID48](#),
 B. Fernandez Barbadillo [ID92](#), P. Fernandez Martinez [ID67](#), M.J.V. Fernoux [ID103](#), J. Ferrando [ID92](#),
 A. Ferrari [ID166](#), P. Ferrari [ID116,115](#), R. Ferrari [ID73a](#), D. Ferrere [ID56](#), C. Ferretti [ID107](#), M.P. Fewell [ID1](#),
 D. Fiacco [ID75a,75b](#), F. Fiedler [ID101](#), P. Fiedler [ID134](#), S. Filimonov [ID39](#), M.S. Filip [ID28b,t](#), A. Filipčić [ID94](#),
 E.K. Filmer [ID161a](#), F. Filthaut [ID115](#), M.C.N. Fiolhais [ID132a,132c,c](#), L. Fiorini [ID168](#), W.C. Fisher [ID108](#),
 T. Fitschen [ID102](#), P.M. Fitzhugh [ID137](#), I. Fleck [ID146](#), P. Fleischmann [ID107](#), T. Flick [ID176](#), M. Flores [ID34d,ag](#),
 L.R. Flores Castillo [ID64a](#), M. Foll [ID127](#), F.M. Follega [ID78a,78b](#), N. Fomin [ID33](#), J.H. Foo [ID160](#),
 A. Formica [ID137](#), A.C. Forti [ID102](#), E. Fortin [ID37](#), A.W. Fortman [ID18a](#), L. Foster [ID18a](#), L. Fountas [ID9,i](#),
 D. Fournier [ID66](#), H. Fox [ID92](#), P. Francavilla [ID74a,74b](#), S. Francescato [ID61](#), S. Franchellucci [ID56](#),
 M. Franchini [ID24b,24a](#), S. Franchino [ID63a](#), D. Francis [ID37](#), L. Franco [ID48](#), L. Franconi [ID48](#), M. Franklin [ID61](#),
 G. Frattari [ID27](#), Y.Y. Frid [ID156](#), J. Friend [ID59](#), N. Fritzsche [ID37](#), A. Froch [ID56](#), D. Froidevaux [ID37](#),
 J.A. Frost [ID136](#), Y. Fu [ID108](#), S. Fuenzalida Garrido [ID139g](#), M. Fujimoto [ID150](#), K.Y. Fung [ID64a](#),
 E. Furtado De Simas Filho [ID82c](#), M. Furukawa [ID158](#), M. Fuste Costa [ID48](#), J. Fuster [ID168](#), A. Gaa [ID55](#),
 A. Gabrielli [ID24b,24a](#), A. Gabrielli [ID160](#), P. Gadow [ID37](#), G. Gagliardi [ID57b,57a](#), L.G. Gagnon [ID18a](#),
 S. Gaid [ID84b](#), S. Galantzan [ID156](#), J. Gallagher [ID1](#), E.J. Gallas [ID128](#), A.L. Gallen [ID166](#), B.J. Gallop [ID136](#),
 K.K. Gan [ID121](#), S. Ganguly [ID158](#), Y. Gao [ID52](#), A. Garabaglu [ID141](#), F.M. Garay Walls [ID139a,139b](#),
 C. García [ID168](#), A. Garcia Alonso [ID116](#), A.G. Garcia Caffaro [ID177](#), J.E. García Navarro [ID168](#),
 M.A. Garcia Ruiz [ID23b](#), M. Garcia-Sciveres [ID18a](#), G.L. Gardner [ID130](#), R.W. Gardner [ID40](#), N. Garelli [ID163](#),
 R.B. Garg [ID148](#), J.M. Gargan [ID33](#), C.A. Garner [ID160](#), C.M. Garvey [ID34a](#), V.K. Gassmann [ID163](#), G. Gaudio [ID73a](#),
 V. Gautam [ID13](#), P. Gauzzi [ID75a,75b](#), J. Gavranovic [ID94](#), I.L. Gavrilenko [ID132a](#), A. Gavrilyuk [ID38](#),
 C. Gay [ID169](#), G. Gayken [ID125](#), E.N. Gazis [ID10](#), A. Gekow [ID121](#), C. Gemme [ID57b](#), M.H. Genest [ID60](#),
 A.D. Gentry [ID114](#), S. George [ID96](#), T. Gerialis [ID46](#), A.A. Gerwin [ID122](#), P. Gessinger-Befurt [ID37](#),
 M. Ghani [ID172](#), K. Ghorbanian [ID95](#), A. Ghosal [ID146](#), A. Ghosh [ID164](#), A. Ghosh [ID7](#), B. Giacobbe [ID24b](#),
 S. Giagu [ID75a,75b](#), T. Giani [ID116](#), A. Giannini [ID62](#), S.M. Gibson [ID96](#), M. Gignac [ID138](#), D.T. Gil [ID86b](#),
 A.K. Gilbert [ID86a](#), B.J. Gilbert [ID42](#), D. Gillberg [ID35](#), G. Gilles [ID116](#), D.M. Gingrich [ID2,ai](#),
 M.P. Giordani [ID69a,69c](#), P.F. Giraud [ID137](#), G. Giugliarelli [ID69a,69c](#), D. Giugni [ID71a](#), F. Giuli [ID76a,76b](#),
 I. Gkialas [ID9,i](#), L.K. Gladilin [ID38](#), C. Glasman [ID100](#), M. Glazewska [ID20](#), R.M. Gleason [ID164](#),
 G. Glemža [ID48](#), M. Glisic [ID125](#), I. Gnesi [ID44b](#), Y. Go [ID30](#), M. Goblirsch-Kolb [ID37](#), B. Gocke [ID49](#),
 D. Godin [ID109](#), B. Gokturk [ID22a](#), S. Goldfarb [ID106](#), T. Golling [ID56](#), M.G.D. Gololo [ID34c](#), A. Golub [ID141](#),
 D. Golubkov [ID38](#), J.P. Gombas [ID108](#), A. Gomes [ID132a,132b](#), G. Gomes Da Silva [ID146](#),
 A.J. Gomez Delegido [ID37](#), R. Gonçalves [ID132a](#), L. Gonella [ID21](#), A. Gongadze [ID154c](#), F. Gonnella [ID21](#),
 J.L. Gonski [ID148](#), R.Y. González Andana [ID52](#), S. González de la Hoz [ID168](#), M.V. Gonzalez Rodrigues [ID48](#),
 R. Gonzalez Suarez [ID166](#), S. Gonzalez-Sevilla [ID56](#), L. Goossens [ID37](#), B. Gorini [ID37](#), E. Gorini [ID70a,70b](#),
 A. Gorišek [ID94](#), T.C. Gosart [ID130](#), A.T. Goshaw [ID51](#), M.I. Gostkin [ID39](#), S. Goswami [ID123](#),
 C.A. Gottardo [ID37](#), S.A. Gotz [ID110](#), M. Goughri [ID36b](#), A.G. Goussiou [ID141](#), N. Govender [ID34c](#),
 R.P. Grabarczyk [ID128](#), I. Grabowska-Bold [ID86a](#), K. Graham [ID35](#), E. Gramstad [ID127](#),
 S. Grancagnolo [ID70a,70b](#), C.M. Grant [ID1](#), P.M. Gravila [ID28f](#), F.G. Gravili [ID70a,70b](#), H.M. Gray [ID18a](#),
 M. Greco [ID111](#), M.J. Green [ID1](#), C. Grefe [ID25](#), A.S. Grefsrud [ID17](#), I.M. Gregor [ID48](#), K.T. Greif [ID164](#),
 P. Grenier [ID148](#), S.G. Grewe [ID111](#), A.A. Grillo [ID138](#), K. Grimm [ID32](#), S. Grinstein [ID13,x](#), J.-F. Grivaz [ID66](#),
 E. Gross [ID174](#), J. Grosse-Knetter [ID55](#), L.H. Grossman [ID18b](#), L. Guan [ID107](#), G. Guerrieri [ID37](#),

R. Guevara ¹²⁷, R. Gugel ¹⁰¹, J.A.M. Guhit ¹⁰⁷, A. Guida ¹⁹, E. Guilloton ¹⁷², S. Guindon ³⁷,
 F. Guo ^{14,113c}, J. Guo ^{143a}, L. Guo ⁴⁸, L. Guo ^{113b,v}, Y. Guo ¹⁰⁷, Y. Guo ⁴², A. Gupta ⁴⁹,
 R. Gupta ¹³¹, S. Gupta ²⁷, S. Gurbuz ²⁵, S.S. Gurdasani ⁴⁸, G. Gustavino ^{75a,75b},
 P. Gutierrez ¹²², L.F. Gutierrez Zagazeta ¹³⁰, M. Gutsche ⁵⁰, C. Gutschow ⁹⁷, C. Gwenlan ¹²⁸,
 C.B. Gwilliam ⁹³, E.S. Haaland ¹²⁷, A. Haas ¹¹⁹, M. Habedank ⁵⁹, C. Haber ^{18a},
 H.K. Hadavand ⁸, A. Haddad ⁴¹, A. Hadeef ⁵⁰, A.I. Hagan ⁹², J.J. Hahn ¹⁴⁶, E.H. Haines ⁹⁷,
 M. Haleem ¹⁷¹, J. Haley ¹²³, G.D. Hallewell ¹⁰³, J.A. Hallford ⁴⁸, K. Hamano ¹⁷⁰,
 H. Hamdaoui ¹⁶⁶, M. Hamer ²⁵, S.E.D. Hammoud ⁶⁶, E.J. Hampshire ⁹⁶, J. Han ^{142a},
 L. Han ^{113a}, L. Han ⁶², S. Han ¹⁴, K. Hanagaki ⁸³, M. Hance ¹³⁸, D.A. Hangal ⁴²,
 H. Hanif ¹⁴⁷, M.D. Hank ¹³⁰, J.B. Hansen ⁴³, P.H. Hansen ⁴³, T. Harenberg ¹⁷⁶,
 S. Harkusha ¹⁷⁸, M.L. Harris ¹⁰⁴, Y.T. Harris ²⁵, J. Harrison ¹³, P.F. Harrison ¹⁷², M.L.E. Hart ⁹⁷,
 N.M. Hartman ¹¹¹, N.M. Hartmann ¹¹⁰, R.Z. Hasan ^{96,136}, Y. Hasegawa ¹⁴⁵, F. Haslbeck ¹²⁸,
 S. Hassan ¹⁷, R. Hauser ¹⁰⁸, M. Haviernik ¹³⁵, C.M. Hawkes ²¹, R.J. Hawkings ³⁷,
 Y. Hayashi ¹⁵⁸, D. Hayden ¹⁰⁸, C. Hayes ¹⁰⁷, R.L. Hayes ¹¹⁶, C.P. Hays ¹²⁸, J.M. Hays ⁹⁵,
 H.S. Hayward ⁹³, M. He ^{14,113c}, Y. He ⁴⁸, Y. He ⁹⁷, N.B. Heatley ⁹⁵, V. Hedberg ⁹⁹,
 J. Heilman ³⁵, S. Heim ⁴⁸, T. Heim ^{18a}, J.J. Heinrich ¹²⁵, L. Heinrich ¹¹¹, J. Hejbal ¹³³,
 M. Helbig ⁵⁰, A. Held ¹⁷⁵, S. Hellesund ¹⁷, C.M. Helling ¹⁶⁹, S. Hellman ^{47a,47b},
 A.M. Henriques Correia ³⁷, H. Herde ⁹⁹, Y. Hernández Jiménez ¹⁵⁰, L.M. Herrmann ²⁵,
 T. Herrmann ⁵⁰, G. Herten ⁵⁴, R. Hertenberger ¹¹⁰, L. Hervas ³⁷, M.E. Hespings ¹⁰¹,
 N.P. Hessey ^{161a}, J. Hessler ¹¹¹, M. Hidaoui ^{36b}, N. Hidic ¹³⁵, E. Hill ¹⁶⁰, T.S. Hillersoy ¹⁷,
 S.J. Hillier ²¹, J.R. Hinds ¹⁰⁸, F. Hinterkeuser ²⁵, M. Hirose ¹²⁶, S. Hirose ¹⁶²,
 D. Hirschbuehl ¹⁷⁶, T.G. Hitchings ¹⁰², B. Hiti ⁹⁴, J. Hobbs ¹⁵⁰, R. Hobincu ^{28e}, N. Hod ¹⁷⁴,
 A.M. Hodges ¹⁶⁷, M.C. Hodgkinson ¹⁴⁴, B.H. Hodgkinson ¹²⁸, A. Hoecker ³⁷, D.D. Hofer ¹⁰⁷,
 J. Hofer ¹⁶⁸, J. Hofner ¹⁰¹, M. Holzbock ³⁷, L.B.A.H. Hommels ³³, V. Homsak ¹²⁸,
 J.J. Hong ⁶⁸, T.M. Hong ¹³¹, B.H. Hooberman ¹⁶⁷, W.H. Hopkins ⁶, M.C. Hoppesch ¹⁶⁷,
 Y. Horii ¹¹², M.E. Horstmann ¹¹¹, S. Hou ¹⁵³, M.R. Housenga ¹⁶⁷, J. Howarth ⁵⁹, J. Hoya ⁶,
 M. Hrabovsky ¹²⁴, T. Hryn'ova ⁴, P.J. Hsu ⁶⁵, S.-C. Hsu ¹⁴¹, T. Hsu ⁶⁶, M. Hu ^{18a}, Q. Hu ⁶²,
 S. Huang ³³, X. Huang ^{14,113c}, Y. Huang ¹³⁵, Y. Huang ^{113b}, Y. Huang ¹⁴, Z. Huang ⁶⁶,
 Z. Hubacek ¹³⁴, F. Huegging ²⁵, T.B. Huffman ¹²⁸, M. Hufnagel Maranha De Faria ^{82a},
 C.A. Hugli ⁴⁸, M. Huhtinen ³⁷, S.K. Huiberts ¹²⁷, R. Hulsken ¹⁰⁵, C.E. Hultquist ^{18a},
 D.L. Humphreys ¹⁰⁴, N. Huseynov ¹², J. Huston ¹⁰⁸, B. Huth ³⁷, J. Huth ⁶¹, L. Huth ⁴⁸,
 R. Hyneman ⁷, G. Iacobucci ⁵⁶, G. Iakovidis ³⁰, L. Iconomidou-Fayard ⁶⁶, J.P. Iddon ³⁷,
 P. Iengo ^{72a,72b}, Y. Iiyama ¹⁵⁸, T. Iizawa ¹⁵⁸, Y. Ikegami ⁸³, D. Iliadis ¹⁵⁷, N. Ilic ¹⁶⁰,
 H. Imam ^{36a}, G. Inacio Goncalves ^{82d}, S.A. Infante Cabanas ^{139c}, T. Ingebretsen Carlson ^{47a,47b},
 J.M. Inglis ⁹⁵, G. Introzzi ^{73a,73b}, M. Iodice ^{77a}, V. Ippolito ^{75a,75b}, R.K. Irwin ⁹³, M. Ishino ¹⁵⁸,
 W. Islam ¹⁷⁵, C. Issever ¹⁹, S. Istin ^{22a,ao}, K. Itabashi ¹²⁶, H. Ito ¹⁷³, R. Iuppa ^{78a,78b},
 A. Ivina ¹⁷⁴, S. Izumiya ¹¹², V. Izzo ^{72a}, P. Jacka ¹³⁴, P. Jackson ¹, P. Jain ⁴⁸, K. Jakobs ⁵⁴,
 T. Jakoubek ¹⁷⁴, J. Jamieson ⁵⁹, W. Jang ¹⁵⁸, S. Jankovych ¹³⁵, M. Javurkova ¹⁰⁴, P. Jawahar ¹⁰²,
 L. Jeanty ¹²⁵, J. Jejelava ^{154a,ae}, P. Jenni ^{54,f}, C.E. Jessiman ³⁵, C. Jia ^{142a}, H. Jia ¹⁶⁹, J. Jia ¹⁵⁰,
 X. Jia ^{111,113c}, Z. Jia ^{113a}, C. Jiang ⁵², Q. Jiang ^{64b}, S. Jiggins ⁴⁸, M. Jimenez Ortega ¹⁶⁸,
 J. Jimenez Pena ¹³, S. Jin ^{113a}, A. Jinaru ^{28b}, O. Jinnouchi ¹⁴⁰, P. Johansson ¹⁴⁴, K.A. Johns ⁷,
 J.W. Johnson ¹³⁸, F.A. Jolly ⁴⁸, D.M. Jones ¹⁵¹, E. Jones ⁴⁸, K.S. Jones ⁸, P. Jones ³³,
 R.W.L. Jones ⁹², T.J. Jones ⁹³, H.L. Joos ⁵⁵, R. Joshi ¹²¹, J. Jovicevic ¹⁶, X. Ju ^{18a},
 J.J. Junggeburth ³⁷, T. Junkermann ^{63a}, A. Juste Rozas ^{13,x}, M.K. Juzek ⁸⁷, S. Kabana ^{139f},
 A. Kaczmarzka ⁸⁷, S.A. Kadir ¹⁴⁸, M. Kado ¹¹¹, H. Kagan ¹²¹, M. Kagan ¹⁴⁸, A. Kahn ¹³⁰,
 C. Kahra ¹⁰¹, T. Kaji ¹⁵⁸, E. Kajomovitz ¹⁵⁵, N. Kakati ¹⁷⁴, N. Kakoty ¹³, I. Kalaitzidou ⁵⁴,
 S. Kandel ⁸, N. Kanellos ¹⁰, N.J. Kang ¹³⁸, D. Kar ^{34j}, E. Karentzos ²⁵, K. Karki ⁸,

O. Karkout ¹¹⁶, S.N. Karpov ³⁹, Z.M. Karpova ³⁹, V. Kartvelishvili ^{92,154b}, A.N. Karyukhin ³⁸, E. Kasimi ¹⁵⁷, J. Katzy ⁴⁸, S. Kaur ³⁵, K. Kawade ¹⁴⁵, M.P. Kawale ¹²², C. Kawamoto ⁸⁸, T. Kawamoto ⁶², E.F. Kay ³⁷, S. Kazakos ¹⁰⁸, V.F. Kazanin ³⁸, J.M. Keaveney ^{34a}, R. Keeler ¹⁷⁰, G.V. Kehris ⁶¹, J.S. Keller ³⁵, J.M. Kelly ¹⁷⁰, J.J. Kempster ¹⁵¹, O. Kepka ¹³³, J. Kerr ^{161b}, B.P. Kerridge ¹³⁶, B.P. Kerševan ⁹⁴, L. Keszezhova ^{29a}, R.A. Khan ¹³¹, A. Khanov ¹²³, A.G. Kharlamov ³⁸, T. Kharlamova ³⁸, E.E. Khoda ¹⁴¹, M. Kholodenko ^{132a}, T.J. Khoo ¹⁹, G. Khoriauli ¹⁷¹, Y. Khoulaki ^{36a}, Y.A.R. Khwaira ¹²⁹, B. Kibirige ^{34j}, D. Kim ⁶, D.W. Kim ^{18b}, Y.K. Kim ⁴⁰, N. Kimura ⁹⁷, M.K. Kingston ⁵⁵, A. Kirchhoff ⁵⁵, C. Kirfel ²⁵, F. Kirfel ²⁵, J. Kirk ¹³⁶, A.E. Kiryunin ¹¹¹, S. Kita ¹⁶², O. Kivernyk ²⁵, M. Klassen ¹⁶³, C. Klein ³⁵, L. Klein ¹⁷¹, M.H. Klein ⁴⁵, S.B. Klein ⁵⁶, U. Klein ⁹³, A. Klimentov ³⁰, T. Klioutchnikova ³⁷, P. Kluit ¹¹⁶, S. Kluth ¹¹¹, E. Kneringer ⁷⁹, T.M. Knight ¹⁶⁰, A. Knue ⁴⁹, M. Kobel ⁵⁰, D. Kobylanskii ¹⁷⁴, S.F. Koch ¹²⁸, M. Kocian ¹⁴⁸, P. Kodyš ¹³⁵, D.M. Koeck ¹²⁵, T. Koffas ³⁵, O. Kolay ⁵⁰, I. Koletsou ⁴, T. Komarek ⁸⁷, K. Köneke ⁵⁵, A.X.Y. Kong ¹, T. Kono ¹²⁰, N. Konstantinidis ⁹⁷, P. Kontaxakis ⁵⁶, B. Konya ⁹⁹, R. Kopeliansky ⁴², S. Koperny ^{86a}, R. Koppenhofer ⁵⁴, K. Korcyl ⁸⁷, K. Kordas ^{157,d}, A. Korn ⁹⁷, S. Korn ⁵⁵, I. Korolkov ¹³, N. Korotkova ³⁸, B. Kortman ¹¹⁶, O. Kortner ¹¹¹, S. Kortner ¹¹¹, W.H. Kostecka ¹¹⁷, M. Kostov ^{29a}, V.V. Kostyukhin ¹⁴⁶, A. Kotsokechagia ³⁷, A. Kotwal ⁵¹, A. Koulouris ³⁷, A. Kourkoumeli-Charalampidi ^{73a,73b}, C. Kourkoumelis ⁹, E. Kourlitis ¹¹¹, O. Kovanda ¹²⁵, R. Kowalewski ¹⁷⁰, W. Kozanecki ¹²⁵, A.S. Kozhin ³⁸, V.A. Kramarenko ³⁸, G. Kramberger ⁹⁴, P. Kramer ²⁵, M.W. Krasny ¹²⁹, A. Krasznahorkay ¹⁰⁴, A.C. Kraus ¹¹⁷, J.W. Kraus ¹⁷⁶, J.A. Kremer ⁴⁸, N.B. Kregel ¹⁴⁶, T. Kresse ⁵⁰, L. Kretschmann ¹⁷⁶, J. Kretschmar ⁹³, P. Krieger ¹⁶⁰, K. Krizka ²¹, K. Kroeninger ⁴⁹, H. Kroha ¹¹¹, J. Kroll ¹³³, J. Kroll ¹³⁰, K.S. Krowpman ¹⁰⁸, U. Kruchonak ³⁹, H. Krüger ²⁵, N. Krumnack ⁸⁰, M.C. Kruse ⁵¹, O. Kuchinskaia ³⁹, S. Kuday ^{3a}, S. Kuehn ³⁷, R. Kuesters ⁵⁴, T. Kuhl ⁴⁸, V. Kukhtin ³⁹, Y. Kulchitsky ³⁹, S. Kuleshov ^{139d,139b}, J. Kull ¹, E.V. Kumar ¹¹⁰, M. Kumar ^{34j}, N. Kumari ⁴⁸, P. Kumari ^{161b}, A. Kupco ¹³³, A. Kupich ³⁸, O. Kuprash ⁵⁴, H. Kurashige ⁸⁵, L.L. Kurchaninov ^{161a}, O. Kurdysh ⁴, A. Kurova ³⁸, M. Kuze ¹⁴⁰, A.K. Kvam ¹⁰⁴, J. Kvita ¹²⁴, N.G. Kyriacou ¹⁴¹, M. Laassiri ³⁰, C. Lacasta ¹⁶⁸, F. Lacava ^{75a,75b}, H. Lacker ¹⁹, D. Lacour ¹²⁹, N.N. Lad ⁹⁷, E. Ladygin ³⁹, A. Lafarge ⁴¹, B. Laforge ¹²⁹, T. Lagouri ¹⁷⁷, F.Z. Lahbabi ^{36a}, S. Lai ^{55,37}, W.S. Lai ⁹⁷, I.K. Lakomic ⁵⁵, J.E. Lambert ¹⁷⁰, S. Lammers ⁶⁸, W. Lampl ⁷, C. Lampoudis ^{157,d}, G. Lamprinoudis ¹⁷¹, A.N. Lancaster ¹¹⁷, E. Lançon ³⁰, U. Landgraf ⁵⁴, M.P.J. Landon ⁹⁵, V.S. Lang ⁵⁴, A.J. Lankford ¹⁶⁴, F. Lanni ³⁷, C.S. Lantz ¹⁶⁷, K. Lantzsch ²⁵, A. Lanza ^{73a}, M. Lanzac Berrocal ¹⁶⁸, J.F. Laporte ¹³⁷, T. Lari ^{71a}, D. Larsen ¹⁷, L. Larson ¹¹, F. Lasagni Manghi ^{24b}, M. Lassnig ³⁷, S.D. Lawlor ¹⁴⁴, R. Lazaridou ¹⁶⁴, M. Lazzaroni ^{71a,71b}, E.T.T. Le ¹⁶⁴, H.D.M. Le ¹⁰⁸, E.M. Le Boulicaut ¹⁷⁷, L.T. Le Pottier ^{18a}, B. Leban ^{24b,24a}, F. Ledroit-Guillon ⁶⁰, T.F. Lee ^{161b}, L.L. Leeuw ^{34c}, M. Lefebvre ¹⁷⁰, C. Leggett ^{18a}, G. Lehmann Miotto ³⁷, M. Leigh ⁵⁶, W.A. Leight ¹⁰⁴, W. Leinonen ¹¹⁵, A. Leisos ^{157,u}, M.A.L. Leite ^{82c}, C.E. Leitgeb ¹⁹, R. Leitner ¹³⁵, K.J.C. Leney ⁴⁵, T. Lenz ²⁵, S. Leone ^{74a}, C. Leonidopoulos ⁵², A. Leopold ¹⁴⁹, J. LePage-Bourbonnais ³⁵, R. Les ¹⁰⁸, C.G. Lester ³³, M. Levchenko ³⁸, J. Levêque ⁴, L.J. Levinson ¹⁷⁴, G. Levrini ^{24b,24a}, M.P. Lewicki ⁸⁷, C. Lewis ¹⁴¹, D.J. Lewis ⁴, L. Lewitt ¹⁴⁴, A. Li ³⁰, B. Li ^{142a}, C. Li ¹⁰⁷, C-Q. Li ¹¹¹, H. Li ^{142a}, H. Li ¹⁰², H. Li ¹⁵, H. Li ⁶², H. Li ^{142a}, J. Li ^{143a}, K. Li ¹⁴, L. Li ^{143a}, R. Li ¹⁷⁷, S. Li ^{14,113c}, S. Li ^{143b,143a}, T. Li ⁵, X. Li ¹⁰⁵, Y. Li ¹⁴, Z. Li ¹⁵⁸, Z. Li ^{14,113c}, Z. Li ⁶², S. Liang ^{14,113c}, Z. Liang ¹⁴, M. Liberatore ¹³⁷, B. Liberti ^{76a}, G.B. Libotte ^{82d}, K. Lie ^{64c}, J. Lieber Marin ^{82e}, H. Lien ⁶⁸, H. Lin ¹⁰⁷, S.F. Lin ¹⁵⁰, L. Linden ¹¹⁰, R.E. Lindley ⁷, J.H. Lindon ³⁷, J. Ling ⁶¹, E. Lipeles ¹³⁰, A. Lipniacka ¹⁷, A. Lister ¹⁶⁹, J.D. Little ⁶⁸, B. Liu ¹⁴, B.X. Liu ^{113b}, D. Liu ¹⁵⁵, D. Liu ¹³⁸, E.H.L. Liu ²¹, J.K.K. Liu ¹¹⁹, K. Liu ^{143b}, K. Liu ^{143b,143a}, M. Liu ⁶²,

M.Y. Liu ⁶², P. Liu ¹⁴, Q. Liu ¹⁴⁸, S. Liu ¹⁵⁰, X. Liu ^{142a}, Y. Liu ^{113b,113c}, Y. Liu ¹⁶⁷,
Y.L. Liu ^{142a}, Y.W. Liu ⁶², Z. Liu ^{66,k}, S.L. Lloyd ⁹⁵, E.M. Lobodzinska ⁴⁸, P. Loch ⁷,
E. Lodhi ¹⁶⁰, K. Lohwasser ¹⁴⁴, E. Loiacono ⁴⁸, J.D. Lomas ²¹, J.D. Long ⁴², I. Longarini ¹⁶⁴,
R. Longo ¹⁶⁷, A. Lopez Solis ¹³, N.A. Lopez-canelas ⁷, N. Lorenzo Martinez ⁴, A.M. Lory ¹¹⁰,
M. Losada ^{118a}, G. Löschcke Centeno ⁴, X. Lou ^{47a,47b}, X. Lou ^{14,113c}, A. Lounis ⁶⁶,
P.A. Love ⁹², M. Lu ⁶⁶, S. Lu ¹³⁰, Y.J. Lu ¹⁵³, H.J. Lubatti ¹⁴¹, C. Luci ^{75a,75b},
F.L. Lucio Alves ^{113a}, F. Luehring ⁶⁸, B.S. Lunday ¹³⁰, O. Lundberg ¹⁴⁹, J. Lunde ³⁷,
N.A. Luongo ⁶, M.S. Lutz ³⁷, A.B. Lux ²⁶, D. Lynn ³⁰, R. Lysak ¹³³, V. Lysenko ¹³⁴,
E. Lytken ⁹⁹, V. Lyubushkin ³⁹, T. Lyubushkina ³⁹, M.M. Lyukova ¹⁵⁰, H. Ma ³⁰, K. Ma ⁶²,
L.L. Ma ^{142a}, W. Ma ⁶², Y. Ma ¹²³, J.C. MacDonald ¹⁰¹, P.C. Machado De Abreu Farias ^{82c},
D. Macina ³⁷, R. Madar ⁴¹, T. Madula ⁹⁷, J. Maeda ⁸⁵, T. Maeno ³⁰, P.T. Mafa ^{34c,j},
H. Maguire ¹⁴⁴, M. Maheshwari ³³, V. Maiboroda ⁶⁶, A. Maio ^{132a,132b,132d}, K. Maj ^{86a},
O. Majersky ⁴⁸, S. Majewski ¹²⁵, R. Makhmanazarov ³⁸, N. Makovec ⁶⁶, V. Maksimovic ¹⁶,
B. Malaescu ¹²⁹, J. Malamant ¹²⁷, Pa. Malecki ⁸⁷, V.P. Maleev ³⁸, F. Malek ^{60,o}, M. Mali ⁹⁴,
D. Malito ⁹⁶, A. Maloizel ⁵, S. Maltezos ¹⁰, A. Malvezzi Lopes ^{82d}, S. Malyukov ³⁹, J. Mamuzic ⁹⁴,
G. Mancini ⁵³, M.N. Mancini ²⁷, G. Manco ^{73a,73b}, J.P. Mandalia ⁹⁵, S.S. Mandarray ¹⁵¹,
I. Mandić ⁹⁴, L. Manhaes de Andrade Filho ^{82a}, I.M. Maniatis ¹⁷⁴, J. Manjarres Ramos ⁹⁰,
D.C. Mankad ¹⁷⁴, A. Mann ¹¹⁰, T. Manoussos ³⁷, M.N. Mantinan ⁴⁰, S. Manzoni ³⁷,
L. Mao ^{143a}, X. Mapekula ^{34c}, A. Marantis ¹⁵⁷, R.R. Marcelo Gregorio ⁹⁵, G. Marchiori ⁵,
C. Marcon ^{71a}, E. Maricic ¹⁶, M. Marinescu ⁴⁸, S. Marium ⁴⁸, M. Marjanovic ¹²²,
A. Markhoos ⁵⁴, M. Markovitch ⁶⁶, M.K. Maroun ¹⁰⁴, M.C. Marr ¹⁴⁷, G.T. Marsden ¹⁰²,
E.J. Marshall ⁹², Z. Marshall ^{18a}, S. Marti-Garcia ¹⁶⁸, J. Martin ⁹⁷, T.A. Martin ¹³⁶,
V.J. Martin ⁵², B. Martin dit Latour ¹⁷, L. Martinelli ^{75a,75b}, M. Martinez ^{13,x},
P. Martinez Agullo ¹⁶⁸, V.I. Martinez Outschoorn ¹⁰⁴, P. Martinez Suarez ³⁷, S. Martin-Haugh ¹³⁶,
G. Martinovicova ¹³⁵, V.S. Martoiu ^{28b}, A.C. Martyniuk ⁹⁷, A. Marzin ³⁷, D. Mascione ^{78a,78b},
L. Masetti ¹⁰¹, J. Masik ¹⁰², A.L. Maslennikov ³⁹, S.L. Mason ⁴², P. Massarotti ^{72a,72b},
P. Mastrandrea ^{74a,74b}, A. Mastroberardino ^{44b,44a}, T. Masubuchi ¹²⁶, T.T. Mathew ¹²⁵,
J. Matousek ¹³⁵, D.M. Mattern ⁴⁹, K. Mauer ⁴⁸, J. Maurer ^{28b}, T. Maurin ⁵⁹, A.J. Maury ⁶⁶,
B. Maček ⁹⁴, C. Mavungu Tsava ¹⁰³, D.A. Maximov ³⁸, A.E. May ¹⁰², E. Mayer ⁴¹,
R. Mazini ^{34j}, I. Maznas ¹¹⁷, S.M. Mazza ¹³⁸, E. Mazzeo ³⁷, J.P. Mc Gowan ¹⁷⁰,
S.P. Mc Kee ¹⁰⁷, C.A. Mc Lean ⁶, C.C. McCracken ¹⁶⁹, E.F. McDonald ¹⁰⁶, A.E. McDougall ¹¹⁶,
L.F. Mcelhinney ⁹², J.A. Mcfayden ¹⁵¹, R.P. McGovern ¹³⁰, R.P. Mckenzie ^{34j}, T.C. McLachlan ⁴⁸,
D.J. McLaughlin ⁹⁷, S.J. McMahon ¹³⁶, C.M. Mcpartland ⁹³, R.A. McPherson ^{170,ab},
S. Mehlhase ¹¹⁰, A. Mehta ⁹³, D. Melini ¹⁶⁸, B.R. Mellado Garcia ^{34j}, A.H. Melo ⁵⁵,
F. Meloni ⁴⁸, A.M. Mendes Jacques Da Costa ¹⁰², L. Meng ⁹², S. Menke ¹¹¹, M. Mentink ³⁷,
E. Meoni ^{44b,44a}, G. Mercado ¹¹⁷, S. Merianos ¹⁵⁷, C. Merlassino ^{69a,69c}, C. Meroni ^{71a,71b},
J. Metcalfe ⁶, A.S. Mete ⁶, E. Meuser ¹⁰¹, C. Meyer ⁶⁸, J-P. Meyer ¹³⁷, Y. Miao ^{113a},
R.P. Middleton ¹³⁶, M. Mihovilovic ⁶⁶, L. Mijović ⁵², G. Mikenberg ¹⁷⁴, M. Mikesstikova ¹³³,
M. Mikuž ⁹⁴, H. Mildner ¹⁰¹, A. Milic ³⁷, D.W. Miller ⁴⁰, E.H. Miller ¹⁴⁸, A. Milov ¹⁷⁴,
D.A. Milstead ^{47a,47b}, T. Min ^{113a}, A.A. Minaenko ³⁸, I.A. Minashvili ^{154b}, A.I. Mincer ¹¹⁹,
B. Mindur ^{86a}, M. Mineev ³⁹, Y. Mino ⁸⁸, L.M. Mir ¹³, M. Miralles Lopez ⁵⁹, M. Mironova ^{18a},
M. Missio ⁴¹, A. Mitra ¹⁷², V.A. Mitsou ¹⁶⁸, Y. Mitsumori ¹¹², O. Miu ¹⁶⁰, P.S. Miyagawa ⁹⁵,
T. Mkrtchyan ³⁷, M. Mlinarevic ⁹⁷, T. Mlinarevic ⁹⁷, M. Mlynarikova ¹³⁵, L. Mlynarska ^{86a},
C. Mo ^{143a}, S. Mobius ²⁰, M.H. Mohamed Farook ¹¹⁴, S. Mohapatra ⁴², M.F. Mohd Soberi ⁵²,
S. Mohiuddin ¹²³, G. Mokgatitswane ^{34j}, L. Moleri ¹⁷⁴, U. Molinatti ¹²⁸, L.G. Mollier ²⁰,
B. Mondal ¹³³, S. Mondal ¹³⁴, K. Mönig ⁴⁸, E. Monnier ¹⁰³, L. Monsonis Romero ¹⁶⁸,
J. Montejo Berlingen ¹³, A. Montella ^{47a,47b}, M. Montella ¹²¹, F. Montekali ^{77a,77b},

F. Monticelli [id⁹¹](#), S. Monzani [id^{69a,69c}](#), A. Morancho Tarda [id⁴³](#), N. Morange [id⁶⁶](#),
 A.L. Moreira De Carvalho [id⁴⁸](#), M. Moreno Llácer [id¹⁶⁸](#), C. Moreno Martinez [id⁵⁶](#), J.M. Moreno Perez [id^{23b}](#),
 P. Morettini [id^{57b}](#), S. Morgenstern [id³⁷](#), M. Morii [id⁶¹](#), M. Morinaga [id¹⁵⁸](#), M. Moritsu [id⁸⁹](#),
 F. Morodei [id^{75a,75b}](#), P. Moschovakos [id³⁷](#), B. Moser [id⁵⁴](#), M. Mosidze [id^{154b}](#), T. Moskalets [id⁴⁵](#),
 P. Moskvitina [id¹¹⁵](#), J. Moss [id³²](#), P. Moszkowicz [id^{86a}](#), T. Motta Quirino [id^{82d}](#), A. Moussa [id^{36d}](#),
 Y. Moyal [id¹⁷⁴](#), H. Moyano Gomez [id¹³](#), E.J.W. Moyse [id¹⁰⁴](#), T.G. Mroz [id⁸⁷](#), S. Muanza [id¹⁰³](#),
 M. Mucha [id²⁵](#), J. Mueller [id¹³¹](#), G.A. Mullier [id¹⁶⁶](#), A.J. Mullin [id³³](#), J.J. Mullin [id⁵¹](#), A.C. Mullins [id⁴⁵](#),
 A.E. Mulski [id⁶¹](#), D.P. Mungo [id¹⁶⁰](#), D. Munoz Perez [id¹⁶⁸](#), F.J. Munoz Sanchez [id¹⁰²](#),
 W.J. Murray [id^{172,136}](#), M. Muškinja [id⁹⁴](#), C. Mwewa [id⁴⁸](#), A.G. Myagkov [id^{38,a}](#), A.J. Myers [id⁸](#),
 G. Myers [id¹⁰⁷](#), M. Myska [id¹³⁴](#), B.P. Nachman [id¹⁴⁸](#), K. Nagai [id¹²⁸](#), K. Nagano [id⁸³](#), R. Nagasaka [id¹⁵⁸](#),
 J.L. Nagle [id^{30,al}](#), E. Nagy [id¹⁰³](#), A.M. Nairz [id³⁷](#), Y. Nakahama [id⁸³](#), K. Nakamura [id⁸³](#), K. Nakkalil [id⁵](#),
 A. Nandi [id^{63b}](#), H. Nanjo [id¹²⁶](#), E.A. Narayanan [id⁴⁵](#), Y. Narukawa [id¹⁵⁸](#), I. Naryshkin [id³⁸](#),
 L. Nasella [id^{71a,71b}](#), S. Nasri [id^{118b}](#), C. Nass [id²⁵](#), G. Navarro [id^{23a}](#), A. Nayaz [id¹⁹](#), P.Y. Nechaeva [id³⁸](#),
 S. Nechaeva [id^{24b,24a}](#), F. Nechansky [id¹³³](#), L. Nedic [id¹²⁸](#), T.J. Neep [id²¹](#), A. Negri [id^{73a,73b}](#),
 M. Negrini [id^{24b}](#), C. Nellist [id¹¹⁶](#), C. Nelson [id¹⁰⁵](#), K. Nelson [id¹⁰⁷](#), S. Nemecek [id¹³³](#), M. Nessi [id^{37,g}](#),
 M.S. Neubauer [id¹⁶⁷](#), J. Newell [id⁹³](#), P.R. Newman [id²¹](#), Y.W.Y. Ng [id¹⁶⁷](#), B. Ngair [id^{118a}](#),
 H.D.N. Nguyen [id¹⁰⁹](#), J.D. Nichols [id¹²²](#), R.B. Nickerson [id¹²⁸](#), R. Nicolaidou [id¹³⁷](#), J. Nielsen [id¹³⁸](#),
 M. Niemeyer [id⁵⁵](#), J. Niermann [id³⁷](#), N. Nikiforou [id³⁷](#), V. Nikolaenko [id^{38,a}](#), I. Nikolic-Audit [id¹²⁹](#),
 P. Nilsson [id³⁰](#), I. Ninca [id⁴⁸](#), G. Ninio [id¹⁵⁶](#), A. Nisati [id^{75a}](#), R. Nisius [id¹¹¹](#), N. Nitika [id¹⁷⁴](#),
 E.K. Nkadimeng [id^{34b}](#), T. Nobe [id¹⁵⁸](#), D. Noll [id¹⁴⁸](#), T. Nommensen [id¹⁵²](#), M.B. Norfolk [id¹⁴⁴](#),
 B.J. Norman [id³⁵](#), L.C. Nosler [id^{18a}](#), M. Noury [id^{36a}](#), J. Novak [id⁹⁴](#), T. Novak [id⁹⁴](#), P. Novotny [id¹⁷⁴](#),
 R. Novotny [id¹³⁴](#), L. Nozka [id¹²⁴](#), K. Ntekas [id¹⁶⁴](#), D. Ntounis [id¹⁴⁸](#), N.M.J. Nunes De Moura Junior [id^{82b}](#),
 J. Ocariz [id¹²⁹](#), I. Ochoa [id^{132a}](#), A. Odella Rodriguez [id¹³](#), S. Oerdek [id^{48,y}](#), J.T. Offermann [id⁴⁰](#),
 A. Ogrodnik [id⁸⁷](#), A. Oh [id¹⁰²](#), C.C. Ohm [id¹⁴⁹](#), H. Oide [id⁸³](#), M.L. Ojeda [id³⁷](#), Y. Okumura [id¹⁵⁸](#),
 L.F. Oleiro Seabra [id^{132a}](#), I. Oleksiyuk [id⁵⁶](#), G. Oliveira Correa [id¹³](#), D. Oliveira Damazio [id³⁰](#),
 J.L. Oliver [id¹](#), R. Omar [id⁶⁸](#), Ö.O. Öncel [id⁵⁴](#), A.P. O'Neill [id²⁰](#), Y. Onoda [id¹⁴⁰](#), A. Onofre [id^{132a,132e,e}](#),
 P.U.E. Onyisi [id¹¹](#), M.J. Oreglia [id⁴⁰](#), D. Orestano [id^{77a,77b}](#), R. Orlandini [id^{77a,77b}](#), R.S. Orr [id¹⁶⁰](#),
 L.M. Osojnak [id⁴²](#), Y. Osumi [id¹¹²](#), G. Otero y Garzon [id³¹](#), H. Otono [id⁸⁹](#), M. Ouchrif [id^{36d}](#),
 F. Ould-Saada [id¹²⁷](#), T. Ovsiannikova [id¹⁴¹](#), M. Owen [id⁵⁹](#), R.E. Owen [id¹³⁶](#), V.E. Ozcan [id^{22a}](#),
 F. Ozturk [id⁸⁷](#), N. Ozturk [id⁸](#), S. Ozturk [id⁸¹](#), H.A. Pacey [id¹²⁸](#), K. Pachal [id^{161a}](#), A. Pacheco Pages [id¹³](#),
 C. Padilla Aranda [id¹³](#), G. Padovano [id^{75a,75b}](#), S. Pagan Griso [id^{18a}](#), J. Pampel [id²⁵](#), J. Pan [id¹⁷⁷](#),
 D.K. Panchal [id¹¹](#), C.E. Pandini [id⁶⁰](#), J.G. Panduro Vazquez [id¹³⁶](#), H.D. Pandya [id¹](#), H. Pang [id¹³⁷](#),
 P. Pani [id⁴⁸](#), G. Panizzo [id^{69a,69c}](#), L. Panwar [id¹²⁹](#), L. Paolozzi [id⁵⁶](#), S. Parajuli [id¹⁶⁷](#), A. Paramonov [id⁶](#),
 C. Paraskevopoulos [id⁵³](#), D. Paredes Hernandez [id^{64b}](#), S.R. Paredes Saenz [id⁵²](#), A. Pareti [id^{73a,73b}](#),
 K.R. Park [id⁴²](#), T.H. Park [id¹¹¹](#), F. Parodi [id^{57b,57a}](#), J.A. Parsons [id⁴²](#), U. Parzefall [id⁵⁴](#), B. Pascual Dias [id⁴¹](#),
 L. Pascual Dominguez [id¹⁰⁰](#), E. Pasqualucci [id^{75a}](#), S. Passaggio [id^{57b}](#), F. Pastore [id⁹⁶](#), P. Patel [id⁸⁷](#),
 U.M. Patel [id⁵¹](#), J.R. Pater [id¹⁰²](#), T. Pauly [id³⁷](#), F. Pauwels [id¹³⁵](#), C.I. Pazos [id¹⁶³](#), M. Pedersen [id¹²⁷](#),
 R. Pedro [id^{132a}](#), S.V. Peleganchuk [id³⁸](#), O. Penc [id¹³³](#), S. Peng [id¹⁵](#), G.D. Penn [id¹⁷⁷](#), K.E. Pensi [id¹¹⁰](#),
 M. Penzin [id³⁸](#), B.S. Peralva [id^{82d}](#), A.P. Pereira Peixoto [id¹⁴¹](#), L. Pereira Sanchez [id¹⁴⁸](#),
 D.V. Perpelitsa [id^{30,al}](#), G. Perera [id¹⁰⁴](#), E. Perez Codina [id³⁷](#), M. Perganti [id¹⁰](#), H. Pernegger [id³⁷](#),
 S. Perrella [id^{75a,75b}](#), K. Peters [id⁴⁸](#), R.F.Y. Peters [id¹⁰²](#), B.A. Petersen [id³⁷](#), T.C. Petersen [id⁴³](#), E. Petit [id¹⁰³](#),
 V. Petousis [id¹³⁴](#), A.R. Petri [id^{71a,71b}](#), C. Petridou [id^{157,d}](#), T. Petru [id¹³⁵](#), M. Pettee [id^{18a}](#), A. Petukhov [id⁸¹](#),
 K. Petukhova [id³⁷](#), R. Pezoa [id^{139g}](#), L. Pezzotti [id^{24b,24a}](#), G. Pezzullo [id¹⁷⁷](#), L. Pfaffenbichler [id³⁷](#),
 A.J. Pflieger [id⁷⁹](#), T.M. Pham [id¹⁷⁵](#), T. Pham [id¹⁰⁶](#), P.W. Phillips [id¹³⁶](#), G. Piacquadio [id¹⁵⁰](#), E. Pianori [id^{18a}](#),
 F. Piazza [id¹²⁵](#), R. Piegaiia [id³¹](#), D. Pietreanu [id^{28b}](#), A.D. Pilkington [id¹⁰²](#), M. Pinamonti [id^{69a,69c}](#),
 J.L. Pinfold [id²](#), G. Pinheiro Matos [id⁴²](#), B.C. Pinheiro Pereira [id^{132a}](#), J. Pinol Bel [id¹³](#),
 A.E. Pinto Pinoargote [id¹²⁹](#), L. Pintucci [id^{69a,69c}](#), K.M. Piper [id¹⁵¹](#), A. Pirttikoski [id⁵⁶](#), D.A. Pizzi [id³⁵](#),

L. Pizzimento ^{64b}, A. Plebani ³³, M.-A. Pleier ³⁰, V. Pleskot ¹³⁵, E. Plotnikova ³⁹, G. Poddar ⁹⁵,
 R. Poettgen ⁹⁹, L. Poggioli ¹²⁹, S. Polacek ¹³⁵, G. Polesello ^{73a}, A. Poley ¹⁴⁷, A. Polini ^{24b},
 C.S. Pollard ¹⁷², Z.B. Pollock ¹²¹, E. Pompa Pacchi ¹²², N.I. Pond ⁹⁷, D. Ponomarenko ⁶⁸,
 L. Pontecorvo ³⁷, S. Popa ^{28a}, G.A. Popeneciu ^{28d}, A. Poreba ³⁷, D.M. Portillo Quintero ^{161a},
 S. Pospisil ¹³⁴, M.A. Postill ¹⁴⁴, P. Postolache ^{28c}, K. Potamianos ¹⁷², P.A. Potepa ^{86a},
 I.N. Potrap ³⁹, C.J. Potter ³³, H. Potti ¹⁵², J. Poveda ¹⁶⁸, M.E. Pozo Astigarraga ³⁷, R. Pozzi ³⁷,
 A. Prades Ibanez ^{76a,76b}, S.R. Pradhan ¹⁴⁴, J. Pretel ¹⁷⁰, D. Price ¹⁰², M. Primavera ^{70a},
 L. Primomo ^{69a,69c}, M.A. Principe Martin ¹⁰⁰, R. Privara ¹²⁴, T. Procter ^{86b}, M.L. Proffitt ¹⁴¹,
 N. Proklova ¹³⁰, K. Prokofiev ^{64c}, G. Proto ¹¹¹, J. Proudfoot ⁶, M. Przybycien ^{86a},
 W.W. Przygoda ^{86b}, A. Psallidas ⁴⁶, J.E. Puddefoot ¹⁴⁴, D. Pudzha ⁵³, H.I. Purnell ¹,
 D. Pyatiizbyantseva ¹¹⁵, J. Qian ¹⁰⁷, R. Qian ¹⁰⁸, D. Qichen ¹²⁸, Y. Qin ¹³, T. Qiu ⁵²,
 A. Quadt ⁵⁵, M. Queitsch-Maitland ¹⁰², G. Quetant ⁵⁶, R.P. Quinn ¹⁶⁹, G. Rabanal Bolanos ⁶¹,
 D. Rafanoharana ¹¹¹, F. Raffaelli ^{76a,76b}, F. Ragusa ^{71a,71b}, J.L. Rainbolt ⁴⁰, S. Rajagopalan ³⁰,
 E. Ramakoti ³⁹, L. Rambelli ^{57b,57a}, I.A. Ramirez-Berend ³⁵, K. Ran ^{107,113c}, D.S. Rankin ¹³⁰,
 N.P. Rapheeha ^{34j}, H. Rasheed ^{28b}, A. Rastogi ^{18a}, S. Rave ¹⁰¹, S. Ravera ^{57b,57a}, B. Ravina ³⁷,
 I. Ravinovich ¹⁷⁴, M. Raymond ³⁷, A.L. Read ¹²⁷, N.P. Radioff ¹⁴⁴, D.M. Rebuzzi ^{73a,73b},
 A.S. Reed ⁵⁹, K. Reeves ²⁷, D. Reikher ³⁷, A. Rej ⁴⁹, C. Rembser ³⁷, H. Ren ⁶², M. Renda ^{28b},
 F. Renner ⁴⁸, A.G. Rennie ⁵⁹, M. Repik ⁵⁶, A.L. Rescia ^{57b,57a}, S. Resconi ^{71a},
 M. Ressegotti ^{57b,57a}, S. Rettie ¹¹⁶, W.F. Rettie ³⁵, M.M. Revering ³³, E. Reynolds ^{18a},
 O.L. Rezanova ³⁹, P. Reznicek ¹³⁵, H. Riani ^{36d}, N. Ribaric ⁵¹, B. Ricci ^{69a,69c}, E. Ricci ^{78a,78b},
 R. Richter ¹¹¹, S. Richter ^{47a,47b}, E. Richter-Was ^{86b}, M. Ridel ¹²⁹, S. Ridouani ^{36d}, P. Rieck ¹¹⁹,
 P. Riedler ³⁷, E.M. Riefel ^{47a,47b}, J.O. Rieger ¹¹⁶, M. Rijssenbeek ¹⁵⁰, M. Rimoldi ^{34c},
 L. Rinaldi ^{24b,24a}, P. Rincke ^{166,55}, G. Ripellino ¹⁶⁶, I. Riu ¹³, J.C. Rivera Vergara ¹⁷⁰,
 F. Rizatdinova ¹²³, E. Rizvi ⁹⁵, B.R. Roberts ⁴⁰, S.S. Roberts ¹³⁸, D. Robinson ³³, A. Robson ⁵⁹,
 A. Rocchi ^{76a,76b}, C. Roda ^{74a,74b}, F.A. Rodriguez ¹¹⁷, S. Rodriguez Bosca ³⁷,
 Y. Rodriguez Garcia ^{23a}, A.M. Rodríguez Vera ¹¹⁷, S. Roe ³⁷, J.T. Roemer ³⁷, O. Røhne ¹²⁷,
 R.A. Rojas ³⁷, C.P.A. Roland ¹²⁹, A. Romaniouk ⁷⁹, E. Romano ^{73a,73b}, M. Romano ^{24b},
 A.C. Romero Hernandez ¹⁶⁷, N. Rompotis ⁹³, L. Roos ¹²⁹, S. Rosati ^{75a}, B.J. Rosser ⁴⁰,
 E. Rossi ¹²⁸, E. Rossi ^{72a,72b}, L.P. Rossi ⁶¹, L. Rossini ⁵⁴, R. Rosten ¹²¹, M. Rotaru ^{28b},
 R. Roth ³⁷, D. Rousseau ⁶⁶, D. Rousso ⁴⁸, S. Roy-Garand ¹⁶⁰, A. Rozanov ¹⁰³,
 Z.M.A. Rozario ⁵⁹, Y. Rozen ¹⁵⁵, A. Rubio Jimenez ¹⁶⁸, V.H. Ruelas Rivera ¹⁹, T.A. Ruggeri ¹,
 A. Ruggiero ¹²⁸, A. Ruiz-Martinez ¹⁶⁸, A. Rummler ³⁷, G.B. Rupnik Boero ³⁷, Z. Rurikova ⁵⁴,
 N.A. Rusakovich ³⁹, S. Ruscelli ⁴⁹, H.L. Russell ¹⁷⁰, G. Russo ^{75a,75b}, J.P. Rutherford ⁷,
 S. Rutherford Colmenares ³³, M. Rybar ¹³⁵, P. Rybczynski ^{86a}, A. Ryzhov ⁴⁵,
 H.F-W. Sadrozinski ¹³⁸, F. Safai Tehrani ^{75a}, S. Saha ¹, M. Sahinsoy ⁸¹, B. Sahoo ¹⁷⁴,
 A. Saibel ¹⁶⁸, B.T. Saifuddin ¹²², M. Saimpert ¹³⁷, G.T. Saito ^{82c}, M. Saito ¹⁵⁸, T. Saito ¹⁵⁸,
 A. Sala ^{71a,71b}, A. Salnikov ¹⁴⁸, J. Salt ¹⁶⁸, A. Salvador Salas ¹⁵⁶, F. Salvatore ¹⁵¹,
 A. Salzburger ³⁷, D. Sammel ⁵⁴, E. Sampson ⁹², D. Sampsonidis ^{157,d}, D. Sampsonidou ¹²⁵,
 M.A.A. Samy ⁵⁹, J. Sánchez ¹⁶⁸, V. Sanchez Sebastian ¹⁶⁸, H. Sandaker ¹²⁷, C.O. Sander ⁴⁸,
 J.A. Sandesara ¹⁷⁵, M. Sandhoff ¹⁷⁶, C. Sandoval ^{23b}, L. Sanfilippo ^{63a}, D.P.C. Sankey ¹³⁶,
 T. Sano ⁸⁸, A. Sansoni ⁵³, M. Santana Queiroz ^{18b}, L. Santi ³⁷, C. Santoni ⁴¹,
 H. Santos ^{132a,132b}, A. Santra ¹⁷⁴, E. Sanzani ^{24b,24a}, K.A. Saoucha ^{84b}, J.G. Saraiva ^{132a,132d},
 J. Sardain ⁷, O. Sasaki ⁸³, K. Sato ¹⁶², C. Sauer ³⁷, E. Sauvan ⁴, P. Savard ^{160,ai}, R. Sawada ¹⁵⁸,
 C. Sawyer ¹³⁶, L. Sawyer ⁹⁸, A.M. Sayed ²⁷, C. Sbarra ^{24b}, A. Sbrizzi ^{24b,24a}, T. Scanlon ⁹⁷,
 J. Schaarschmidt ¹⁴¹, U. Schäfer ¹⁰¹, A.C. Schaffer ^{66,45}, D. Schaile ¹¹⁰, R.D. Schamberger ¹⁵⁰,
 C. Scharf ¹⁹, M.M. Schefer ²⁰, V.A. Schegelsky ³⁸, D. Scheirich ¹³⁵, M. Schernau ^{139f},
 C. Scheulen ⁵⁶, C. Schiavi ^{57b,57a}, M. Schioppa ^{44b,44a}, B. Schlag ¹⁴⁸, S. Schlenker ³⁷,

J. Schmeing [id176](#), E. Schmidt [id111](#), M.A. Schmidt [id176](#), K. Schmieden [id25](#), C. Schmitt [id101](#),
 N. Schmitt [id101](#), S. Schmitt [id48](#), N.A. Schneider [id110](#), L. Schoeffel [id137](#), A. Schoening [id63b](#),
 P.G. Scholer [id35](#), E. Schopf [id146](#), M. Schott [id25](#), S. Schramm [id56](#), T. Schroer [id56](#),
 H-C. Schultz-Coulon [id63a](#), M. Schumacher [id54](#), B.A. Schumm [id138](#), Ph. Schune [id137](#), H.R. Schwartz [id7](#),
 A. Schwartzman [id148](#), T.A. Schwarz [id107](#), Ph. Schwemling [id137](#), R. Schwienhorst [id108](#),
 F.G. Sciacca [id20](#), A. Sciandra [id30](#), G. Sciolla [id27](#), F. Scuri [id74a](#), C.D. Sebastiani [id37](#), K. Sedlaczek [id117](#),
 S.C. Seidel [id114](#), A. Seiden [id138](#), B.D. Seidlitz [id42](#), C. Seitz [id48](#), J.M. Seixas [id82b](#), G. Sekhniaidze [id72a](#),
 L. Selem [id60](#), N. Semprini-Cesari [id24b,24a](#), A. Semushin [id178](#), D. Sengupta [id56](#), V. Senthilkumar [id168](#),
 L. Serin [id66](#), M. Sessa [id72a,72b](#), H. Severini [id122](#), F. Sforza [id57b,57a](#), A. Sfyrla [id56](#), Q. Sha [id14](#),
 H. Shaddix [id117](#), A.H. Shah [id33](#), R. Shaheen [id149](#), J.D. Shahinian [id130](#), M. Shamim [id37](#), L.Y. Shan [id14](#),
 M. Shapiro [id18a](#), A. Sharma [id37](#), A.S. Sharma [id169](#), P. Sharma [id30](#), P.B. Shatalov [id38](#), K. Shaw [id151](#),
 S.M. Shaw [id102](#), Q. Shen [id14](#), D.J. Sheppard [id147](#), P. Sherwood [id97](#), L. Shi [id97](#), X. Shi [id14](#),
 S. Shimizu [id83](#), I.P.J. Shipsey [id128,*](#), S. Shirabe [id89](#), M. Shiyakova [id39,z](#), M.J. Shochet [id40](#),
 D.R. Shope [id127](#), B. Shrestha [id122](#), S. Shrestha [id121,an](#), I. Shreyber [id39](#), M.J. Shroff [id170](#), P. Sicho [id133](#),
 A.M. Sickles [id167](#), E. Sideras Haddad [id34j,165](#), A.C. Sidley [id116](#), A. Sidoti [id24b](#), F. Siegert [id50](#),
 Dj. Sijacki [id16](#), F. Sili [id62](#), J.M. Silva [id52](#), I. Silva Ferreira [id82b](#), M.V. Silva Oliveira [id30](#),
 S.B. Silverstein [id47a](#), S. Simion [id66](#), R. Simoniello [id37](#), E.L. Simpson [id102](#), H. Simpson [id151](#),
 L.R. Simpson [id6](#), S. Simsek [id81](#), S. Sindhu [id55](#), P. Sinervo [id160](#), S.N. Singh [id27](#), S. Singh [id30](#),
 S. Sinha [id48](#), S. Sinha [id102](#), M. Sioli [id24b,24a](#), K. Sioulas [id9](#), I. Siral [id37](#), E. Sitnikova [id48](#),
 J. Sjölin [id47a,47b](#), A. Skaf [id55](#), E. Skorda [id21](#), P. Skubic [id122](#), M. Slawinska [id87](#), I. Slazyk [id17](#),
 I. Sliusar [id127](#), V. Smakhtin [id174](#), B.H. Smart [id136](#), S.Yu. Smirnov [id139b](#), Y. Smirnov [id34c](#),
 L.N. Smirnova [id38,a](#), O. Smirnova [id99](#), A.C. Smith [id42](#), D.R. Smith [id164](#), J.L. Smith [id102](#), M.B. Smith [id35](#),
 R. Smith [id148](#), H. Smitmanns [id101](#), M. Smizanska [id92](#), K. Smolek [id134](#), P. Smolyanskiy [id134](#),
 A.A. Snesarev [id39](#), H.L. Snoek [id116](#), R.M. Snyder [id51](#), S. Snyder [id30](#), R. Sobie [id170,ab](#), A. Soffer [id156](#),
 C.A. Solans Sanchez [id37](#), E.Yu. Soldatov [id39](#), U. Soldevila [id168](#), A.A. Solodkov [id34j](#), S. Solomon [id27](#),
 A. Soloshenko [id39](#), K. Solovieva [id54](#), O.V. Solovyanov [id41](#), P. Sommer [id50](#), A. Sonay [id13](#),
 A. Sopcak [id134](#), A.L. Soppio [id52](#), F. Sopkova [id29b](#), J.D. Sorenson [id114](#), I.R. Sotarriva Alvarez [id140](#),
 V. Sothilingam [id63a](#), O.J. Soto Sandoval [id139c,139b](#), S. Sottocornola [id68](#), R. Soualah [id84a](#),
 Z. Soumami [id36e](#), D. South [id48](#), N. Soybelman [id174](#), S. Spagnolo [id70a,70b](#), D. Sperlich [id54](#),
 B. Spisso [id72a,72b](#), D.P. Spiteri [id59](#), L. Splendori [id103](#), M. Spousta [id135](#), E.J. Staats [id35](#), R. Stamen [id63a](#),
 E. Stanecka [id87](#), W. Stanek-Maslouska [id48](#), M.V. Stange [id50](#), B. Stanislaus [id18a](#), M.M. Stanitzki [id48](#),
 E.A. Starchenko [id38](#), G.H. Stark [id138](#), J. Stark [id90](#), P. Staroba [id133](#), P. Starovoitov [id84b](#),
 R. Staszewski [id87](#), C. Stauch [id110](#), G. Stavropoulos [id46](#), A. Stefl [id37](#), A. Stein [id101](#), P. Steinberg [id30](#),
 B. Stelzer [id147,161a](#), H.J. Stelzer [id131](#), O. Stelzer [id161a](#), H. Stenzel [id58](#), T.J. Stevenson [id151](#),
 G.A. Stewart [id37](#), J.R. Stewart [id123](#), G. Stoicea [id28b](#), M. Stolarski [id132a](#), S. Stonjek [id111](#),
 A. Straessner [id50](#), J. Strandberg [id149](#), S. Strandberg [id47a,47b](#), M. Stratmann [id176](#), M. Strauss [id122](#),
 T. Strebler [id103](#), P. Strizenec [id29b](#), R. Ströhmer [id171](#), D.M. Strom [id125](#), R. Stroynowski [id45](#),
 A. Strubig [id47a,47b](#), S.A. Stucci [id30](#), B. Stugu [id17](#), J. Stupak [id122](#), N.A. Styles [id48](#), D. Su [id148](#),
 S. Su [id62](#), X. Su [id62](#), D. Suchy [id29a](#), A.D. Sudhakar Ponnu [id55](#), L. Sudit [id174](#), K. Sugizaki [id130](#),
 V.V. Sulin [id38](#), D.M.S. Sultan [id128](#), L. Sultanaliyeva [id25](#), S. Sultansoy [id3b](#), S. Sun [id175](#), W. Sun [id14](#),
 N. Sur [id99](#), N. Suri Jr [id177](#), M.R. Sutton [id151](#), M. Svatos [id133](#), P.N. Swallow [id33](#), M. Swiatlowski [id161a](#),
 A. Swoboda [id37](#), I. Sykora [id29a](#), M. Sykora [id135](#), T. Sykora [id135](#), D. Ta [id101](#), K. Tackmann [id48,y](#),
 A. Taffard [id164](#), R. Tafirout [id161a](#), Y. Takubo [id83](#), M. Talby [id103](#), A.A. Talyshev [id38](#), K.C. Tam [id64b](#),
 N.M. Tamir [id156](#), A. Tanaka [id158](#), J. Tanaka [id158](#), R. Tanaka [id66](#), M. Tanasini [id150](#), Z. Tao [id169](#),
 S. Tapia Araya [id139g](#), S. Tapprogge [id101](#), A. Tarek Abouelfadl Mohamed [id37](#), S. Tarem [id155](#),
 K. Tariq [id14](#), G. Tarna [id37](#), G.F. Tartarelli [id71a](#), M.J. Tartarin [id90](#), P. Tas [id135](#), M. Tasevsky [id133](#),
 E. Tassi [id44b,44a](#), A.C. Tate [id167](#), Y. Tayalati [id36e,aa](#), G.N. Taylor [id106](#), W. Taylor [id161b](#),

R.J. Taylor Vara [ID168](#), A.S. Tegetmeier [ID90](#), P. Teixeira-Dias [ID96](#), J.J. Teoh [ID160](#), K. Terashi [ID158](#),
 J. Terron [ID100](#), S. Terzo [ID13](#), M. Testa [ID53](#), R.J. Teuscher [ID160,ab](#), A. Thaler [ID79](#), O. Theiner [ID56](#),
 T. Thevenaux-Pelzer [ID103](#), D.W. Thomas [ID96](#), J.P. Thomas [ID21](#), E.A. Thompson [ID18a](#), P.D. Thompson [ID21](#),
 E. Thomson [ID130](#), R.E. Thornberry [ID45](#), C. Tian [ID62](#), Y. Tian [ID56](#), V. Tikhomirov [ID81](#),
 Yu.A. Tikhonov [ID39](#), S. Timoshenko [ID38](#), D. Timoshyn [ID135](#), E.X.L. Ting [ID1](#), P. Tipton [ID177](#),
 A. Tishelman-Charny [ID30](#), K. Todome [ID140](#), S. Todorova-Nova [ID135](#), L. Toffolin [ID69a,69c](#), M. Togawa [ID83](#),
 J. Tojo [ID89](#), S. Tokár [ID29a](#), O. Toldaiev [ID68](#), G. Tolkachev [ID103](#), M. Tomoto [ID83](#), L. Tompkins [ID148,n](#),
 E. Torrence [ID125](#), H. Torres [ID90](#), D.I. Torres Arza [ID139g](#), E. Torró Pastor [ID168](#), M. Toscani [ID31](#),
 C. Toscirì [ID40](#), M. Tost [ID11](#), D.R. Tovey [ID144](#), T. Trefzger [ID171](#), P.M. Tricarico [ID13](#), A. Tricoli [ID30](#),
 I.M. Trigger [ID161a](#), S. Trincas-Duvoid [ID129](#), D.A. Trischuk [ID170](#), A. Tropina [ID39](#), D. Truncali [ID76a,76b](#),
 L. Truong [ID34c](#), M. Trzebinski [ID87](#), A. Trzupiek [ID87](#), F. Tsai [ID150](#), M. Tsai [ID107](#), A. Tsiamis [ID157](#),
 P.V. Tsiarehka [ID39](#), S. Tsigaridas [ID161a](#), A. Tsirigotis [ID157,u](#), V. Tsiskaridze [ID154a](#), E.G. Tskhadadze [ID154a](#),
 Y. Tsujikawa [ID88](#), I.I. Tsukerman [ID38](#), V. Tsulaia [ID18a](#), S. Tsuno [ID83](#), K. Tsuru [ID120](#), D. Tsybychev [ID150](#),
 Y. Tu [ID64b](#), A. Tudorache [ID28b](#), V. Tudorache [ID28b](#), S.B. Tuncay [ID128](#), S. Turchikhin [ID57b,57a](#),
 I. Turk Cakir [ID3a](#), R. Turra [ID71a](#), T. Turtuvshin [ID39,ac](#), P.M. Tuts [ID42](#), S. Tzamarias [ID157,d](#),
 Y. Uematsu [ID83](#), F. Ukegawa [ID162](#), P.A. Ulloa Poblete [ID139c,139b](#), E.N. Umaka [ID30](#), G. Unal [ID37](#),
 A. Undrus [ID30](#), G. Unel [ID164](#), J. Urban [ID29b](#), P. Urrejola [ID139e](#), G. Usai [ID8](#), R. Ushioda [ID159](#),
 M. Usman [ID109](#), F. Ustuner [ID52](#), Z. Uysal [ID81](#), V. Vacek [ID134](#), B. Vachon [ID105](#), T. Vafeiadis [ID37](#),
 A. Vaitkus [ID97](#), C. Valderanis [ID110](#), E. Valdes Santurio [ID47a,47b](#), M. Valente [ID37](#), S. Valentinetti [ID24b,24a](#),
 A. Valero [ID168](#), E. Valiente Moreno [ID168](#), A. Vallier [ID90](#), J.A. Valls Ferrer [ID168](#), D.R. Van Arneman [ID116](#),
 A. Van Der Graaf [ID49](#), H.Z. Van Der Schyf [ID34j](#), P. Van Gemmeren [ID6](#), M. Van Rijnbach [ID37](#),
 S. Van Stroud [ID97](#), I. Van Vulpen [ID116](#), P. Vana [ID135](#), M. Vanadia [ID76a,76b](#), U.M. Vande Voorde [ID149](#),
 W. Vandelli [ID37](#), E.R. Vandewall [ID148](#), D. Vannicola [ID156](#), L. Vannoli [ID53](#), R. Vari [ID75a](#), M. Varma [ID177](#),
 E.W. Varnes [ID7](#), C. Varni [ID79](#), D. Varouchas [ID66](#), L. Varriale [ID168](#), K.E. Varvell [ID152](#), M.E. Vasile [ID28b](#),
 L. Vaslin [ID83](#), M.D. Vassilev [ID148](#), A. Vasyukov [ID39](#), L.M. Vaughan [ID123](#), R. Vavricka [ID135](#),
 T. Vazquez Schroeder [ID13](#), J. Veatch [ID32](#), V. Vecchio [ID102](#), M.J. Veen [ID104](#), I. Veliscek [ID30](#),
 I. Velkovska [ID94](#), L.M. Veloce [ID160](#), F. Veloso [ID132a,132c](#), A.G. Veltman [ID52](#), S.H. Venetianer [ID163](#),
 S. Veneziano [ID75a](#), A. Ventura [ID70a,70b](#), A. Verbytskyi [ID111](#), M. Verducci [ID74a,74b](#), C. Vergis [ID95](#),
 M. Verissimo De Araujo [ID82b](#), W. Verkerke [ID116](#), J.C. Vermeulen [ID116](#), C. Vernieri [ID148](#),
 M. Vessella [ID164](#), M.C. Vetterli [ID147,ai](#), A. Vgenopoulos [ID101](#), N. Viaux Maira [ID139g,af](#), T. Vickey [ID144](#),
 O.E. Vickey Boeriu [ID144](#), G.H.A. Viehhauser [ID128](#), L. Vigani [ID63b](#), M. Vigl [ID111](#), M. Villa [ID24b,24a](#),
 M. Villaplana Perez [ID168](#), E.M. Villhauer [ID40](#), E. Vilucchi [ID53](#), M. Vincent [ID168](#), M.G. Vincter [ID35](#),
 A. Visibile [ID116](#), A. Visive [ID116](#), C. Vittori [ID37](#), I. Vivarelli [ID24b,24a](#), M.I. Vivas Albornoz [ID48](#),
 E. Voevodina [ID111](#), F. Vogel [ID110](#), J.C. Voigt [ID50](#), P. Vokac [ID134](#), Yu. Volkotrub [ID86b](#), L. Vomberg [ID25](#),
 E. Von Toerne [ID25](#), B. Vormwald [ID37](#), K. Vorobev [ID51](#), M. Vos [ID168](#), K. Voss [ID146](#), M. Vozak [ID37](#),
 L. Vozdecky [ID122](#), N. Vranjes [ID16](#), M. Vranjes Milosavljevic [ID16](#), M. Vreeswijk [ID116](#), N.K. Vu [ID143b,143a](#),
 R. Vuillermet [ID37](#), O. Vujinovic [ID101](#), I. Vukotic [ID40](#), I.K. Vyas [ID35](#), J.F. Wack [ID33](#), S. Wada [ID162](#),
 C. Wagner [ID148](#), J.M. Wagner [ID18a](#), W. Wagner [ID176](#), S. Wahdan [ID176](#), H. Wahlberg [ID91](#), C.H. Waits [ID122](#),
 J. Walder [ID136](#), R. Walker [ID110](#), K. Walkingshaw Pass [ID59](#), W. Walkowiak [ID146](#), A. Wall [ID130](#),
 E.J. Wallin [ID99](#), T. Wamorkar [ID148](#), K. Wandall-Christensen [ID168](#), A. Wang [ID62](#), A.Z. Wang [ID138](#),
 C. Wang [ID48](#), C. Wang [ID11](#), H. Wang [ID18a](#), J. Wang [ID64c](#), P. Wang [ID102](#), P. Wang [ID97](#), R. Wang [ID61](#),
 R. Wang [ID6](#), S.M. Wang [ID153](#), S. Wang [ID14](#), T. Wang [ID115](#), T. Wang [ID62](#), W.T. Wang [ID128](#), W. Wang [ID14](#),
 X. Wang [ID167](#), X. Wang [ID143a](#), X. Wang [ID48](#), Y. Wang [ID150](#), Y. Wang [ID114](#), Z. Wang [ID107](#),
 Z. Wang [ID143b](#), Z. Wang [ID107](#), C. Wanotayaroj [ID83](#), A. Warburton [ID105](#), A.L. Warnerbring [ID146](#),
 S. Waterhouse [ID96](#), A.T. Watson [ID21](#), H. Watson [ID52](#), M.F. Watson [ID21](#), E. Watton [ID37](#), G. Watts [ID141](#),
 B.M. Waugh [ID97](#), J.M. Webb [ID54](#), C. Weber [ID30](#), M.S. Weber [ID20](#), S.M. Weber [ID63a](#), C. Wei [ID62](#),
 Y. Wei [ID54](#), A.R. Weidberg [ID128](#), E.J. Weik [ID119](#), J. Weingarten [ID49](#), C. Weiser [ID54](#), C.J. Wells [ID48](#),

T. Wenaus ¹, T. Wengler ³⁷, N.S. Wenke ¹¹¹, N. Wermes ²⁵, M. Wessels ^{63a}, A.M. Wharton ⁹², A.S. White ⁶¹, A. White ⁸, M.J. White ¹, D. Whiteson ¹⁶⁴, L. Wickremasinghe ¹²⁶, W. Wiedenmann ¹⁷⁵, M. Wielers ¹³⁶, R. Wierda ¹⁴⁹, C. Wiglesworth ⁴³, H.G. Wilkens ³⁷, J.J.H. Wilkinson ³³, D.M. Williams ⁴², H.H. Williams ¹³⁰, S. Williams ³³, S. Willocq ¹⁰⁴, B.J. Wilson ¹⁰², D.J. Wilson ¹⁰², P.J. Windischhofer ⁴⁰, F.I. Winkel ³¹, F. Winklmeier ¹²⁵, B.T. Winter ⁵⁴, M. Wittgen ¹⁴⁸, M. Wobisch ⁹⁸, T. Wojtkowski ⁶⁰, Z. Wolfs ¹¹⁶, J. Wollrath ³⁷, M.W. Wolter ⁸⁷, H. Wolters ^{132a,132c}, M.C. Wong ¹³⁸, E.L. Woodward ⁴², S.D. Worm ⁴⁸, B.K. Wosiek ⁸⁷, K.W. Woźniak ⁸⁷, S. Wozniowski ⁵⁵, K. Wraight ⁵⁹, C. Wu ¹⁶⁰, C. Wu ²¹, J. Wu ¹⁵⁸, M. Wu ^{113b}, M. Wu ¹¹⁵, S.L. Wu ¹⁷⁵, S. Wu ^{14,ak}, X. Wu ⁶², Y.Q. Wu ¹⁶⁰, Y. Wu ⁶², Z. Wu ⁴, Z. Wu ^{113a}, J. Wuerzinger ¹¹¹, T.R. Wyatt ¹⁰², B.M. Wynne ⁵², S. Xella ⁴³, L. Xia ^{113a}, M. Xie ⁶², A. Xiong ¹²⁵, D. Xu ¹⁴, H. Xu ⁶², L. Xu ⁶², R. Xu ¹³⁰, T. Xu ¹⁰⁷, W. Xu ^{113a}, Y. Xu ¹⁴¹, Z. Xu ⁵², R. Xue ¹³¹, B. Yabsley ¹⁵², S. Yacoob ^{34a}, Y. Yamaguchi ⁸³, E. Yamashita ¹⁵⁸, H. Yamauchi ¹⁶², T. Yamazaki ^{18a}, Y. Yamazaki ⁸⁵, S. Yan ⁵⁹, Z. Yan ¹⁰⁴, H.J. Yang ^{143a,143b}, H.T. Yang ⁶², S. Yang ⁶², T. Yang ^{64c}, X. Yang ³⁷, X. Yang ¹⁴, Y. Yang ¹⁵⁸, Y. Yang ⁶², W-M. Yao ^{18a}, C.L. Yardley ¹⁵¹, J. Ye ¹⁴, S. Ye ³⁰, X. Ye ⁶², Y. Yeh ⁹⁷, I. Yeletsikh ³⁹, B. Yeo ^{18b}, M.R. Yexley ⁹⁷, T.P. Yildirim ¹²⁸, K. Yorita ¹⁷³, C.J.S. Young ³⁷, C. Young ¹⁴⁸, I.N.L. Young ⁵⁹, N.D. Young ¹²⁵, Y. Yu ⁶², J. Yuan ^{14,113c,ak}, M. Yuan ¹⁰⁷, R. Yuan ^{143b}, L. Yue ⁹⁷, M. Zaazoua ⁶², B. Zabinski ⁸⁷, I. Zahir ^{36a}, A. Zaio ^{57b,57a}, Z.K. Zak ⁸⁷, T. Zakareishvili ¹⁶⁸, S. Zambito ⁵⁶, J.A. Zamora Saa ^{139d}, J. Zang ¹⁵⁸, R. Zanzottera ^{71a,71b}, O. Zaplatilek ¹³⁴, C. Zeitnitz ¹⁷⁶, H. Zeng ¹⁴, D.T. Zenger Jr ²⁷, O. Zenin ³⁸, T. Ženiš ^{29a}, S. Zenz ⁹⁵, D. Zerwas ⁶⁶, B. Zhang ¹⁷², D.F. Zhang ¹⁴⁴, G. Zhang ^{14,ak}, J. Zhang ^{142a}, J. Zhang ⁶, L. Zhang ⁶², L. Zhang ^{113a}, P. Zhang ^{14,113c}, R. Zhang ^{113a}, S. Zhang ⁹⁰, T. Zhang ¹⁵⁸, Y. Zhang ¹⁴¹, Y. Zhang ⁹⁷, Y. Zhang ⁶², Y. Zhang ^{113a}, Z. Zhang ^{18a}, Z. Zhang ^{142a}, Z. Zhang ⁶⁶, H. Zhao ¹⁴¹, T. Zhao ^{142a}, Y. Zhao ³⁵, Z. Zhao ⁶², Z. Zhao ⁶², A. Zhemchugov ³⁹, J. Zheng ^{113a}, K. Zheng ¹⁶⁷, X. Zheng ⁶², Z. Zheng ¹⁴⁸, D. Zhong ¹⁶⁷, B. Zhou ¹⁰⁷, B. Zhou ^{143b,143a}, H. Zhou ⁷, N. Zhou ^{143a}, Y. Zhou ¹⁵, Y. Zhou ^{113a}, Y. Zhou ⁷, J. Zhu ¹⁰⁷, X. Zhu ^{143b}, Y. Zhu ^{143a}, Y. Zhu ⁶², X. Zhuang ¹⁴, K. Zhukov ⁶⁸, N.I. Zimine ³⁹, J. Zinsser ^{63b}, M. Ziolkowski ¹⁴⁶, L. Živković ¹⁶, A. Zoccoli ^{24b,24a}, K. Zoch ⁶¹, A. Zografos ³⁷, T.G. Zorbas ¹⁴⁴, O. Zormpa ⁴⁶, L. Zwalinski ³⁷.

¹Department of Physics, University of Adelaide, Adelaide; Australia.

²Department of Physics, University of Alberta, Edmonton AB; Canada.

^{3(a)}Department of Physics, Ankara University, Ankara; ^(b)Division of Physics, TOBB University of Economics and Technology, Ankara; Türkiye.

⁴LAPP, Université Savoie Mont Blanc, CNRS/IN2P3, Annecy; France.

⁵APC, Université Paris Cité, CNRS/IN2P3, Paris; France.

⁶High Energy Physics Division, Argonne National Laboratory, Argonne IL; United States of America.

⁷Department of Physics, University of Arizona, Tucson AZ; United States of America.

⁸Department of Physics, University of Texas at Arlington, Arlington TX; United States of America.

⁹Physics Department, National and Kapodistrian University of Athens, Athens; Greece.

¹⁰Physics Department, National Technical University of Athens, Zografou; Greece.

¹¹Department of Physics, University of Texas at Austin, Austin TX; United States of America.

¹²Institute of Physics, Azerbaijan Academy of Sciences, Baku; Azerbaijan.

¹³Institut de Física d'Altes Energies (IFAE), Barcelona Institute of Science and Technology, Barcelona; Spain.

¹⁴Institute of High Energy Physics, Chinese Academy of Sciences, Beijing; China.

¹⁵Physics Department, Tsinghua University, Beijing; China.

- ¹⁶Institute of Physics, University of Belgrade, Belgrade; Serbia.
- ¹⁷Department for Physics and Technology, University of Bergen, Bergen; Norway.
- ¹⁸(^a) Physics Division, Lawrence Berkeley National Laboratory, Berkeley CA; (^b) University of California, Berkeley CA; United States of America.
- ¹⁹Institut für Physik, Humboldt Universität zu Berlin, Berlin; Germany.
- ²⁰Albert Einstein Center for Fundamental Physics and Laboratory for High Energy Physics, University of Bern, Bern; Switzerland.
- ²¹School of Physics and Astronomy, University of Birmingham, Birmingham; United Kingdom.
- ²²(^a) Department of Physics, Bogazici University, Istanbul; (^b) Department of Physics Engineering, Gaziantep University, Gaziantep; (^c) Department of Physics, Istanbul University, Istanbul; Türkiye.
- ²³(^a) Facultad de Ciencias y Centro de Investigaciones, Universidad Antonio Nariño, Bogotá; (^b) Departamento de Física, Universidad Nacional de Colombia, Bogotá; Colombia.
- ²⁴(^a) Dipartimento di Fisica e Astronomia A. Righi, Università di Bologna, Bologna; (^b) INFN Sezione di Bologna; Italy.
- ²⁵Physikalisches Institut, Universität Bonn, Bonn; Germany.
- ²⁶Department of Physics, Boston University, Boston MA; United States of America.
- ²⁷Department of Physics, Brandeis University, Waltham MA; United States of America.
- ²⁸(^a) Transilvania University of Brasov, Brasov; (^b) Horia Hulubei National Institute of Physics and Nuclear Engineering, Bucharest; (^c) Department of Physics, Alexandru Ioan Cuza University of Iasi, Iasi; (^d) National Institute for Research and Development of Isotopic and Molecular Technologies, Physics Department, Cluj-Napoca; (^e) National University of Science and Technology Politehnica, Bucharest; (^f) West University in Timisoara, Timisoara; (^g) Faculty of Physics, University of Bucharest, Bucharest; Romania.
- ²⁹(^a) Faculty of Mathematics, Physics and Informatics, Comenius University, Bratislava; (^b) Department of Subnuclear Physics, Institute of Experimental Physics of the Slovak Academy of Sciences, Kosice; Slovak Republic.
- ³⁰Physics Department, Brookhaven National Laboratory, Upton NY; United States of America.
- ³¹Universidad de Buenos Aires, Facultad de Ciencias Exactas y Naturales, Departamento de Física, y CONICET, Instituto de Física de Buenos Aires (IFIBA), Buenos Aires; Argentina.
- ³²California State University, CA; United States of America.
- ³³Cavendish Laboratory, University of Cambridge, Cambridge; United Kingdom.
- ³⁴(^a) Department of Physics, University of Cape Town, Cape Town; (^b) iThemba Labs, Western Cape; (^c) Department of Mechanical Engineering Science, University of Johannesburg, Johannesburg; (^d) National Institute of Physics, University of the Philippines Diliman (Philippines); (^e) Department of Physics, Stellenbosch University, Matieland; (^f) University of KwaZulu-Natal, School of Agriculture and Science, Mathematics, Westville; (^g) University of South Africa, Department of Physics, Pretoria; (^h) University of Pretoria, Department of Mechanical and Aeronautical Engineering, Pretoria; (ⁱ) University of Zululand, KwaDlangezwa; (^j) School of Physics, University of the Witwatersrand, Johannesburg; South Africa.
- ³⁵Department of Physics, Carleton University, Ottawa ON; Canada.
- ³⁶(^a) Faculté des Sciences Ain Chock, Université Hassan II de Casablanca; (^b) Faculté des Sciences, Université Ibn-Tofail, Kénitra; (^c) Faculté des Sciences Semlalia, Université Cadi Ayyad, LPHEA-Marrakech; (^d) LPMR, Faculté des Sciences, Université Mohamed Premier, Oujda; (^e) Faculté des sciences, Université Mohammed V, Rabat; (^f) Institute of Applied Physics, Mohammed VI Polytechnic University, Ben Guerir; Morocco.
- ³⁷CERN, Geneva; Switzerland.
- ³⁸Affiliated with an institute formerly covered by a cooperation agreement with CERN.
- ³⁹Affiliated with an international laboratory covered by a cooperation agreement with CERN.

- ⁴⁰ Enrico Fermi Institute, University of Chicago, Chicago IL; United States of America.
- ⁴¹ LPC, Université Clermont Auvergne, CNRS/IN2P3, Clermont-Ferrand; France.
- ⁴² Nevis Laboratory, Columbia University, Irvington NY; United States of America.
- ⁴³ Niels Bohr Institute, University of Copenhagen, Copenhagen; Denmark.
- ⁴⁴ ^(a) Dipartimento di Fisica, Università della Calabria, Rende; ^(b) INFN Gruppo Collegato di Cosenza, Laboratori Nazionali di Frascati; Italy.
- ⁴⁵ Physics Department, Southern Methodist University, Dallas TX; United States of America.
- ⁴⁶ National Centre for Scientific Research "Demokritos", Agia Paraskevi; Greece.
- ⁴⁷ ^(a) Department of Physics, Stockholm University; ^(b) Oskar Klein Centre, Stockholm; Sweden.
- ⁴⁸ Deutsches Elektronen-Synchrotron DESY, Hamburg and Zeuthen; Germany.
- ⁴⁹ Fakultät Physik, Technische Universität Dortmund, Dortmund; Germany.
- ⁵⁰ Institut für Kern- und Teilchenphysik, Technische Universität Dresden, Dresden; Germany.
- ⁵¹ Department of Physics, Duke University, Durham NC; United States of America.
- ⁵² SUPA - School of Physics and Astronomy, University of Edinburgh, Edinburgh; United Kingdom.
- ⁵³ INFN e Laboratori Nazionali di Frascati, Frascati; Italy.
- ⁵⁴ Physikalisches Institut, Albert-Ludwigs-Universität Freiburg, Freiburg; Germany.
- ⁵⁵ II. Physikalisches Institut, Georg-August-Universität Göttingen, Göttingen; Germany.
- ⁵⁶ Département de Physique Nucléaire et Corpusculaire, Université de Genève, Genève; Switzerland.
- ⁵⁷ ^(a) Dipartimento di Fisica, Università di Genova, Genova; ^(b) INFN Sezione di Genova; Italy.
- ⁵⁸ II. Physikalisches Institut, Justus-Liebig-Universität Giessen, Giessen; Germany.
- ⁵⁹ SUPA - School of Physics and Astronomy, University of Glasgow, Glasgow; United Kingdom.
- ⁶⁰ LPSC, Université Grenoble Alpes, CNRS/IN2P3, Grenoble INP, Grenoble; France.
- ⁶¹ Laboratory for Particle Physics and Cosmology, Harvard University, Cambridge MA; United States of America.
- ⁶² Department of Modern Physics and State Key Laboratory of Particle Detection and Electronics, University of Science and Technology of China, Hefei; China.
- ⁶³ ^(a) Kirchhoff-Institut für Physik, Ruprecht-Karls-Universität Heidelberg, Heidelberg; ^(b) Physikalisches Institut, Ruprecht-Karls-Universität Heidelberg, Heidelberg; Germany.
- ⁶⁴ ^(a) Department of Physics, Chinese University of Hong Kong, Shatin, N.T., Hong Kong; ^(b) Department of Physics, University of Hong Kong, Hong Kong; ^(c) Department of Physics and Institute for Advanced Study, Hong Kong University of Science and Technology, Clear Water Bay, Kowloon, Hong Kong; China.
- ⁶⁵ Department of Physics, National Tsing Hua University, Hsinchu; Taiwan.
- ⁶⁶ IJCLab, Université Paris-Saclay, CNRS/IN2P3, 91405, Orsay; France.
- ⁶⁷ Centro Nacional de Microelectrónica (IMB-CNM-CSIC), Barcelona; Spain.
- ⁶⁸ Department of Physics, Indiana University, Bloomington IN; United States of America.
- ⁶⁹ ^(a) INFN Gruppo Collegato di Udine, Sezione di Trieste, Udine; ^(b) ICTP, Trieste; ^(c) Dipartimento Politecnico di Ingegneria e Architettura, Università di Udine, Udine; Italy.
- ⁷⁰ ^(a) INFN Sezione di Lecce; ^(b) Dipartimento di Matematica e Fisica, Università del Salento, Lecce; Italy.
- ⁷¹ ^(a) INFN Sezione di Milano; ^(b) Dipartimento di Fisica, Università di Milano, Milano; Italy.
- ⁷² ^(a) INFN Sezione di Napoli; ^(b) Dipartimento di Fisica, Università di Napoli, Napoli; Italy.
- ⁷³ ^(a) INFN Sezione di Pavia; ^(b) Dipartimento di Fisica, Università di Pavia, Pavia; Italy.
- ⁷⁴ ^(a) INFN Sezione di Pisa; ^(b) Dipartimento di Fisica E. Fermi, Università di Pisa, Pisa; Italy.
- ⁷⁵ ^(a) INFN Sezione di Roma; ^(b) Dipartimento di Fisica, Sapienza Università di Roma, Roma; Italy.
- ⁷⁶ ^(a) INFN Sezione di Roma Tor Vergata; ^(b) Dipartimento di Fisica, Università di Roma Tor Vergata, Roma; Italy.
- ⁷⁷ ^(a) INFN Sezione di Roma Tre; ^(b) Dipartimento di Matematica e Fisica, Università Roma Tre, Roma; Italy.

- ⁷⁸(^a)INFN-TIFPA;(^b)Università degli Studi di Trento, Trento; Italy.
- ⁷⁹Universität Innsbruck, Department of Astro and Particle Physics, Innsbruck; Austria.
- ⁸⁰Department of Physics and Astronomy, Iowa State University, Ames IA; United States of America.
- ⁸¹Istinye University, Sariyer, Istanbul; Türkiye.
- ⁸²(^a)Departamento de Engenharia Elétrica, Universidade Federal de Juiz de Fora (UFJF), Juiz de Fora;(^b)Universidade Federal do Rio De Janeiro COPPE/EE/IF, Rio de Janeiro;(^c)Instituto de Física, Universidade de São Paulo, São Paulo;(^d)Rio de Janeiro State University, Rio de Janeiro;(^e)Federal University of Bahia, Bahia; Brazil.
- ⁸³KEK, High Energy Accelerator Research Organization, Tsukuba; Japan.
- ⁸⁴(^a)Khalifa University of Science and Technology, Abu Dhabi;(^b)University of Sharjah, Sharjah; United Arab Emirates.
- ⁸⁵Graduate School of Science, Kobe University, Kobe; Japan.
- ⁸⁶(^a)AGH University of Krakow, Faculty of Physics and Applied Computer Science, Krakow;(^b)Marian Smoluchowski Institute of Physics, Jagiellonian University, Krakow; Poland.
- ⁸⁷Institute of Nuclear Physics Polish Academy of Sciences, Krakow; Poland.
- ⁸⁸Faculty of Science, Kyoto University, Kyoto; Japan.
- ⁸⁹Research Center for Advanced Particle Physics and Department of Physics, Kyushu University, Fukuoka ; Japan.
- ⁹⁰L2IT, Université de Toulouse, CNRS/IN2P3, UPS, Toulouse; France.
- ⁹¹Instituto de Física La Plata, Universidad Nacional de La Plata and CONICET, La Plata; Argentina.
- ⁹²Physics Department, Lancaster University, Lancaster; United Kingdom.
- ⁹³Oliver Lodge Laboratory, University of Liverpool, Liverpool; United Kingdom.
- ⁹⁴Department of Experimental Particle Physics, Jožef Stefan Institute and Department of Physics, University of Ljubljana, Ljubljana; Slovenia.
- ⁹⁵Department of Physics and Astronomy, Queen Mary University of London, London; United Kingdom.
- ⁹⁶Department of Physics, Royal Holloway University of London, Egham; United Kingdom.
- ⁹⁷Department of Physics and Astronomy, University College London, London; United Kingdom.
- ⁹⁸Louisiana Tech University, Ruston LA; United States of America.
- ⁹⁹Fysiska institutionen, Lunds universitet, Lund; Sweden.
- ¹⁰⁰Departamento de Física Teórica C-15 and CIAFF, Universidad Autónoma de Madrid, Madrid; Spain.
- ¹⁰¹Institut für Physik, Universität Mainz, Mainz; Germany.
- ¹⁰²School of Physics and Astronomy, University of Manchester, Manchester; United Kingdom.
- ¹⁰³CPPM, Aix-Marseille Université, CNRS/IN2P3, Marseille; France.
- ¹⁰⁴Department of Physics, University of Massachusetts, Amherst MA; United States of America.
- ¹⁰⁵Department of Physics, McGill University, Montreal QC; Canada.
- ¹⁰⁶School of Physics, University of Melbourne, Victoria; Australia.
- ¹⁰⁷Department of Physics, University of Michigan, Ann Arbor MI; United States of America.
- ¹⁰⁸Department of Physics and Astronomy, Michigan State University, East Lansing MI; United States of America.
- ¹⁰⁹Group of Particle Physics, University of Montreal, Montreal QC; Canada.
- ¹¹⁰Fakultät für Physik, Ludwig-Maximilians-Universität München, München; Germany.
- ¹¹¹Max-Planck-Institut für Physik (Werner-Heisenberg-Institut), München; Germany.
- ¹¹²Graduate School of Science and Kobayashi-Maskawa Institute, Nagoya University, Nagoya; Japan.
- ¹¹³(^a)Department of Physics, Nanjing University, Nanjing;(^b)School of Science, Shenzhen Campus of Sun Yat-sen University;(^c)University of Chinese Academy of Science (UCAS), Beijing; China.
- ¹¹⁴Department of Physics and Astronomy, University of New Mexico, Albuquerque NM; United States of America.

- ¹¹⁵Institute for Mathematics, Astrophysics and Particle Physics, Radboud University/Nikhef, Nijmegen; Netherlands.
- ¹¹⁶Nikhef National Institute for Subatomic Physics and University of Amsterdam, Amsterdam; Netherlands.
- ¹¹⁷Department of Physics, Northern Illinois University, DeKalb IL; United States of America.
- ¹¹⁸(^a)New York University Abu Dhabi, Abu Dhabi; (^b)United Arab Emirates University, Al Ain; United Arab Emirates.
- ¹¹⁹Department of Physics, New York University, New York NY; United States of America.
- ¹²⁰Ochanomizu University, Otsuka, Bunkyo-ku, Tokyo; Japan.
- ¹²¹Ohio State University, Columbus OH; United States of America.
- ¹²²Homer L. Dodge Department of Physics and Astronomy, University of Oklahoma, Norman OK; United States of America.
- ¹²³Department of Physics, Oklahoma State University, Stillwater OK; United States of America.
- ¹²⁴Palacký University, Joint Laboratory of Optics, Olomouc; Czech Republic.
- ¹²⁵Institute for Fundamental Science, University of Oregon, Eugene, OR; United States of America.
- ¹²⁶Graduate School of Science, University of Osaka, Osaka; Japan.
- ¹²⁷Department of Physics, University of Oslo, Oslo; Norway.
- ¹²⁸Department of Physics, Oxford University, Oxford; United Kingdom.
- ¹²⁹LPNHE, Sorbonne Université, Université Paris Cité, CNRS/IN2P3, Paris; France.
- ¹³⁰Department of Physics, University of Pennsylvania, Philadelphia PA; United States of America.
- ¹³¹Department of Physics and Astronomy, University of Pittsburgh, Pittsburgh PA; United States of America.
- ¹³²(^a)Laboratório de Instrumentação e Física Experimental de Partículas - LIP, Lisboa; (^b)Departamento de Física, Faculdade de Ciências, Universidade de Lisboa, Lisboa; (^c)Departamento de Física, Universidade de Coimbra, Coimbra; (^d)Centro de Física Nuclear da Universidade de Lisboa, Lisboa; (^e)Departamento de Física, Escola de Ciências, Universidade do Minho, Braga; (^f)Departamento de Física Teórica y del Cosmos, Universidad de Granada, Granada (Spain); (^g)Departamento de Física, Instituto Superior Técnico, Universidade de Lisboa, Lisboa; Portugal.
- ¹³³Institute of Physics of the Czech Academy of Sciences, Prague; Czech Republic.
- ¹³⁴Czech Technical University in Prague, Prague; Czech Republic.
- ¹³⁵Charles University, Faculty of Mathematics and Physics, Prague; Czech Republic.
- ¹³⁶Particle Physics Department, Rutherford Appleton Laboratory, Didcot; United Kingdom.
- ¹³⁷IRFU, CEA, Université Paris-Saclay, Gif-sur-Yvette; France.
- ¹³⁸Santa Cruz Institute for Particle Physics, University of California Santa Cruz, Santa Cruz CA; United States of America.
- ¹³⁹(^a)Departamento de Física, Pontificia Universidad Católica de Chile, Santiago; (^b)Millennium Institute for Subatomic physics at high energy frontier (SAPHIR), Santiago; (^c)Instituto de Investigación Multidisciplinario en Ciencia y Tecnología, y Departamento de Física, Universidad de La Serena; (^d)Universidad Andres Bello, Department of Physics, Santiago; (^e)Universidad San Sebastian, Recoleta; (^f)Instituto de Alta Investigación, Universidad de Tarapacá, Arica; (^g)Departamento de Física, Universidad Técnica Federico Santa María, Valparaíso; Chile.
- ¹⁴⁰Department of Physics, Institute of Science, Tokyo; Japan.
- ¹⁴¹Department of Physics, University of Washington, Seattle WA; United States of America.
- ¹⁴²(^a)Institute of Frontier and Interdisciplinary Science and Key Laboratory of Particle Physics and Particle Irradiation (MOE), Shandong University, Qingdao; (^b)School of Physics, Zhengzhou University; China.
- ¹⁴³(^a)State Key Laboratory of Dark Matter Physics, School of Physics and Astronomy, Shanghai Jiao Tong University, Key Laboratory for Particle Astrophysics and Cosmology (MOE), SKLPPC, Shanghai; (^b)State

Key Laboratory of Dark Matter Physics, Tsung-Dao Lee Institute, Shanghai Jiao Tong University, Shanghai; China.

¹⁴⁴Department of Physics and Astronomy, University of Sheffield, Sheffield; United Kingdom.

¹⁴⁵Department of Physics, Shinshu University, Nagano; Japan.

¹⁴⁶Department Physik, Universität Siegen, Siegen; Germany.

¹⁴⁷Department of Physics, Simon Fraser University, Burnaby BC; Canada.

¹⁴⁸SLAC National Accelerator Laboratory, Stanford CA; United States of America.

¹⁴⁹Department of Physics, Royal Institute of Technology, Stockholm; Sweden.

¹⁵⁰Departments of Physics and Astronomy, Stony Brook University, Stony Brook NY; United States of America.

¹⁵¹Department of Physics and Astronomy, University of Sussex, Brighton; United Kingdom.

¹⁵²School of Physics, University of Sydney, Sydney; Australia.

¹⁵³Institute of Physics, Academia Sinica, Taipei; Taiwan.

¹⁵⁴(^a) E. Andronikashvili Institute of Physics, Iv. Javakhishvili Tbilisi State University, Tbilisi; (^b) High Energy Physics Institute, Tbilisi State University, Tbilisi; (^c) University of Georgia, Tbilisi; Georgia.

¹⁵⁵Department of Physics, Technion, Israel Institute of Technology, Haifa; Israel.

¹⁵⁶Raymond and Beverly Sackler School of Physics and Astronomy, Tel Aviv University, Tel Aviv; Israel.

¹⁵⁷Department of Physics, Aristotle University of Thessaloniki, Thessaloniki; Greece.

¹⁵⁸International Center for Elementary Particle Physics and Department of Physics, University of Tokyo, Tokyo; Japan.

¹⁵⁹Graduate School of Science and Technology, Tokyo Metropolitan University, Tokyo; Japan.

¹⁶⁰Department of Physics, University of Toronto, Toronto ON; Canada.

¹⁶¹(^a) TRIUMF, Vancouver BC; (^b) Department of Physics and Astronomy, York University, Toronto ON; Canada.

¹⁶²Division of Physics and Tomonaga Center for the History of the Universe, Faculty of Pure and Applied Sciences, University of Tsukuba, Tsukuba; Japan.

¹⁶³Department of Physics and Astronomy, Tufts University, Medford MA; United States of America.

¹⁶⁴Department of Physics and Astronomy, University of California Irvine, Irvine CA; United States of America.

¹⁶⁵University of West Attica, Athens; Greece.

¹⁶⁶Department of Physics and Astronomy, University of Uppsala, Uppsala; Sweden.

¹⁶⁷Department of Physics, University of Illinois, Urbana IL; United States of America.

¹⁶⁸Instituto de Física Corpuscular (IFIC), Centro Mixto Universidad de Valencia - CSIC, Valencia; Spain.

¹⁶⁹Department of Physics, University of British Columbia, Vancouver BC; Canada.

¹⁷⁰Department of Physics and Astronomy, University of Victoria, Victoria BC; Canada.

¹⁷¹Fakultät für Physik und Astronomie, Julius-Maximilians-Universität Würzburg, Würzburg; Germany.

¹⁷²Department of Physics, University of Warwick, Coventry; United Kingdom.

¹⁷³Waseda University, Tokyo; Japan.

¹⁷⁴Department of Particle Physics and Astrophysics, Weizmann Institute of Science, Rehovot; Israel.

¹⁷⁵Department of Physics, University of Wisconsin, Madison WI; United States of America.

¹⁷⁶Fakultät für Mathematik und Naturwissenschaften, Fachgruppe Physik, Bergische Universität Wuppertal, Wuppertal; Germany.

¹⁷⁷Department of Physics, Yale University, New Haven CT; United States of America.

¹⁷⁸Yerevan Physics Institute, Yerevan; Armenia.

^a Also at Affiliated with an institute formerly covered by a cooperation agreement with CERN.

^b Also at An-Najah National University, Nablus; Palestine.

^c Also at Borough of Manhattan Community College, City University of New York, New York NY; United

States of America.

^d Also at Center for Interdisciplinary Research and Innovation (CIRI-AUTH), Thessaloniki; Greece.

^e Also at Centre of Physics of the Universities of Minho and Porto (CF-UM-UP); Portugal.

^f Also at CERN, Geneva; Switzerland.

^g Also at Département de Physique Nucléaire et Corpusculaire, Université de Genève, Genève; Switzerland.

^h Also at Departament de Física de la Universitat Autònoma de Barcelona, Barcelona; Spain.

ⁱ Also at Department of Financial and Management Engineering, University of the Aegean, Chios; Greece.

^j Also at Department of Mathematical Sciences, University of South Africa, Johannesburg; South Africa.

^k Also at Department of Modern Physics and State Key Laboratory of Particle Detection and Electronics, University of Science and Technology of China, Hefei; China.

^l Also at Department of Physics, Bolu Abant İzzet Baysal University, Bolu; Türkiye.

^m Also at Department of Physics, King's College London, London; United Kingdom.

ⁿ Also at Department of Physics, Stanford University, Stanford CA; United States of America.

^o Also at Department of Physics, Stellenbosch University; South Africa.

^p Also at Department of Physics, University of Fribourg, Fribourg; Switzerland.

^q Also at Department of Physics, University of Thessaly; Greece.

^r Also at Department of Physics, Westmont College, Santa Barbara; United States of America.

^s Also at Faculty of Physics, Sofia University, 'St. Kliment Ohridski', Sofia; Bulgaria.

^t Also at Faculty of Physics, University of Bucharest; Romania.

^u Also at Hellenic Open University, Patras; Greece.

^v Also at Henan University; China.

^w Also at Imam Mohammad Ibn Saud Islamic University; Saudi Arabia.

^x Also at Institutio Catalana de Recerca i Estudis Avancats, ICREA, Barcelona; Spain.

^y Also at Institut für Experimentalphysik, Universität Hamburg, Hamburg; Germany.

^z Also at Institute for Nuclear Research and Nuclear Energy (INRNE) of the Bulgarian Academy of Sciences, Sofia; Bulgaria.

^{aa} Also at Institute of Applied Physics, Mohammed VI Polytechnic University, Ben Guerir; Morocco.

^{ab} Also at Institute of Particle Physics (IPP); Canada.

^{ac} Also at Institute of Physics and Technology, Mongolian Academy of Sciences, Ulaanbaatar; Mongolia.

^{ad} Also at Institute of Physics, Azerbaijan Academy of Sciences, Baku; Azerbaijan.

^{ae} Also at Institute of Theoretical Physics, Ilia State University, Tbilisi; Georgia.

^{af} Also at Millennium Institute for Subatomic physics at high energy frontier (SAPHIR), Santiago; Chile.

^{ag} Also at National Institute of Physics, University of the Philippines Diliman (Philippines); Philippines.

^{ah} Also at The Collaborative Innovation Center of Quantum Matter (CICQM), Beijing; China.

^{ai} Also at TRIUMF, Vancouver BC; Canada.

^{aj} Also at Università di Napoli Parthenope, Napoli; Italy.

^{ak} Also at University of Chinese Academy of Sciences (UCAS), Beijing; China.

^{al} Also at University of Colorado Boulder, Department of Physics, Colorado; United States of America.

^{am} Also at University of Siena; Italy.

^{an} Also at Washington College, Chestertown, MD; United States of America.

^{ao} Also at Yeditepe University, Physics Department, Istanbul; Türkiye.

* Deceased